TKK Dissertations 24
Espoo 2006

EVALUATION OF POWER SYSTEM HARMONIC EFFECTS ON TRANSFORMERS

Hot Spot Calculation and Loss of Life Estimation

Doctoral Dissertation

Asaad A. Elmoudi

Helsinki University of Technology
Department of Electrical and Communications Engineering
Power Systems and High Voltage Engineering

TKK Dissertations 24
Espoo 2006

EVALUATION OF POWER SYSTEM HARMONIC EFFECTS ON TRANSFORMERS

Hot Spot Calculation and Loss of Life Estimation

Doctoral Dissertation

Asaad A. Elmoudi

Dissertation for the degree of Doctor of Science in Technology to be presented with due permission of the Department of Electrical and Communications Engineering for public examination and debate in Auditorium S4 at Helsinki University of Technology (Espoo, Finland) on the 20th of April, 2006, at 12 noon.

Helsinki University of Technology
Department of Electrical and Communications Engineering
Power Systems and High Voltage Engineering

Teknillinen korkeakoulu
Sähkö- ja tietoliikennetekniikan osasto
Sähköverkot ja suurjännitetekniikka

Distribution:
Helsinki University of Technology
Department of Electrical and Communications Engineering
Power Systems and High Voltage Engineering
P.O. Box 3000
FI - 02015 TKK
FINLAND
URL: http://powersystems.tkk.fi/
Tel. +358-9-4511
Fax +358-9-451 5012
E-mail: asaad.elmoudi@tkk.fi

ISBN 951-22-8077-9
ISBN 951-22-8078-7 (PDF)
ISSN 1795-2239
ISSN 1795-4584 (PDF)
URL: http://lib.tkk.fi/Diss/2006/isbn9512280787/

TKK-DISS-2105

Edita Prima Oy
Helsinki 2006

HELSINKI UNIVERSITY OF TECHNOLOGY

P. O. BOX 1000, FI-02015 TKK

http://www.tkk.fi

ABSTRACT OF DOCTORAL DISSERTATION

Author Asaad Ali Elmoudi

Name of the dissertation

Evaluation of Power System Harmonic Effects on Transformers
Hot Spot Calculation and Loss of Life Estimation

Date of manuscript September 2005 | Date of the dissertation 20.04.2006

☒ Monograph ☐ Article dissertation

Department Department of Electrical and Communications Engineering
Laboratory Power Systems and High Voltage Engineering
Field of research Power Systems
Opponents Professor Timo Vekara & Dr. Kaj Juslin
Supervisor Professor Matti Lehtonen

Abstract

The significance of harmonics in power systems has increased substantially due to the use of solid state controlled loads and other high frequency producing devices. An important consideration when evaluating the impact of harmonics is their effect on power system components and loads. Transformers are major components in power systems. The increased losses due to harmonic distortion can cause excessive winding loss and hence abnormal temperature rise.

Existing standards give a procedure to determine the capability of an existing transformer subject to non-sinusoidal load currents based on conservative assumptions. The eddy current loss generated by the electromagnetic field is assumed to vary with the square of the rms current and the square of the frequency (harmonic order *h*). Actually, due to skin effect, the electromagnetic flux may not totally penetrate the strands in the winding at high frequencies. In addition, the temperature rise due to harmonics is estimated based on constant harmonic load currents and the average daily or monthly temperatures to which a transformer would be subjected while in service.

It is the purpose of this research effort to quantify the increased winding losses due to harmonics and the corresponding temperature rise in transformers. This is accomplished using a 2-D FEM model adapted for winding loss calculation. A corrected harmonic loss factor that considers conductor skin effect is proposed and verified by measurements. Thermal dynamic models are investigated and modified to consider a time varying distorted load cycle. The increased temperature is used with an industry accepted insulation loss of life formula to evaluate a transformer's capability.

Keywords Temperature, Power Transformers, Thermal Factors, Power Quality Problems

ISBN 951-22-8077-9 | ISSN 1795-2239

ISBN 951-22-8078-7 (PDF) | ISSN 1795-4584 (PDF)

ISBN (others) | Number of pages xiv + 136 p.

Publisher Helsinki University of Technology, Power Systems and High Voltage Engineering

Print distribution Power Systems and High Voltage Engineering

The dissertation can be read at http://lib.tkk.fi/Diss/2006/isbn9512280787/

PREFACE

First and foremost thanks to God. Without his help and blessing I would not have been able to finish this work.

Then, I would like to thank my supervisor Prof. Matti Lehtonen for his encouragement and unlimited support. Thanks go to Dr. Hasse Nordman ABB Vaasa, for providing us with measured data. I would like to acknowledge my university in Libya (7^{th} of April University) for awarding me a scholarship to continue my studies.

I would also like to thank all the Libyan students in Helsinki for their support, in particular Naser for his suggestions and help. Thanks to all members of the Power Systems and High Voltage Engineering, in particular Dejan, Pirjo and John, for his help in the measurements and reviewing the language in the thesis.

Thanks to my dear wife Fatma for her patience and unlimited support. Thanks also to my Mother and Father, whose hearts are always with me and whose prayers light my way in this life.

In, Espoo, Aug. 2005
Asaad

Contents

List of Symbols and Abbreviations

$\mathbf{A}$	Magnetic vector potential
$\mathbf{B}$	Magnetic flux density
c	Empirical value typically taken equal to one
C_{th-Oil}	Top oil model thermal capacitance
C_{th-H}	Winding thermal capacitance at hot spot location
Cp	Specific heat of a material
$\mathbf{D}$	Electric flux density
d	Conductor diameter in the direction of B.
$\mathbf{E}$	Electric field strength
f	Rated frequncy
F_{AA}	Accelerated ageing factor
F_{WE}	Winding eddy current loss factor
F_{WE-x}	Winding eddy current loss factor for axial winding eddy loss component
F_{WE-r}	Winding eddy current loss factor for radial winding eddy loss component
F_{OSL}	Other stray loss factor
g	Average winding to average oil temperature rise at rated load.
H	Hot spot factor due to the increased eddy losses at the winding end.
$\mathbf{H}$	Magnetic field strength.
H_H	Per unit winding height to hot spot location
h	Harmonic order
I_h	Rms current at harmonic order h,
I_R	Rms fundamental current under rated frequency and load conditions
$I\ (pu)$	Normalised current
$\mathbf{J_S}$	Source current density
K	Load factor (supplied load/rated load)

K_W	Temperature correction for winding losses
L	Per unit load
L_F	Per unit loss factor
l	Length of the conductor in the z-direction
m	Empirically derived exponent depends on the cooling method
M	Mass of transformer component
n	Empirically derived exponent depends on the cooling method
P_{NL}	No load losses.
P_{LL}	Load Losses.
P_T	Total losses.
P_{dc}	Loss due to load current and dc winding resistance conventionally I^2R_{dc}.
P_{EC}	Winding eddy losses.
P_{OSL}	Other stray losses in clamp, tanks, etc.
P_{SL}	Total stray losses in windings and other structural parts.
P_W	Winding losses
P_{W-ave}	pu average winding losses
$P_{W-\max}$	pu winding losses at the hot spot location
$P_W(pu)$	Increased winding losses due to harmonics at the hottest spot location.
q	A harmonic number exponent of winding eddy loss.
q_{Tot}	Heat generated by total losses
q_W	Heat generated by losses at the hot spot location
R	Ratio of load losses at rated current to no load losses
R_{th-Oil}	Oil thermal resistance
R_{th-H}	Thermal resistance at the hot spot location
r	A harmonic number exponent of other stray loss.
r_0	Outer radius of the solution region in meters
T	Conductor thickness (height h or width w) perpendicular to B.

U_h	Harmonic voltage
V_q	Potential difference of conductor between conductor ends
w	Winding eddy loss as a fraction of the total stray losses at fundamental frequency.
Θ_{DAO}	Average temperature of oil in winding ducts
Θ_{DO}	Temperature of oil exiting winding ducts
Θ_{BO}	Temperature of bottom oil entering winding
Θ_H	Ultimate hot spot temperature.
Θ_W	Average winding temperature.
Θ_K	Temperature factor for resistance change with temperature; 234.5 for Copper and 225 for Aluminium.
Θ_A	Ambient temperature.
Θ_O	Average oil temperature.
Θ_{Oil}	Top oil temperature
$\Delta\Theta_{TO}$	Top oil temperature rise over ambient temperature.
$\Delta\Theta_H$	Hot spot temperature rise over top oil temperature.
Θ_{WO}	Temperature of oil in ducts at hot spot location
$\Delta\Theta_{BO}$	Bottom oil temperature rise over ambient temperature.
$\Delta\Theta_{WO}$	Oil temperature rise at winding hot spot over bottom oil
$\Delta\Theta_{HSWO}$	Winding hot spot temperature rise over oil at hot spot location
$\Delta\Theta_{DO}$	Temperature rise of oil at top of duct over bottom oil temperature
ε	Electric permittivity.
ε_0	Electric permittivity of vacuum.
ε_r	Relative electric permittivity.
μ	Permeability.
μ_0	Permeability of vacuum
μ_r	Relative permeability.
μ_w	Viscosity of oil film in ducts at instant time

σ	Electrical conductivity.
ω	Angular frequency $2\pi f$
$\xi = \frac{T}{\delta}$	Relative skin depth to strand dimension.
δ	Depth of penetration at harmonic frequency
δ_R	Depth of penetration at power frequency 50 Hz.
τ_{TO}	Top oil time rise constant.
τ_H	Hot spot rise time constant
τ_W	Winding time constant
x	Empirically derived exponent depends on the cooling method.
y	Empirically derived exponent, depends on the cooling method
z	Empirically derived exponent, depends on the cooling method

Subscripts

R	Rated
i	Initial
u	Ultimate
H	Hot spot location
pu	Per unit value

CTC	Continuously Transposed Cable
FEM	Finite Element Method
HV	High voltage
IEC	The International Electrotechnical Commission
IEEE	The Institute of Electrical and Electronics Engineers
LV	Low voltage
rms	Root mean square
THD	Total Harmonic Distortion
YNd11	Transformer connection type
2-D	Two dimensional
3-D	Three dimensional

Chapter One

Introduction

1.1 Motivation and Objectives

Harmonics and distortion in power system current and voltage waveforms have been present for decades. However, today the number of harmonic producing devices is increasing rapidly. These loads use diodes, silicon controlled rectifiers (SCR), power transistors, etc. Due to their tremendous advantages in efficiency and controllability, power electronic loads are expected to become significant in the future, and can be found at all power levels, from low-voltage appliances to high voltage converters. One result of this is a significant increase in the level of harmonics and distortion in power system networks.

This thesis deals with the effects of power system harmonics on power system transformers. The main target is transformer units in transmission substations and industrial plants.

Many transformers designed to operate at rated frequency have had their loads gradually replaced with non-linear loads that inject harmonic currents. These harmonic currents will increase losses and hence cause abnormal temperature rises which will decrease the expected lifetime. Such conditions require either transformer de-rating to return to the normal life expectancy or upgrading with a larger and more economical unit. Therefore the need for investigating the harmonic problems is obvious.

The commonly used method to predict the hot spot temperature as the sum of the ambient temperature, the top oil rise over ambient and the hot spot rise over top oil is described in the IEEE and IEC loading guides [8]-[9]. Their steady state temperature relationship is similar.

In the IEC the hot spot temperature rise is taken as the average winding temperature rise above the average oil temperature times a hot spot factor *H,* usually assumed to be 1.3 for power transformers. The average oil temperature derivation starts from the bottom oil temperature. The best method to measure the hot spot would be the direct measurement of the actual hot spot with fibre optic sensors. However, this may not be practical for existing transformers and difficulty in justifying the added costs has limited their use on new transformers. On existing transformers the most common method is to simulate the hot spot temperature. The IEC working group proposed a number of formulas for calculating the *H* factor, but no standard formula has been adopted [13].

The loading guides and recommended practices give a procedure to determine the capability of an existing transformer subject to non-sinusoidal load currents. The methodology determines a de-rated current magnitude that allows for the increased harmonics based on conservative assumptions [27]-[28].

The eddy current losses generated by the electromagnetic field are assumed to vary with the square of the rms current and the square of the frequency (harmonic order *h*). Actually, due to skin effect, the electromagnetic flux may not totally penetrate the

conductors in the winding at high frequencies. It is also assumed that the per unit eddy losses at the hot spot location are four times the average per unit eddy losses.

In practice a transformer's critical point is usually in the upper end of the windings where the conductors are exposed to an inclined magnetic field with two components, an axial component and a radial component. The eddy current losses are the contribution of these two components. The conductor dimensions are found to vary in a wide range. This situation requires a more precise prediction when a transformer is subject to non-sinusoidal load current. A corrected harmonic loss factor to predict transformer capability when subject to non-sinusoidal load current is presented in [30] as a more accurate estimate. A similar factor is proposed as an alternative method for calculating the winding eddy loss enhancement factor [27].

The increased transformer temperatures due to harmonics are estimated based on constant harmonic load currents with average daily or monthly temperatures. Transformer loading generally changes with time as does the ambient temperature. A transformer may operate far below rated load followed by a short period where the rated load is exceeded. An accurate and applicable method is needed to estimate the effect of harmonics on the transformer temperatures and hence the transformer loss of life. Such a method should consider the actual distorted load cycle and temperature variation to which a transformer would be subjected while in service.

It should be noted that there is no universal agreement on a "correct" thermal dynamic model. The commonly used transient equations are reported in the IEC and IEEE loading guides [8]-[9]. The IEEE model does not properly account for variations in ambient temperature, which is conservative, and an improved top oil model is proposed in [42]. The ambient temperature is included in the top oil rise model where it allows the top oil temperature to respond dynamically to changes in ambient temperature. A few techniques have been developed to consider the effect of harmonics based on the existing loading guides [39], [48]-[49].

In Annex G of the IEEE loading guide, [9] and [41], a more rigorous method is suggested. The equations require the use of bottom oil temperature rise over ambient at rated conditions. Duct oil temperature is introduced, which may be higher than the top oil temperature under certain conditions, leading to a more accurate hot spot temperature located at some point in the winding duct. The improved equations consider liquid type, cooling mode, resistance and fluid viscosity changes with temperature and ambient temperature, and load changes during a load cycle. The temperature equations are based on the conservation of energy over any time interval Δt. Over such an interval, there must be a balance between all energy changes in Joules. At each step new calculated temperature values are added to the old values. The equations are programmed in Basic as documented in [9] and [41]. The total winding loss figure is used in the hot spot equation calculation [41] and only the losses due to the dc resistance for a test winding [40]. The winding eddy and other stray losses are separated from the losses due to winding resistance in the equations to permit a future consideration of oil and winding effects due to the increased losses when harmonic currents are present.

A thermal model in the form of an equivalent circuit based on the fundamentals of heat transfer theory was proposed by Swift in [44]. The proposed thermal model was established to determine the hot spot temperature. The top oil temperature is calculated from the oil-to-air model. The top oil temperature becomes the ambient temperature for the winding-to-oil model. The top oil model was validated using data from a 250 MVA transformer in the field [45].

It is the objective of this research to accurately estimate the increased transformer losses and temperature due to harmonic load currents. A FEM (finite element method) model is adapted to estimate the losses in each turn/disc to determine the hot spot temperature. A corrected loss factor which considers skin effect is proposed and verified experimentally. A thermal model which considers a time varying load and temperature is developed and verified by factory measurements. The hot spot temperature is used to evaluate a transformer loss of life based on an industry accepted formula.

1.2 Contributions

The main contributions of this thesis can be summarised as follows:

- A FEM model is adapted and used to predict transformer winding losses. Knowledge of the flux density is used with the appropriate conductor dimensions to predict the eddy losses for a specific design. The model can be used to locate the winding hot spot location, to predict the eddy losses in an individual turn/disc, and to calculate the hot spot factor *H*. Such information is very important for winding hot spot determination.

- A corrected eddy current loss factor is derived that considers the field penetration in the conductor due to skin effect. The factor can be applied to more accurately predict the increased losses due to harmonics and hence the temperature rise. The factor is verified experimentally.

- The hot spot equation in Annex G of the IEEE loading guide is modified using the calculated winding losses that cause the hot spot. The thermal dynamic model is also modified to consider distorted load cycle variation.

- The winding-to-oil model proposed by Swift is developed to predict the hot spot temperature based on loading, oil temperature and the estimated losses that cause a winding hot spot. The thermal dynamic model is also modified to consider distorted load cycle variation. The loss of insulation life function is developed to be used to assess a transformer loading capability.

1.3 Outline of the thesis

Transformer losses and temperature rises are reviewed in chapter 2. In chapter 3 the concepts necessary for understanding the modelling of transformers by numerical simulation of the relevant fields by FEM is presented. An adapted transformer simulation model, field solution and loss calculation are explained in chapter 4. A corrected eddy loss factor developed to predict the transformer losses and the steady state temperature for any harmonic spectrum is presented in chapter 5. Chapter 6 re-examines and reviews the applicability of the existing thermal dynamic models used within transformers. Chapter 7 presents the thermal models in the presence of a distorted varying load cycle. A test setup and results to validate the corrected loss factor is presented in Appendix I. Appendix II gives the input data used in finite element method (FEM). Details of the simulink models can be found in Appendix III.

Chapter Two

Transformer Losses and Temperature Rise

Stray losses can be particularly high in power transformers with large ratings. Transformer designers today are challenged by high loss evaluation, high reliability requirements, and low cost and weight requirements, for which they need advanced techniques and tools that lead to optimum design and product performance improvements. Among the most important of these calculations and techniques are those for winding eddy losses, stray losses in other structural parts and, in general, potential regions of excessive heating. All of these can be determined by the strength of the electromagnetic leakage field of the transformer winding. This chapter reviews transformer losses and the calculation of transformer temperature rise. It also presents transformer winding eddy current losses from the point of view of their estimation. Such information is important for winding hot spot calculation.

2.1 Transformer losses

Transformer losses are generally classified into no load or core losses and load losses as shown in Fig 2.1.

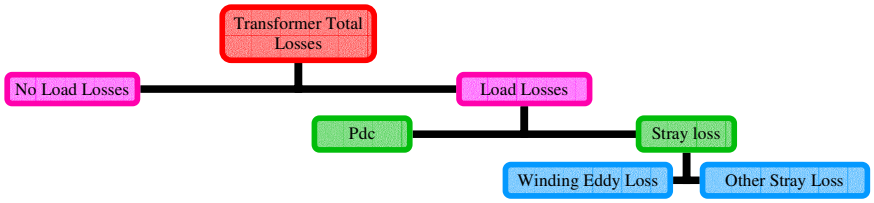

Fig. 2.1 Transformer loss classification

This can be expressed in equation form:

$$P_T = P_{NL} + P_{LL} \qquad (W) \tag{2.1}$$

where,

P_{NL} are the no load losses.

P_{LL} are the load losses.

P_T are the total losses.

P_{NL} are the losses due to the voltage excitation of the core. P_{LL} is, in accordance with convention, subdivided into P_{dc} losses (I^2R_{dc}) and stray losses caused by electromagnetic fields in the windings, core clamps, magnetic shields, enclosure or tank walls, etc. P_{dc} is calculated by measuring the dc resistance of the winding and multiplying it by the square of the load current. The stray losses can be further divided into winding eddy losses and structural part stray losses. Winding eddy losses consist of eddy current losses and circulating current losses, which are all considered to be winding eddy current losses. Other stray losses are due to losses in structures other than windings, such as clamps, tank or enclosure walls, etc.; this can be expressed as:

$$P_{LL} = P_{dc} + P_{EC} + P_{OSL} \qquad (W) \tag{2.2}$$

where,

P_{dc} are the losses due to load current and dc winding resistance.

P_{EC} are the winding eddy losses.

P_{OSL} are other stray losses in clamps, tanks, etc.

The total stray losses P_{SL} are determined by subtracting P_{dc} from the load losses measured during the impedance test, i.e.:

$$P_{SL} = P_{EC} + P_{OSL} = P_{LL} - P_{dc} \qquad (W) \tag{2.3}$$

There is no test method to distinguish the winding eddy losses from the stray losses that occur in structural parts.

2.2 Structure of core type transformers

Core type power transformers have high voltage HV and low voltage LV windings as concentric cylinders surrounding a vertical core leg of rectangular or circular cross-section. Oil immersed transformers are contained within a steel tank. Fig. 2.2 shows the top view of a core type transformer.

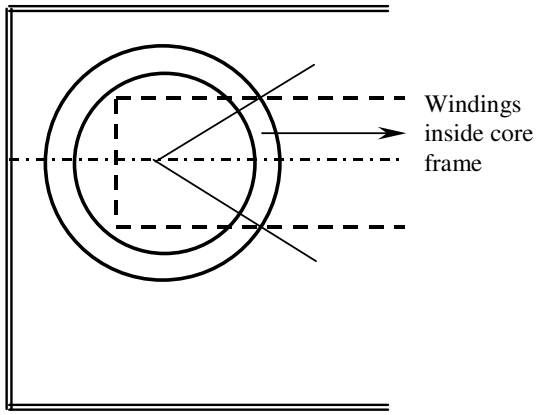

Fig. 2.2 Top view of a core type transformer

The main parts of a transformer, which are subject to leakage flux, are illustrated in Fig 2.3.

- The magnetic circuit, i.e. the iron core.
- The primary, secondary and regulating winding.
- The yoke clamps.
- The flitch plate.
- The tank and the tank shields (shunts).

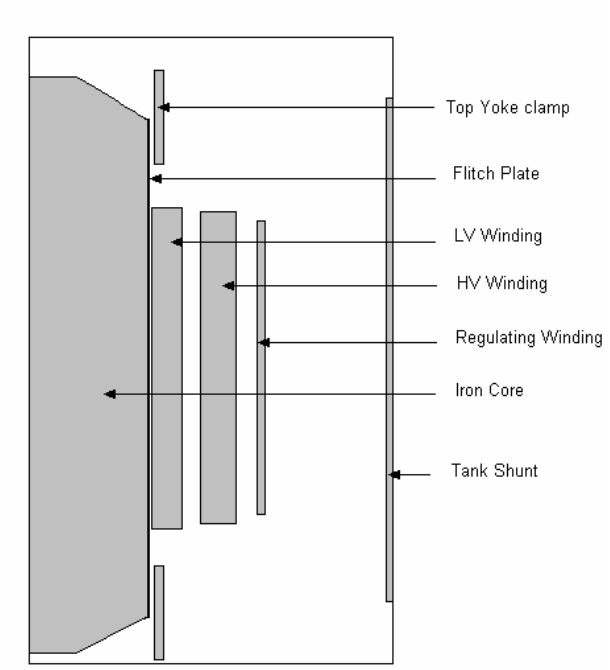

Fig. 2.3 A 2-D transformer cross-section illustrates essential parts subject to leakage flux

As mentioned in the previous section, the stray flux has the effect of creating eddy current losses within the windings. The eddy current losses are concentrated in the end discs due to the radial flux. Flux shunts can be used to divert the flux to avoid too large radial components.

On high-current transformers, it is also the case that the generated stray flux can give rise to eddy current losses in the tank. In this situation a reduction in the magnitude of losses can be obtained by the provision of a flux shunt or shields to prevent currents flowing in the tank. This will prevent an excessive temperature

rise in the tank. The flux shunts will themselves experience losses but they are usually arranged to operate at modest flux density and, like the core, are laminated. The stray flux departing radially through the inner surface of the winding hits the core and fittings such as the flitch plate mounted in the core for holding the core lamination together vertically. Although the losses occurring in the flitch plate may not form a significant part of total transformer losses, the loss density may attain local levels that may lead to high local temperature if the material and type of flitch plate is not selected properly.

A thorough knowledge of the leakage flux is necessary to define the local stray losses that cause local hot spots. Due to the fact that transformer loading is based on the winding hot spot temperature, the winding losses are the most critical stray loss component.

2.3 A review of winding stray loss evaluation in transformers

Many references [3]-[4] on basic eddy current theory have tried to make eddy current analysis understandable and practically applicable for solving complex engineering problems. These references still give a foundation to researchers for analysis of the various stray loss components.

2.3.1 Winding eddy current loss

2-D FEM is the most commonly used numerical technique to compute winding eddy losses. Knowledge of the flux density distribution in the windings can be used in choosing the proper axial and radial conductor dimensions. Continuously transposed conductors (CTC) can be used in large power transformers with smaller axial and radial dimensions to minimise the eddy losses in the low voltage winding. The eddy losses in individual turns/discs must be accurately estimated to calculate the hottest spot in the transformer, which is generally located at the top of the windings.

Anderson [5] developed a leakage flux program based on a simple form of the finite element method and used it to calculate the eddy current losses in the windings due to the axial and radial flux components. Komulainen and Nordman [6] used 2-D

FEM to get a magneto-static solution for loss calculation. Pavlik et al. [7] have approximated leakage flux using a series of 2-D FEM solutions to investigate the contribution of different loss components. The authors studied the impact of magnetic eddy current shields, placed to cover the tank wall, on the other stray loss components, such as flitch plates, core edges and windings.

Analysis of winding eddy losses by 3-D FEM would be more accurate, however, the computation cost and complexity would increase. In practice, a reduction to 2-D based on construction symmetry is possible without significant loss of accuracy.

2.3.2 Circulating current losses

Losses due to circulating currents in the windings are caused by differences in the value of the leakage field linking the parallel strands. It is clear that circulating current losses depend strongly on the physical location of each strand in the leakage field. The losses can be avoided if the location of each conductor is linked with an equal amount of leakage flux. Circulating currents can be reduced to a negligibly small value by continuous transposition or by employing a number of transpositions at pre-determined intervals along the winding height.

2.4 Transformer loading guides

The most common model used for top oil and hot spot temperature calculations is described in the IEC 354 Loading Guide for oil immersed transformers [8]. A simplified temperature distribution in a transformer is shown in Fig. 2.4. This diagram is based on the following assumptions:

- The oil temperature inside and along the windings increases linearly from bottom to top.
- The winding temperature increases linearly from bottom to top, with a constant temperature difference *g*.

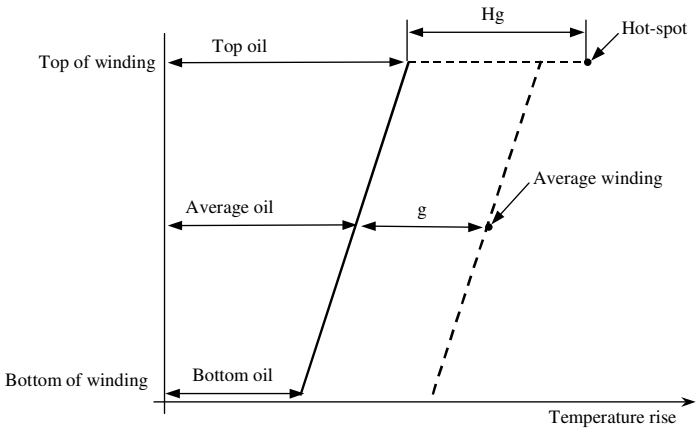

Fig. 2.4 Transformer thermal diagram according to IEC 354

- The hot spot temperature rise at the top of the winding is higher than the average temperature rise of the winding. To consider non-linearities such as the increase in stray losses at the top of the winding, the difference in temperature between the hot spot and the oil at the top of the winding is defined as *Hg*. The hot spot factor *H* may vary from 1.1 to 1.5, depending on the transformer size, short circuit impedance and winding design.

The steady state temperature relations in IEEE [9] are similar to Fig 2.4 from the IEC loading guide.

The ultimate hot spot temperature for a transformer under any load *K* is equal to the sum of the ambient temperature, the top oil temperature rise over ambient and the hot spot temperature rise over top oil. This can be expressed by the equation below:

$$\Theta_H = \Theta_A + \Delta\Theta_{TO} + \Delta\Theta_H \tag{2.4}$$

where

Θ_A is the ambient temperature, °C.

$\Delta\Theta_{TO}$ is the oil temperature rise over ambient, °C.

$\Delta\Theta_H$ is the hot spot temperature rise over top oil temperature, °C.

Θ_H is the ultimate hot spot temperature, °C.

The top oil temperature rise over ambient temperature is given by the following equation:

$$\Delta\Theta_{TO} = \Delta\Theta_{TO-R}\left(\frac{1+R\cdot K^2}{1+R}\right)^n \tag{2.5}$$

where

$\Delta\Theta_{TO-R}$ is the top oil temperature rise over ambient at rated load.

R is the ratio of load losses at rated current to no load losses

K is the load factor (supplied load/rated load)

n is an empirically derived exponent that depends on the cooling method

The hot spot temperature rise over top oil temperature is given by :

$$\Delta\Theta_H = H\cdot g\ \cdot K^{2m} \tag{2.6}$$

where

$\Delta\Theta_H$ is the hot spot to top oil rise.

H is the hot spot factor due to the increased eddy losses at the winding end.

g is the average winding to average oil temperature rise at rated load.

m is an empirically derived exponent that depends on the cooling method

The suggested exponents n and m define the non-linearity and depend on the transformer cooling method. The four modes of cooling used are: natural convection of oil in the transformer and natural convection of cooling air over the radiators (OA/ONAN), natural convection of oil with forced convection of air over the radiators (FA/ONAF), non-directed forced oil flow and forced air flow (NDFOA/OFAF) and directed forced oil flow and forced air flow (DFOA/ODAF). The exponents used are:

Table 2.1 Exponents used in temperature calculation equations

Type of Cooling	IEC		IEEE	
	n	m	n	m
OA/ONAN	0.9	0.8	0.8	0.8
FA/ONAF	0.9	0.8	0.9	0.8
NDFOA/OFAF	1.0	0.8	0.9	0.8
DFOA/ODAF	1.0	1.0	1.0	1.0

2.5 Determination of the hot spot factor *H*

A standard thermal test to measure the average temperature rise does not simulate the additional losses due to the high eddy currents in the end windings. These losses are covered by the hot spot factor in order to calculate the ultimate hot spot temperature. CIGRE Working Group 12-09 [11] analysed data collected during detailed tests to quantify the *H* factor used in the IEC loading guide. A statistical analysis of these data showed that the value of this factor is distributed between 1 and 1.5. A typical value of 1.1 has been given for distribution transformers and 1.3 for medium size and large transformers. IEC 76-2 [12] states that the hot spot factor varies considerably in large power transformers depending on design and that the manufacturer should be consulted for information unless actual measurements have been made.

Direct hot spot temperature measurements indicate that the range of variation is between 1.1 to 2.2 and *H* does not represent a constant. The *H* factor should be predicted correctly for a specific transformer design due to the fact that an unrealistically high value will penalise the user in determining loading capability while an unrealistically low value understates the ultimate winding hottest spot temperature.

2.5.1 Analytical determination of the winding hot-spot factor *H*

The working group 12-09 [13] proposed a number of formulas for calculating the hot-spot factor *H* to explain the range of variation and to predict its value when designing a specific transformer. However, no standard formula has been adopted.

2.5.2 Determination of winding hot-spot temperature by direct measurement

Direct temperature measurement techniques using fibre optic sensors are currently available and are in use in some large power transformers. Ideally, the best method is to directly measure the winding hot spot temperature through a fibre optic sensor. This may not be practical for existing transformers and may be difficult to justify in terms of cost for new transformers.

These devices are capable of indicating the temperature only at the spots where sensors are located. The proper choice of location for the sensors in the transformer windings is crucial to accurately determine the hottest spot temperature. Therefore, their accuracy in measuring the winding hottest spot is dependent on the ability to predict the hottest spot location prior to the sensors' placement. However, even with these disadvantages, many consider fibre optic sensors the best tool available for measuring winding hot spot temperatures. The working group 12-09 survey [14] suggests that eight sensors would be adequate if placed in the winding locations where the highest temperatures are expected.

Chapter three

Modeling and Simulation of Electromagnetic Fields

The notation and basic laws of electric and magnetic fields are explained in this chapter. Furthermore, that which is necessary to understand in the modelling of devices by numerical simulation of such fields by FEM is presented.

3.1 Electromagnetic fields

The fundamental physical equations for electromagnetic field calculations are the Maxwell equations:

$$\nabla \times \mathbf{E} = \frac{-\partial \mathbf{B}}{\partial t} \tag{3.1}$$

$$\nabla \times \mathbf{H} = \mathbf{J} + \frac{\partial \mathbf{D}}{\partial t} \tag{3.2}$$

$$\nabla \cdot \mathbf{B} = 0 \tag{3.3}$$

where,

E is the electric field strength

B is the magnetic flux density.

H is the magnetic field strength.

J is the current density

D is the electric flux density

Constitutive relations between the different field vectors are as follows

$$\mathbf{B} = \mu\mathbf{H} = \mu_0\mu_r\mathbf{H} \tag{3.4}$$

$$\mathbf{J} = \sigma\mathbf{E} \tag{3.5}$$

$$\mathbf{D} = \varepsilon\mathbf{E} = \varepsilon_0\varepsilon_r\mathbf{E} \tag{3.6}$$

where

ε is the electric permittivity

ε_0 is the permittivity of a vacuum

ε_r is the relative permittivity

μ is the permeability

μ_0 is the permeability of a vacuum

μ_r is the relative permeability.

σ is the electrical conductivity

3.2 Magnetic vector potential formulation

Maxwell's equations are not solved directly. They are usually solved by combining equations to eliminate variables, using potential functions from which the field can be derived and seeking simplifying assumptions valid for the particular problem. The proper choice of a potential depends on the type of field problem. The magnetic vector potential is commonly used in the solution of 2-D magnetic fields.

In a 2-D field the vector potential **A** and the current density have only a *z* component when the magnetic field is in the *x-y* plane. In the axi-symmetric case **A** and the current density have only ϕ components and the magnetic field is in the *r-z* plane.

$$(0,0,A_Z)\ or\ (0,0,A_\phi) = \mathbf{A}$$

$$(0,0,J_Z)\ or\ (0,0,J_\phi) = \mathbf{J}$$

$$(B_x,B_y,0)\ or\ (B_r,B_z,0) = \mathbf{B}$$

The magnetic vector potential **A** is defined as the curl of the magnetic flux density **B**.

$$\nabla \times \mathbf{A} = \mathbf{B} \tag{3.7}$$

According to equation (3.3)

$$\nabla \cdot (\nabla \times \mathbf{A}) = 0$$

The displacement current is usually omitted from the equation for electrical devices operated at low frequency. Hence, a magneto-static problem can be described using equation (3.2)

$$\nabla \times (\frac{1}{\mu} \nabla \times \mathbf{A}) = \mathbf{J} \tag{3.8}$$

A vector calculus identity can be used to simplify the above equation.

$$\nabla \times (\nabla \times A) = \nabla(\nabla \cdot \mathbf{A}) - \nabla^2 \mathbf{A} \tag{3.9}$$

Substituting (3.9) into (3.8) leads to the formulation of the magneto-static field

$$\frac{1}{\mu} \nabla^2 \mathbf{A} = -\mathbf{J} \tag{3.10}$$

where, in order to define the vector field **A** uniquely, a Coulomb gauge is used

$$\nabla \cdot \mathbf{A} = 0 \tag{3.11}$$

This is the magneto-vector potential formulation of the magneto-static fields.

To consider quasi-static fields for eddy current calculations, a magneto-dynamic formulation is to be used. Equation (3.1) is used in addition to equation (3.7)

$$\nabla \times \mathbf{E} = \frac{-\partial \mathbf{B}}{\partial t} = -\frac{\partial (\nabla \times \mathbf{A})}{\partial t} = -\nabla \times \frac{\partial \mathbf{A}}{\partial t} \tag{3.12}$$

Rearranging equation (3.12) and introducing the magnetic scalar potential function ϕ yields

$$\nabla \times \left[\mathbf{E} + \frac{\partial \mathbf{A}}{\partial t} \right] = 0 = -\nabla \times \nabla \phi \tag{3.13}$$

Equation (3.13) can be reduced as follows:

$$\mathbf{E} + \frac{\partial \mathbf{A}}{\partial t} = -\nabla \phi \tag{3.14}$$

Using equation (3.5) we get the current density *J* as:

$$\mathbf{J} = -\sigma \frac{\partial \mathbf{A}}{\partial t} - \sigma \nabla \phi \tag{3.15}$$

Using equations (3.8) and (3.15) yields a formulation of the quasi-static field in the time domain

$$\nabla \times (\frac{1}{\mu} \nabla \times \mathbf{A}) = -\sigma \frac{\partial \mathbf{A}}{\partial t} - \sigma \nabla \phi \tag{3.16}$$

Using vector calculus (3.16) is then reduced to

$$-\nabla . (\frac{1}{\mu} \nabla \mathbf{A}) + \sigma \frac{\partial \mathbf{A}}{\partial t} = \sigma \nabla \phi = \mathbf{J_s} \tag{3.17}$$

The scalar potential can be used to describe an external voltage or current in a conductor.

$$-\nabla \cdot (\frac{1}{\mu}\nabla \mathbf{A}) + \sigma \frac{\partial \mathbf{A}}{\partial t} = \sigma \frac{\mathbf{V}}{\ell} = \mathbf{J_s} \tag{3.18}$$

In order to solve this equation, a time discretisation in addition to spatial discretisation must be performed. A time stepping technique has to be used. However, this equation can be simplified assuming sinusoidal field variation at angular frequency ω or using phasor representation. Thus

$$\frac{\partial}{\partial t} A = j\omega A$$

Substituting the above into equation (3.18) yields an equation that describes the time harmonic problem:

$$-\nabla \cdot (\frac{1}{\mu}\nabla \mathbf{A}) + j\omega\sigma \mathbf{A} = \sigma \frac{\mathbf{V}}{\ell} = \mathbf{J_s} \tag{3.19}$$

3.2.1 Magnetic field solution using FEM

The fundamental idea behind the finite element method is to subdivide the region to be studied into small sub-regions called finite elements. The field variable is approximated in each finite element by a simple function, usually a polynomial. The coefficients of the polynomials are chosen in such a way that a variational principle (e.g. the minimisation of the field energy) is approximately satisfied [15].

3.2.2 Boundary conditions

Boundary conditions are necessary to make the boundary value problem a well posed problem with a unique solution. Dirichlet and Neuman boundary conditions must be applied in an appropriate way to reduce the size of the problem significantly. FEM programs are limited in terms of the number of elements available to approximate the geometry of the problem. The correct and appropriate application of the boundary conditions is therefore the key to define the problem and arrive at an accurate solution in an efficient way.

Dirichlet boundary condition

The value of the vector potential is defined on the boundary of the problem.

$$A = A_0$$

This is mainly applied in its homogenous form A= 0 keeping the flux from crossing the boundary.

The non-homogenous Dirichlet boundary can be used to force a prescribed flux between two boundaries by the following equation, assuming no flux variation in the z-direction [16].

$$\phi = \int_s B \cdot ds = \oint_l A \cdot dl = L(A_2 - A_1)$$

where,

L is the distance between the two boundaries

Neuman boundary condition.

This boundary condition specifies the normal derivative of A along the boundary. The homogenous form, where the field is perpendicular to the boundary, is the most common.

$$\frac{\partial A}{\partial n} = 0$$

Open boundary condition

This boundary condition can be applied to approximate an unbounded solution region [17].

$$\frac{1}{\mu}\frac{\partial A}{\partial n} + \frac{c}{\mu_0 r_0} A = 0$$

where

c is a constant which is set equal to one

r_0 is the outer radius of the solution region in meters

3.2.3 An example of solving a problem using FEM

Consider the magneto-static linear homogeneous equation

$$\nabla^2 \mathbf{A} = -\mu_0 \mathbf{J}$$

The corresponding energy minimum functional is

$$F(A)=\frac{1}{2}\int_{\Omega}(|\nabla A|^2-2\mu_0 JA)d\Omega \tag{3.20}$$

The vector potential is approximated by the linear shape function:

$$A=a+bx+cy$$

The coefficients a, b and c are found from the values of the magnetic vector potential A_1, A_2 and A_3 at the three nodes of an element Fig.3.1

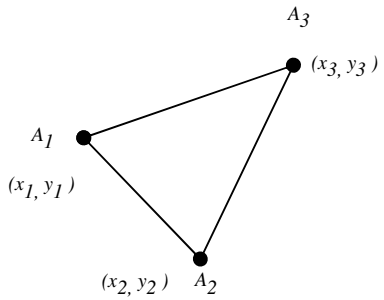

Fig 3.1 Triangular finite element

The magnetic vector potential within an element is:

$$A=\begin{bmatrix}1 & x & y\end{bmatrix}\begin{bmatrix}1 & x_1 & y_1\\ 1 & x_2 & y_2\\ 1 & x_3 & y_3\end{bmatrix}^{-1}\begin{bmatrix}A_1\\ A_2\\ A_3\end{bmatrix}$$

Using shape functions, the magnetic vector potential is approximated by:

$$A=\sum_{i=1}^{3}A_i N_i(x,y)$$

where

$$N_1=\frac{1}{2\Delta^e}\left[(x_2y_3-x_3y_2)+(y_2-y_3)x+(x_3-x_2)y)\right]$$

$$N_i=\frac{1}{2\Delta^e}\left[a_i+b_ix+c_iy)\right]$$

where

Δ^e is the area of an element

The shape functions are one at one node and zero at both other nodes.

$$N_i(x_j, y_j) = \begin{cases} 0 & i \neq j \\ 1 & i = j \end{cases}$$

The first term of equation (3.20) is a 3x3 element matrix *S*

$$S_{ij}^e = \frac{1}{4\Delta^e}(b_i b_j + c_i c_j) \tag{3.21}$$

This is the stiffness matrix associated with one element

The second term is

$$\int_{\Delta^e} J_0^{(e)} \mu_0 A d\Omega = \mu_0 \sum_{i=1}^{i=3} J_0^{(e)} A_i N_i = \mu_0 \sum_{i=1}^{i=3} J_0^{(e)} A_i \frac{\Delta^e}{3}$$

$$T_i^{(e)} = \mu_0 J_0^{(e)} \frac{\Delta^e}{3} \tag{3.22}$$

where
$T_i^{(e)}$ is the source vector function with one element

The contribution of one element to the energy functional can be written in matrix form

$$F^{(e)}(A) = \frac{1}{2} A^T S^{(e)} A - A^T T^{(e)}$$

The overall functional of the problem is the sum of the functionals of all elements

$$F(A) = \sum F^{(e)}(A)$$

The system of linear equations is obtained by forcing the partial derivative with respect to the nodal potentials to zero. This is the minimisation of the energy functional.

$$\frac{\partial F(A)}{\partial A_i} = 0 \qquad i = 1, ..., n$$

$$S\ A = T$$

The matrices *S* and *T* are obtained by summing the contribution of the individual elements. This is a system of linear equations and the solution of this system provides the distribution of the magnetic vector potential through the domain.

3.3 Time harmonic problem

In principal, time harmonic eddy current/skin effect analysis is facilitated by solving the harmonic equation:

$$-\nabla \cdot \left(\mu^{-1} \nabla \mathbf{A}\right) + j\omega\sigma \mathbf{A} = \mathbf{J_s}$$

where,

J_s is the source current density

3.3.1 The source term modelling

Stranded Conductors

For regions without eddy current (stranded conductors) σ = 0 and the source vector is:

$$\mathbf{J_s} = J_0$$

where

J_0 is the applied current density

Transformer winding turns may consist of a number of conductors connected in parallel. The eddy currents caused by internal currents can be neglected at the relevant frequency. For this case the source vector can be written in terms of the current per strand or turn for stranded conductor *p* [16].

$$J_0 = \frac{N_{t,p}}{\Delta_{str,p}} I_{str,p} \tag{3.23}$$

where,

$N_{t,p}$ is the number of turns of the winding or strands of conductor *p*.

$\Delta_{str,p}$ is the area of the stranded conductor in the FEM mesh

Solid conductors or foil (sheet) winding

When skin effect is significant, individual conductors have to be modelled [16].

$$J_s = \frac{\sigma}{\ell} V_q \tag{3.24}$$

where,

l is the length of the conductor in the z-direction

V_q is the potential difference between the ends of the conductor

For sheet-wound (foil) windings where several conductors carry identical total currents a circuit constraint is often needed, which complicates the solution. The total current density in the conductor is given by

$$J = J_s - j\omega\sigma\mathbf{A} \tag{3.25}$$

The quantity specified by design engineers is the surface integral of J over each conductor cross-section, i.e. the total current I flowing in each conductor.

$$I = \iint J_s ds - j\omega\sigma \iint \mathbf{A} ds \tag{3.26}$$

Different techniques are cited in the literature to solve the problem. First, Konard [18] substituted the source current density into the time harmonic equation, which yields the integrodifferential equation with A as the unknown variable and I as the forcing function.

$$\nabla \cdot (\mu^{-1} \nabla \mathbf{A}) - j\omega\sigma\mathbf{A} + j\omega \frac{\sigma}{a} \iint \mathbf{A} ds = -\frac{I}{a} \tag{3.27}$$

where

a is the area of the conductor cross-section

In another form, Weiss and Csendes [19] solved the time harmonic equation in one step with a symmetric matrix containing two unknowns, $\mathbf{A}$ and $\mathbf{J_s}$.

$$\begin{bmatrix} -\nabla\cdot\frac{1}{\mu}\nabla + j\omega\sigma & -j\omega\sigma \\ -j\omega\sigma & j\omega\sigma \end{bmatrix}\begin{bmatrix} \mathbf{A} \\ G \end{bmatrix} = \begin{bmatrix} 0 \\ I \end{bmatrix} \tag{3.28}$$

where,

$$G = \frac{\mathbf{J}_s}{j\omega\sigma}$$

And finally, Konard et. al. [20] used the superposition method and assumed that one can find a finite element solution of the time harmonic equation if J_s is given.

3.4 Loss computation using FEM

Transformer turns usually consist of copper conductors in the shape of small rectangular strands. These strands are immersed in an alternating magnetic field as shown in Fig. 3.2. The losses are found from a magneto-static solution in which the eddy current region is given zero conductivity. The strand dimensions are small compared to the skin depth and the strands are frequently transposed. To a good approximation, the current density is uniform.

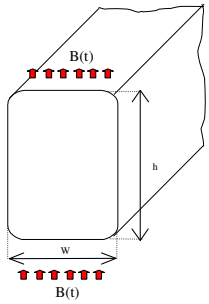

Fig. 3.2 A conductor strand subject to axial and radial components of the magnetic field

The FEM solution gives the familiar leakage flux over the windings. Using the local value of the flux density from the field solution, the eddy current for each strand is obtained using the formula valid for strand dimensions that are small compared to skin depth [21]:

$$P_{EC} \simeq \frac{\pi^2 f^2 T^2 B^2}{3\rho} \quad \mathrm{W/m^3} \tag{3.29}$$

While for round conductors where diameter d is small compared to the skin depth,

$$P_{EC} \simeq \frac{\pi^2 f^2 d^2 B^2}{4\rho} \quad \text{W/m}^3 \tag{3.30}$$

where,

B is the rms value of the magnetic flux density.

T is the conductor thickness (height h or width w) in the direction of B.

d is the conductor diameter in the direction of B.

ρ is the conductor resistivity.

It should be noted that the eddy losses are proportional to the square of the frequency and strand dimension. The eddy losses are predicted based on the assumption that eddy currents do not affect the impinging field. This is only the eddy loss component. The losses due to the current and dc resistance must be added and integrated and corrected over the winding to obtain the losses per unit length, i.e., in the post-processing, the losses are determined by adding the loss integrals of the finite elements.

$$P_W = P_{dc} + P_{EC} \quad \text{W/m}^3 \tag{3.31}$$

$$P_W = \iint_A \left(P_{dc} + P_{EC}\right) dA = \sum_e q_e = \sum_e \left(\rho J^2 + P_{EC}\right) \Omega_e \quad \text{W/m} \tag{3.32}$$

where

q_e are the loss integrals of the finite elements e

The loss density for a conductor modelled with the eddy current term included can be calculated as follows [18]:

$$P_W = \frac{\left|J^2\right|}{\sigma} \quad \text{W/m}^3$$

where the total current density may be evaluated from (3.25),

$$J = J_s + J_e = \frac{I_s}{a} - j\omega\sigma\mathbf{A}$$

The losses per unit length of conductor are obtained by integrating the losses over the cross-section

$$P_W = \iint_A \frac{\left|J\right|^2}{\sigma} dA \quad \text{W/m}$$

Chapter Four

Transformer Simulation Model

Analysis of the winding eddy losses by 3-D FEM would be more accurate, however the computation cost and complexity would increase. Fortunately, in many cases a reduction to 2-D is possible without significant loss of accuracy. The 2-D finite element method is the most commonly used method to compute eddy losses. Utilising transformer symmetry, half of the transformer is modelled instead of the full height. High order elements have been used for more accurate field solution. All the transformers have been simulated using axi-symmetric (r-z) and plane (x-y) solutions. It was observed that the solution remains almost unchanged. The appropriate solution was applied for different 2-D cross-sections.

4.1 Transformer FEM model

The main parts of a transformer in a 2-D model are the windings, core clamps, tank shunts and walls.

The windings: the most delicate part of the model since the loss computation needs to be accurately determined. For windings in which the conductors are small strands, i.e. smaller than skin depth, the skin effect can be neglected. In such a model currents

simply appear as a given source current density in the right hand side of equation (3.19). The windings were modelled with the conductors occupying the area that in reality is covered by insulation. The increased conductor size was then corrected by appropriate factors in the loss calculation. The insulation could have been modelled but this would have increased the number of elements used, i.e. a very dense mesh would have been required, which is not justified. Fortunately, the insulation does not have a significant effect on the losses.

The iron core: only half of the core width is modelled with linear isotropic permeability. The edge of the core is taken to be the axis of symmetry with zero magnetic potential.

Tank walls or shields: Magnetic or electrical conductor materials can be included in the model.

Specific knowledge of the leakage magnetic flux, and the conductors shape and their placement in the field is needed to evaluate the eddy losses due to stray magnetic flux. A 2-D simulation model was adapted to simulate the field based on data obtained in the short circuit test; the easiest way is to apply rated currents.

4.2 FEM analysis and results

In this work a transformer model was adapted using the FEM analysis software FEMLAB [22]. The FEM analysis was carried out on different industrial transformers to estimate the winding eddy current losses. Circulating current losses in CTC or properly transposed windings is small and their contribution to the eddy current loss was considered negligible.

4.2.1 Transformer field solution

Fig 4.1 shows the field solution of a 31.5 MVA, 115/6.3 kV transformer. The leakage flux in the windings flows axially up through the coils and then bends radially across the windings. From Fig 4.2 it can be seen that the component of the leakage flux has its greatest concentration at the interface between the two windings and then decreases progressing away from the gap between the windings. The inner LV winding typically has a higher attraction of the leakage flux due to the high

permeance of the core. The leakage flux in the HV winding is divided between the core and the core clamps and other structural parts [23].

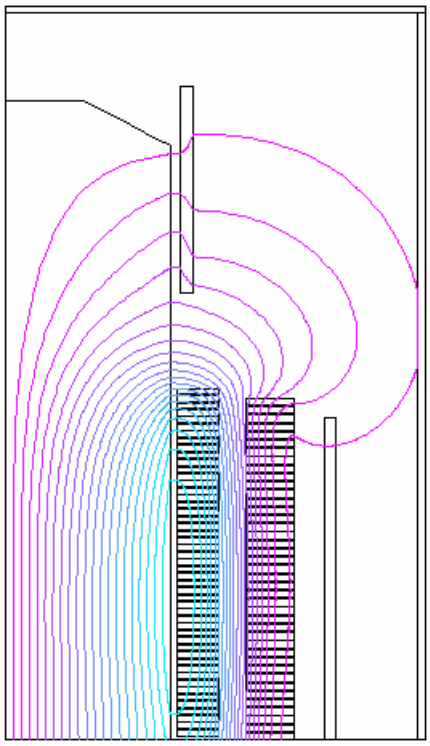

Fig.4.1 Transformer field solution in plane (x,y)

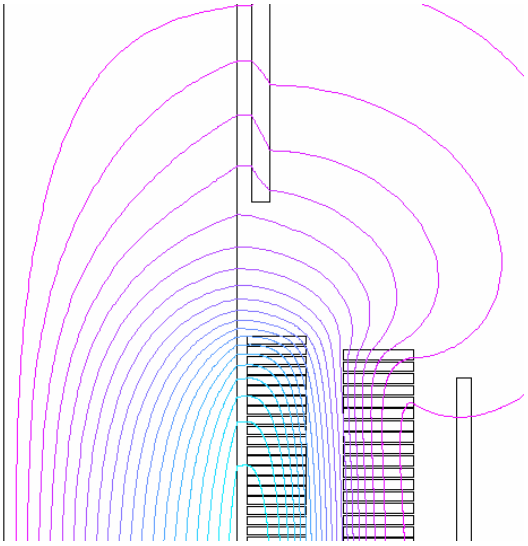

Fig. 4.2 Detailed transformer field solution

In the upper end of the windings, the conductors are exposed to an inclined magnetic field with two components, an axial component and a radial component. The eddy current loss is the contribution of these two components. Fig. 4.3 shows the axial and radial flux components distributed over the transformer windings, as post-processed from FEM analysis.

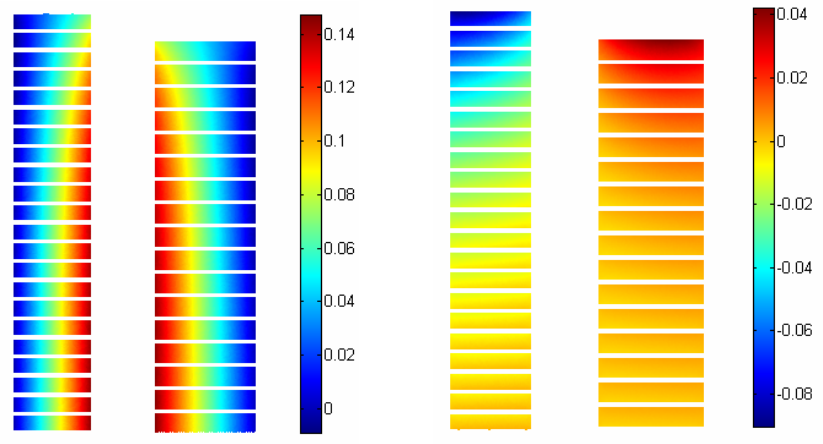

Fig. 4.3 Axial (left) and radial (right) flux density distributed over the transformer windings

Similar leakage flux distribution over the transformer windings has been observed for different 2-D projections. Fig. 4.4 shows the leakage flux for the windings inside the core.

Fig. 4.4 Stray field pattern for windings inside the core

4.2.2 Winding loss computation

Since the eddy current term is neglected, the contribution of eddy currents is generated by the leakage flux that penetrates the winding, but does not have a significant effect on the impinging field as long as the size of the strands is smaller than the skin depth. Each strand is subject to two components of flux density normal to its sides, which produces eddy currents. For each component the eddy current loss is obtained using equation (3.29), which is valid for strand dimensions that are small compared to skin depth. This gives the eddy current loss per unit volume for each component of flux density. The radial loss component of flux density B_x occurs in the strand height dimension. The axial component of flux density B_y occurs in the strand width dimension. The eddy losses strongly depend on the strand dimension and the magnetic field strength. These losses are added to the P_{dc} losses and are integrated over the winding area using equation (3.32). A transformer designer can predict the losses for a specific design.

4.2.3 FEM analysis carried out on different transformers

FEM analysis carried out on different transformers for winding loss estimation and compared with measured losses is described next. For the model details see Appendix II.

Case 1: A 31.5 MVA unit

This is a 31.5 MVA, 115±9×1.67%/6.3 kV unit with Z=12.06% and a YNd11 connection, ONAF cooled. The LV is a Helical winding, consisting of 3 transposed cables in parallel in each turn and a strand dimension of 2.05×5.2 mm. The high voltage winding is a disc winding consisting of 25 strands in parallel in each disc and a strand dimension of 2.35×13.5 mm.

The measured transformer losses (at principal tapping position 10) are shown in the table below:

Table 4.1 Measured rated losses (kW) for the 31.5 MVA transformer

P_{dc}	Load Losses P_{LL}	Stray Losses $P_{EC} + P_{SL}$
123.9	146.3	22.4

Transformer winding loss calculations

The winding losses estimated by FEM in each individual disc/turn were calculated at a reference temperature of 75 °C, where disc 1 is the top disc, as shown in the table below:

Table 4.2 The estimated winding losses per disc (W/m) over the transformer's HV winding

Disc No.	P_{dc}	Axial winding eddy loss	Radial winding eddy loss	P_{EC}	$P_W = P_{dc} + P_{EC}$
1	102.43	4.82	48.20	53.02	155.45
2	102.43	6.15	22.13	28.28	130.71
3	102.43	7.24	10.66	17.90	120.33
4	102.43	8.14	5.35	13.48	115.92
5	102.43	8.88	2.80	11.68	114.11
6	102.43	9.48	1.55	11.03	113.47
7	102.43	9.99	0.92	10.91	113.34
8	102.43	10.41	0.59	11.00	113.43
9	102.43	10.76	0.41	11.18	113.61
10	102.43	11.06	0.32	11.37	113.81
11	102.43	11.30	0.26	11.56	113.99

In order to estimate the winding losses, they were multiplied by the winding mean length. The stray losses in other structural parts could then be obtained by subtracting the calculated winding eddy current losses from the total stray losses and were found to be as follows:

P_{dc} LV	60.9 kW
P_{dc} HV	62.9 kW
Eddy losses LV	3.53 kW
Eddy losses HV	7.86 kW
Other stray losses	11 kW

Determination of the transformer windings hot-spot factor *H*

Fig 4.6 shows the eddy loss density (W/m^3) over the transformer windings, which enables us to predict the hot spot location. It can be seen that in this case the highest losses are in the HV winding. This is due to the larger conductors used.

The 2-D FEM calculations can be used in a simple way to calculate the hot spot factor. The *H* factor can be predicted as the ratio of the calculated disc/turn losses that generates the hot spot to the total winding average disc/turn losses as follows:

$$H = \left(\frac{P_{W-\max}(pu)}{P_{W-ave}(pu)} \right)^{0.8} \tag{4.1}$$

where

$P_{W-\max}$ are the winding losses at the hottest spot location (pu)

P_{W-ave} are the average winding losses (pu)

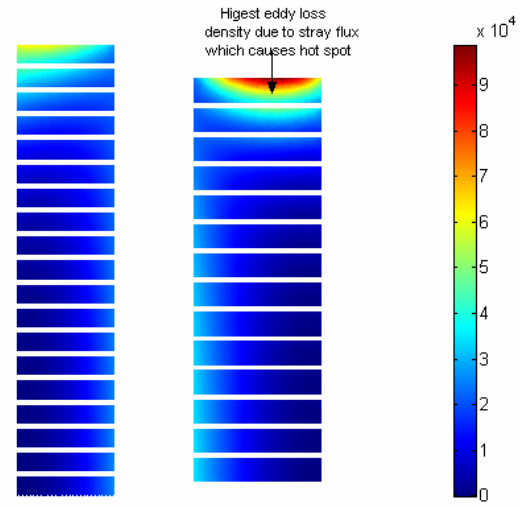

Fig. 4.6 Eddy loss density in the upper discs due to the axial and radial flux density over both windings

For the example case, using equation (4.1) and pu values, the hot spot factor

$$H = \left(\frac{1.52}{1.13} \right)^{0.8} = 1.27 \simeq 1.3$$

Case 2: A **250 MVA unit**

This is a 250 MVA, 230±8×1.5%/118 kV unit with Z =12% and a YN0ynd11 connection, ONAF cooled. The LV winding consists of 2 turns per disc and 2 transposed stranded cables in parallel in each turn with a strand dimension of 1.35×5.9 mm. The high voltage winding is 4 turns per disc, with 1 transposed cable in each turn. The strand dimension is 1.35×6.95 mm.

The measured transformer losses (at principle tapping position 9) are shown in the table below:

Table 4.3 Measured losses (kW) for the 250 MVA transformer

P_{dc} (HV+LV+Reg)	P_{LL} Load losses	Stray losses $P_{EC} + P_{SL}$
411.8	484.64	72.86

The 2-D FEM field solution is shown in Fig. 4.7.

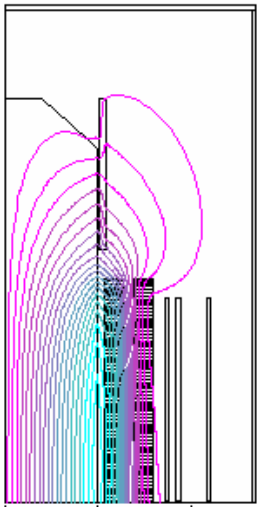

Fig. 4.7 Transformer field solution

Transformer winding loss calculations

The estimated winding losses per individual disc/turn, calculated at a reference temperature of 75°C are presented in the table below:

Table 4.4 The estimated winding losses per disc (W/m) over the transformer's LV winding

Disc No.	P_{dc}	Axial winding eddy loss	Radial winding eddy loss	Eddy losses P_{EC}	Total losses $P_W = P_{dc} + P_{Ec}$
1	126.20	2.55	79.78	82.33	208.53
2	126.20	3.12	58.55	61.67	187.87
3	126.20	3.65	44.32	47.96	174.16
4	126.20	4.14	34.28	38.42	164.62
5	126.20	4.60	26.95	31.55	157.75
6	126.20	5.01	21.46	26.47	152.67
7	126.20	5.39	17.25	22.64	148.84
8	126.20	5.74	13.97	19.71	145.91
9	126.20	6.05	11.40	17.45	143.65
10	126.20	6.34	7.98	14.31	140.51
11	126.20	6.59	6.33	12.92	139.12
12	126.20	6.83	5.00	11.83	138.03

The transformer losses were estimated to be as follows:

P_{dc} LV	199.2
P_{dc} HV	187
P_{dc} Reg.	24.4
Eddy losses LV	21.62
Eddy losses HV	19.63
Other stray losses	31.66

Determination of transformer windings hot-spot factor *H*

Fig. 4.8 shows the eddy loss density W/m^3 due to leakage flux over the transformer windings, which enables us to predict the hottest spot location in the windings. It can be seen that the highest eddy loss is in the LV winding mainly caused by the radial magnetic flux component.

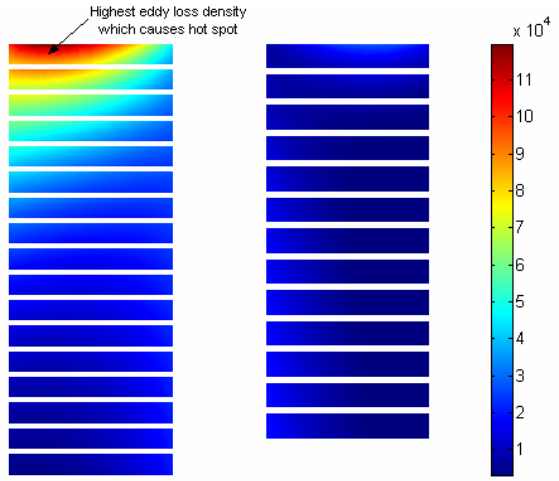

Fig.4.8 Eddy loss density due to the axial and radial flux denity over upper discs of both windings

The calculated hot spot factor using pu values $= \left(\frac{1.65}{1.10}\right)^{0.8} = 1.38 \simeq 1.4$

The calculated hot spot factor is found to be in good agreement with the value obtained from measurements 1.4 [46].

Case 3: A 2500 KVA prototype unit

A 2500 kVA, 20.5/0.71 kV unit with a Dy11 connection and ONAN without an external cooler. The LV winding is a foil winding, consisting of 18 foils and each foil is 640×2 mm. The high voltage winding consists of flat conductors, 3.15×9 mm.

The measured transformer losses are shown in the table below:

Table 4.5 Measured results (kW) for the 2500 kVA transformer

P_{dc}	P_{LL} Load losses	Stray losses $P_{EC} + P_{SL}$
17.400	18.8	1.35

For this transformer each layer of the HV winding and each conductor were modelled as shown in Fig. 4.9. This allowed estimation of the loss distribution over the transformer windings.

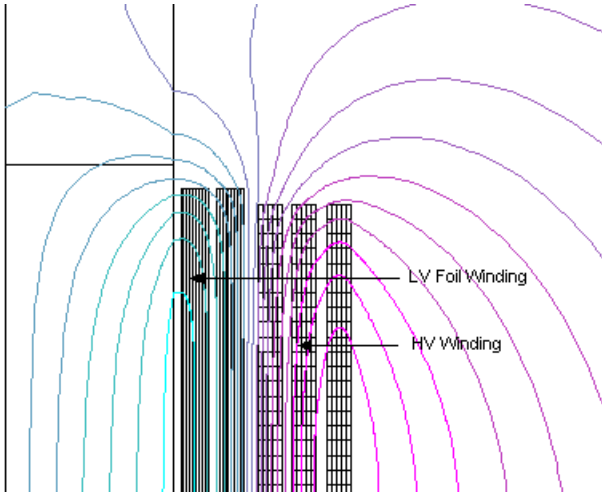

Fig 4.9 Field solution for the 2500 KVA transformer

Figs. 4.10 and 4.11 show the eddy loss density W/m^3 due to leakage flux over the transformer winding, which enables us to predict the highest winding losses that cause the hot spot. The HV winding has the highest loss density in the upper conductors. In the LV winding the highest eddy losses are found in the outer foils, due to the axial flux density component, and decrease towards the core.

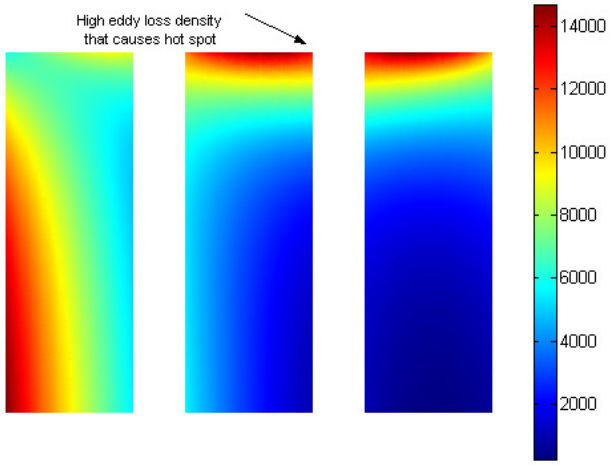

Fig 4.10 Eddy loss distribution over the HV winding

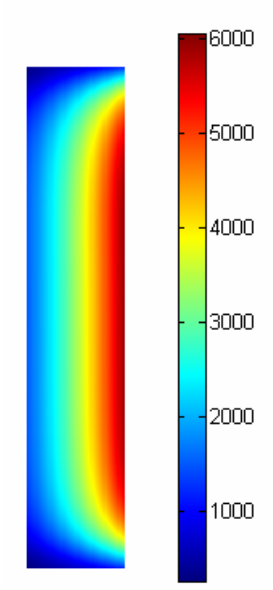

Fig.4.11 Eddy loss distribution over the LV outer layer foils

The transformer's estimated losses are

P_{dc} LV	7416 W
P_{dc} HV	9926 W
Eddy losses LV	135 W
Eddy losses HV	621 W
Stray losses	650 W

The calculated hot spot factor $= \left(\frac{1.13}{1.04}\right)^{0.8} = 1.07 \simeq 1.1$

This is in good agreement with the value obtained from the measurements made on this unit 1.13 [45].

The calculation carried out is a good approximation. However, when skin effect is significant, the conductors have to be modelled including an eddy current term (for the internal eddy current distribution) and the techniques explained in section 3.3.1 is to be used. This is necessary for foil or sheet windings in order to predict the losses more accurately. The solution of this problem would require a magneto-dynamic solution. For the time being commercial software is insufficient. This also implies that the elements cannot be larger than the skin depth close to the boundaries, i.e., a very fine mesh would be needed.

Case 4: A 50 kVA transformer

A 50 kVA, 20.5/0.41 kV, ONAN unit. The LV winding consists of 4.5×6.5 mm flat conductors. The high voltage winding consists of round conductors of 0.6 mm diameter.

The measured transformer losses are shown in Table 4.6

Table 4.6 Measured results (kW) for the 50 kVA transformer

P_{dc}	P_{LL} Load losses	Stray losses $P_{EC} + P_{SL}$
1.106	1.119	0.013

Each conductor in the LV winding was modelled while in the HV winding the small round conductors were modelled as 19 layers. Fig. 4.12 shows the field solution for the transformer.

It was observed that the flux density is small and the radial flux affects only the upper conductors of the LV winding. Calculations based only on axial magnetic flux would have no effect on the result.

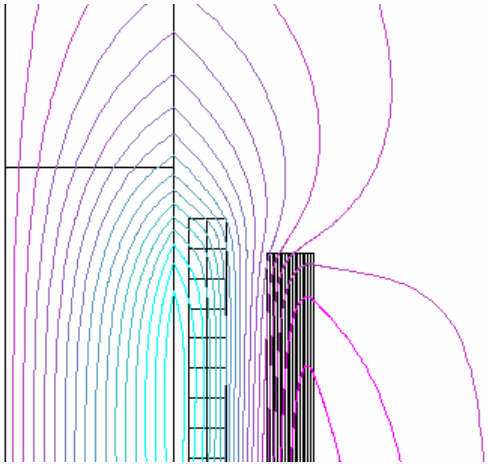

Fig. 4.12 Field solution for 50 kVA Transformer

The estimated losses in the transformer are

P_{dc} HV	651
P_{dc} LV	339
Eddy losses HV	0.2
Eddy losses LV	6.5
Stray losses	6

The upper part of the transformer was modelled in detail. The HV winding small conductors were modelled as shown in Fig. 4.13.

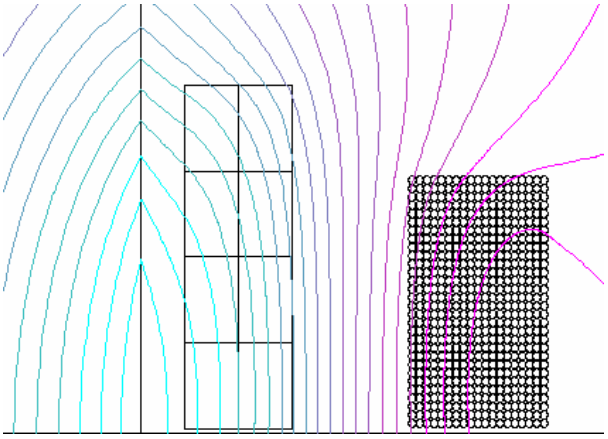

Fig 4.13 Transformer upper part with detailed HV winding

Fig. 4.14 shows the winding losses W/m^3 over the HV winding, which was found to have the highest loss density because it is made of small round conductors of 0.63 mm

diameter. Furthermore, the stray field was small and, considering the conductor dimensions used, the eddy losses were also small. As a result, the losses can be considered constant over the winding.

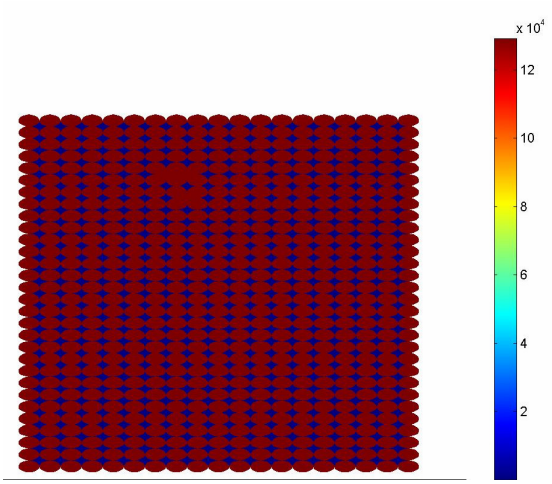

Fig. 4.14 Winding loss density distribution over the upper part of the HV winding, W/m^3

Chapter Five

Consideration of Non-sinusoidal Loading on Transformers

Harmonics and distortion in power system current and voltage waveforms emerged during the early history of ac power systems. However, today the number of harmonic producing devices is increasing rapidly. These loads use diodes, silicon controlled rectifiers (SCR), power transistors, etc. Due to their tremendous advantages in efficiency and controllability, power electronic loads are expected to become significant in the future and can be found at all power levels, from low-voltage appliances to high-voltage converters. One result of this is a significant increase in the level of harmonics and distortion in power system networks.

Transformers are major components in power systems and increased harmonic distortion can cause excessive winding loss and hence abnormal temperature rise. Increased losses have traditionally been assumed to vary with the square of the frequency. This chapter reviews the effect of power system harmonics on transformers. A corrected winding eddy current loss factor for typical stranded transformer windings is presented and implemented to predict a transformer temperature rise under non-sinusoidal load currents. This corrected loss factor is

compared with the loss factor based on the square of the harmonic order that is used in practical situations.

5.1 Effect of power system harmonics on transformers

Traditionally, transformer losses are divided into no load losses and load losses as described in section 2.1. The same loss grouping is retained when considering the influence of power system harmonics. The effect of harmonics on the various losses is considered next.

5.1.1 Effect of voltage harmonics

According to Faraday's law the terminal voltage determines the transformer flux level.

$$N_1 . \frac{d\phi}{dt} \cong u_1(t)$$

Transferring this equation into the frequency domain shows the relation between the voltage harmonics and the flux components.

$$N_1 \cdot j(h\omega) \cdot \phi_h \cong U_h \qquad h = 1, 3, ...$$

This equation shows that the flux magnitude is proportional to the voltage harmonic and inversely proportional to the harmonic order *h*. Furthermore, within most power systems the harmonic distortion of the system voltage THD_v is well below 5% and the magnitudes of the voltage harmonics components are small compared to the fundamental component, rarely exceeding a level of 2-3%. This is determined by the low internal impedance of most supply systems carrying harmonics. Therefore neglecting the effect of harmonic voltage and considering the no load losses caused by the fundamental voltage component will only give rise to an insignificant error. This is confirmed by measurements [24]-[26].

5.1.2 Effect of current harmonics

In most power systems, current harmonics are of more significance. These harmonic current components cause additional losses in the windings and other structural parts.

P_{dc} Losses

If the rms value of the load current is increased due to harmonic components, then these losses will increase with the square of the current.

Winding eddy losses

Conventionally, the eddy current losses generated by the electromagnetic flux are assumed to vary with the square of the rms current and the square of the frequency (harmonic order *h*), [27]-[28]
i.e.

$$P_{EC} = P_{EC-R} \sum_{h=1}^{h=\max} h^2 \left(\frac{I_h}{I_R} \right)^2 \tag{5.1}$$

where

P_{EC} is the winding eddy loss due to non-sinusoidal current

P_{EC-R} is the winding eddy current loss under rated conditions

h is the harmonic order

I_h is the rms current at harmonic order *h*,

I_R is the rms fundamental current under rated frequency and load conditions

Actually, due to the skin effect, the electromagnetic flux may not totally penetrate the strands in the winding at high frequencies. Although conservative, the power of 2 is usually used in calculations [29].

The increased eddy current losses produced by a non-sinusoidal load current can cause excessive winding losses and hence abnormal temperature rise. Therefore the influence of the current harmonics is more important, not only because of the assumed square of the harmonic order but also because of the relatively large harmonic currents present in the power system.

Other stray losses

Other losses occur due to the stray flux, which introduces losses in the core, clamps, tank and other iron parts. When transformers are subject to harmonic load currents these losses also increase. These stray losses may elevate the temperature of the structural parts. For oil filled transformers, these stray losses increase the oil temperature and thus the hot spot temperature. The other stray losses are assumed to vary with the square of the rms current and the harmonic frequency to the power of 0.8, [27]-[28].
i.e.

$$P_{OSL} = P_{OSL-R} \sum_{h=1}^{h=\max} h^{0.8} \left(\frac{I_h}{I_R} \right)^2 \tag{5.2}$$

where,

P_{OSL} are the stray losses in the structural parts due to nonsinusoidal current

P_{OSL-R} are the stray losses in the structural parts under rated conditions

The factor of 0.8 has been verified in studies by manufacturers and others, and is accepted in the standards.

Temperature rises

All effects of harmonic currents discussed so far will increase the transformer losses. These increased losses will obviously increase the temperature rise of the transformer from its sinusoidal value. Therefore, the increased losses due to the harmonic current spectrum must be addressed.

5.2 Winding eddy-current loss factor for transformers

The winding loss at a certain spot can be calculated as:

$$P_W = P_{dc} + P_{EC} \quad \text{W/m} \tag{5.3}$$

The normalised winding loss with the P_{dc} losses can be expressed as:

$$\frac{P_W}{P_{dc-R}} = \frac{P_{dc}}{P_{dc-R}} + \frac{P_{EC}}{P_{dc-R}} \tag{5.4}$$

The first term,

$$\frac{P_{dc}}{P_{dc-R}} = \left(\frac{I}{I_R}\right)^2 = \frac{\sum_{h=1}^{h=\max} I_h^2}{I_R^2} \tag{5.5}$$

The contribution of eddy current losses caused by the magnetic field is obtained using (3.29):

$$P_{EC} \simeq \frac{\pi^2 f^2 T^2 B^2}{3\rho} \tag{5.6}$$

The leakage magnetic field B is directly proportional to the load current I, i.e.

$$B = K_B I$$

When the load current is periodic but non-sinusoidal, its rms value,

$$I = \sqrt{\sum_{h=1}^{h=\max} I_h^2}$$

where

I_h is the rms current harmonic of order h,

Hence,

$$P_{EC} \simeq K \sum_{h=1}^{h=\max} h^2 I_h^2 \tag{5.7}$$

where,

$K = \frac{\pi^2 f^2 T^2 K_B^2}{3\rho}$ and where f is the rated frequency.

When the transformer is loaded at rated current I_R, the corresponding rated eddy current losses are

$$P_{EC-R} = K I_R^2 \tag{5.8}$$

From (5.7) and (5.8)

$$P_{EC} = P_{EC-R} \sum_{h=1}^{h=\max} h^2 \left(\frac{I_h}{I_R} \right)^2 \tag{5.9}$$

Hence, the eddy current losses produced by a harmonic current load can be predicted based on the eddy current losses at rated current and fundamental frequency.

Substituting (5.5) and (5.9) into (5.4) gives:

$$\frac{P_W}{P_{dc-R}} = \left[\frac{\sum_{h=1}^{h=\max} I_h^2}{I_R^2} + \frac{P_{EC-R}}{P_{dc-R}} \sum_{h=1}^{h=\max} h^2 \left(\frac{I_h}{I_R} \right)^2 \right] \tag{5.10}$$

Equation (5.10) was derived based on the assumption that the measured applied currents are taken at the rated currents of the transformer. Since this is seldom encountered in the field, a new term is defined based on the winding eddy losses at the measured current and power frequency, which may be read directly on a meter. A harmonic loss factor is defined in the IEEE standard [28].

$$\frac{P_W}{P_{dc-R}} = \frac{\sum_{h=1}^{h=h_{\max}} I_h^2}{I_R^2} \left[1 + \frac{P_{EC-R}}{P_{dc-R}} \frac{\sum_{h=1}^{h=h_{\max}} h^2 I_h^2}{\sum_{h=1}^{h=h_{\max}} I_h^2} \right]$$

or

The harmonic loss factor can be normalized to either the fundamental or the rms current

$$F_{HL} = \frac{\sum_{h=1}^{h=h_{\max}} h^2 I_h^2}{\sum_{h=1}^{h=h_{\max}} I_h^2} = \frac{\sum_{h=1}^{h=h_{\max}} h^2 \left(\frac{I_h}{I_1} \right)^2}{\sum_{h=1}^{h=h_{\max}} \left(\frac{I_h}{I_1} \right)^2}$$

$$P_W(pu) = I^2(pu)\left[1 + P_{EC-R}(pu)F_{HL}\right] \tag{5.11}$$

where,

$I^2(pu)$ is the normalized current squared.

$P_{EC-R}(pu)$ is the normalized eddy current loss under rated conditions.

F_{HL} is the harmonic loss factor.

The harmonic loss factor can be used to predict the increased eddy losses. This is very important when calculating the temperature rise, which is the limiting factor in transformer loading.

The harmonic loss factor is a key indicator of the current harmonic impact on the winding eddy losses. Under rated sinusoidal current $I(pu) = 1,\ F_{HL} = 1$ and the hot spot specific power loss is

$$P_W(pu) = 1 + P_{EC-R}(pu)$$

5.3 Corrected winding eddy current loss factor

The assumption that the eddy current losses in a winding are proportional to the square of the harmonic order is only reasonable for transformers with small conductors. For larger conductors such an assumption leads to conservative results. Markov and Emanual suggested a corrected harmonic loss factor that leads to a more accurate prediction of transformer capability when subject to non-sinusoidal load current [30]. Their corrected loss factor, based on the specific eddy current loss equation is [32]:

$$P_{EC} \approx \omega B^2 p \tag{5.12}$$

$$p = \frac{1}{\xi}\left[\frac{\sinh\xi - \sin\xi}{\cosh\xi + \cos\xi}\right]$$

where

$\xi = \dfrac{T}{\delta}$ is the relative skin depth compared to strand dimension.

T is the conductor thickness

$\delta_R = \sqrt{\rho / \mu \ \pi f}$ is the penetration depth at power frequency 50 Hz.

$\delta = \sqrt{\frac{\rho}{\mu \pi f h}} = \frac{\delta_R}{\sqrt{h}}$ is the penetration depth at harmonic frequency

For copper and aluminium conductors at 50 Hz and 75 °C, $\delta_R \approx 10.2$ mm and 13.2 mm, respectively.

The relative skin depth compared to strand dimension for harmonic order *h* is

$$\xi_h = \frac{T}{\delta_R / \sqrt{h}} = \xi_R \sqrt{h}$$

Normalising the eddy current loss produced by a harmonic current load to the eddy current losses at rated condition, a corrected harmonic loss factor $h \ F(\xi_h) / F(\xi_R)$ is obtained [30].

$$\frac{P_{EC}}{P_{EC-R}} = \frac{\sum_{h=1}^{h=\max} h \ F(\xi_h) \ I_h^2}{F(\xi_R) \ I_R^2}$$

Fig. 5.1 demonstrates the corrected eddy losses factor as a function of the harmonic order *h*, for different copper conductor dimensions at 75 °C immersed in an alternating field with the harmonic frequencies based on a 50 Hz fundamental. The loss factor obtained using the square of the harmonic order h^2 is also shown.

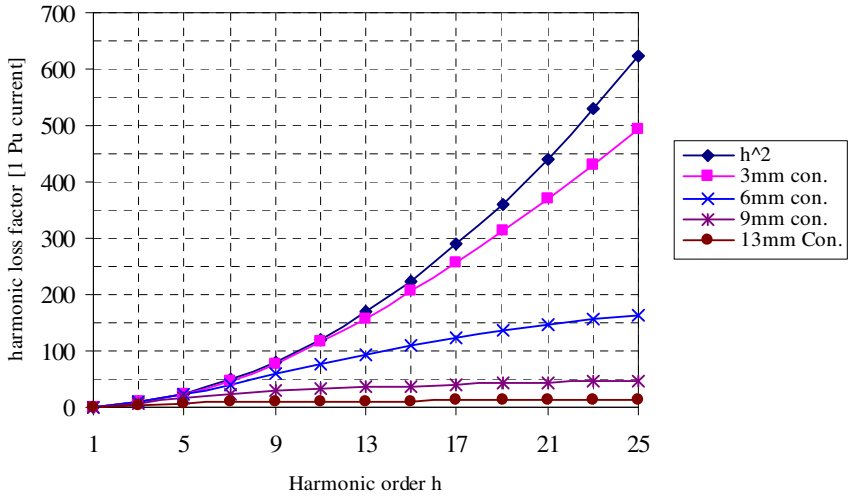

Fig. 5.1 Corrected winding eddy loss factor as a function of harmonic order h for different rectangular copper conductor dimensions [30]

It can be observed where the skin effect begins to have an effect. For small strand thicknesses the skin effect only becomes important at higher harmonics. For larger strands the difference is already significant at lower harmonics, i.e. the winding eddy current loss factor h^2 predicts losses that are higher than the actual losses.

A more accurate winding eddy current loss factor is suggested in this thesis, based on the following equation [3] and published in [31]

$$P_{EC} \simeq \frac{\pi^2 f^2 T^2 B^2}{3\rho} F(\xi) \tag{5.13}$$

where

$$F(\xi) = \frac{3}{\xi} \frac{\sinh \xi - \sin \xi}{\cosh \xi - \cos \zeta}$$

When the current is non-sinusoidal as in (5.7),

$$P_{EC} = K' F(\xi)\ h^2 I^2 \tag{5.14}$$

where,

$$K' = \frac{\pi^2 T^2 f^2 K_B^2}{3\rho}$$

f is the rated frequency

hence,

$$P_{EC} = K' \sum_{h=1}^{h=\max} F(\xi_h)\ h^2 I_h^2 \tag{5.15}$$

Normalising the eddy current losses produced by a harmonic current load to the eddy current losses at rated condition a corrected eddy loss factor $h^2 F(\xi_h)/F(\xi_R)$ is achieved.

$$\frac{P_{EC}}{P_{EC-R}} = \frac{\sum_{h=1}^{h=\max} F(\xi_h)\ h^2 I_h^2}{F(\xi_R)\ I_R^2} \tag{5.16}$$

Substituting (5.5) and (5.16) into (5.4) gives:

$$\frac{P_W}{P_{dc-R}} = \left[\frac{\sum_{h=1}^{h=\max} I_h^2}{I_R^2} + \frac{P_{EC-R}}{P_{dc-R}} \frac{\sum_{h=1}^{h=\max} h^2 F(\xi_h) \left(\frac{I_h}{I_R} \right)^2}{F(\xi_R)} \right] \tag{5.17}$$

When the strand dimension is smaller than the penetration depth at the harmonic frequency, equation (5.17) is reduced to (5.10), which is the correct limiting case.

The importance of the above corrected loss factor which is based on (5.16), is shown in Fig. 5.2. The harmonic loss factors are presented as a function of the harmonic order, for different copper conductor thicknesses at 75°C immersed in alternating fields. The fundamental frequency is 50 Hz. The graph of the square of the harmonic order h^2 is added for comparison.

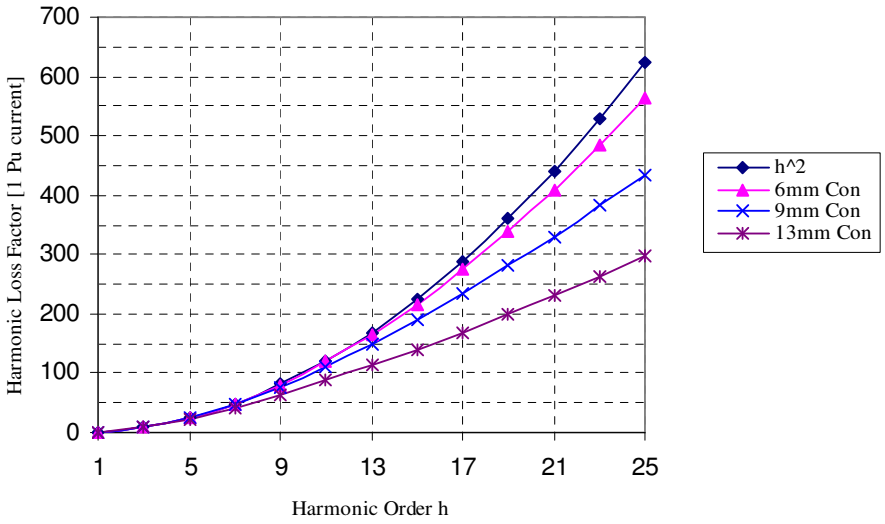

Fig. 5. 2 Corrected winding eddy-current loss factor as a function of harmonic order h for different rectangular copper conductor thickness [31]

It can be seen that for small conductors skin effect is insignificant and only for large conductor dimensions at high harmonics does the difference become significant. It can be said that using the assumed eddy current loss factor h^2 predicts losses accurately for small conductors and low harmonics but produces a certain degree of error for a combination of large conductors and higher frequencies.

The corrected loss factor in (5.16) was verified by laboratory measurements using the calorimetric method (see Appendix I). The corrected loss factor was found to be in good agreement with measurements and most importantly, what error there is would appear to be on the conservative side at high frequencies.

In practical transformers the critical point is usually in the upper end of the windings where the conductors are exposed to an inclined magnetic field with two components, an axial component and a radial component. The eddy current losses are the contribution of these two components. The side dimensions of conductors are found to be in a wide range. This requires an equivalent eddy-current loss factor that will account for both axial and radial eddy current losses.

The enhanced eddy losses due to any non-sinusoidal loading can be predicted more accurately using a corrected winding eddy loss factor that accounts for the strand thickness. The eddy current loss at rated current can be obtained using

$$P_{EC} = P_{EC-x} \sum_{h=1}^{h=\max} \frac{F_x(\xi_h)}{F_x(\xi_R)} h^2 \left(\frac{I_h^2}{I_R^2} \right) + P_{EC-r} \sum_{h=1}^{h=\max} \frac{F_r(\xi_h)}{F_r(\xi_R)} h^2 \left(\frac{I_h^2}{I_R^2} \right) \tag{5.18}$$

where

$F_{WE-x} = \frac{F_x(\xi_h)}{F_x(\xi_R)} h^2$ and $F_{WE-r} = \frac{F_r(\xi_h)}{F_r(\xi_R)} h^2$ are the winding eddy current corrected loss factors for the axial and radial strand dimensions, respectively

5.4 Transformer stray loss components

There is no test method to distinguish the winding eddy losses from the stray losses that occur in structural parts. Transformer stray losses are frequency dependent, and vary with the exponent of the harmonic order. The stray loss components can be estimated by thorough loss measurements at different frequencies, or simply, as recommended in [33], based on load loss measurements at fundamental frequency and at 150 or 250 Hz:

$$P_1 = P_{dc} + P_{EC} + P_{SL} \tag{5.19}$$

$$P_h = P_{dc} + P_{EC} \times h^2 + P_{SL} \times h^{0.8} \tag{5.20}$$

The result will be based on well established measurements in the factory, a good estimation. Exact results are not required.

Furthermore, Bendapudi [34] evaluated the frequency-dependent factors of winding eddy losses and other stray losses for specific transformer designs based on measurements at different frequencies. The harmonic loss factor K_n was defined as:

$$K_n = \frac{P_1 - P_0}{P_1}\left[wn^q + (1-w)n^r \right] + \frac{P_0}{P_1} \tag{5.21}$$

where,

n is the harmonic order

K_n is the harmonic factor P_n / P_1

P_n is the load loss at the nth harmonic

P_1 is the load loss at fundamental frequency

P_0 is the loss due to the DC resistance

w are the winding eddy losses as a fraction of the total stray losses at fundamental frequency.

$(1-w)$ are the other stray losses as a fraction of the total stray losses at fundamental frequency.

The value of w is based on the calculation of the particular transformer design. Curve fitting was used to determine the best value for q and r.

J. Drisen [35] suggested a practical method to determine the winding frequency dependent factor with short circuit tests at harmonic frequencies. The loss factor was defined as:

$$K(f) = \frac{R_{AC}(f) - R_{DC}}{R_{AC}(f_1) - R_{DC}} \tag{5.22}$$

These authors also developed an advanced FEM tool and studied a wire and foil transformer.

5.4.1 A method of load loss estimation

A relatively simple method based on factory measurements to estimate the loss variation due to harmonics that can be applied at the design stage is proposed. The winding stray losses and other stray losses vary with the exponent of the harmonic order. For the total load losses P_{LL} we may write:

$$\frac{P_{LL}}{P_{dc}} = 1 + \frac{P_{SL}}{P_{dc}}\left[w\ h^q + (1-w)\ h^r \right] \tag{5.23}$$

where,

P_{SL} are the total stray losses

P_{dc} are the losses due to the dc resistance.

w Are the winding eddy losses as a fraction of the total stray losses at fundamental frequency.

$(1-w)$ are the other stray losses as a fraction of the total stray losses at fundamental frequency.

The dc loss component is independent of frequency and the influence of the skin effect can be neglected for the frequency range being considered.
Factory measurements of load losses at frequencies 20 Hz, 30 Hz, 40 Hz, 50 Hz, 60 Hz, 80 Hz, 165 Hz and 250 Hz, fitted with (5.23), are shown in Fig.5.3

The values of *q, r* and *w* that produced a fit with the test results are:

w	0.51
Winding eddy loss exponent q	2
Other stray loss exponent r	1

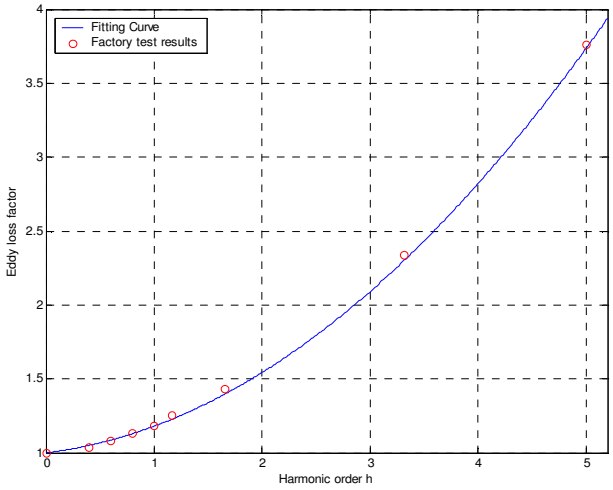

Fig. 5.3 Eddy loss factor as a function of the harmonic order

This seems to be reasonable since the estimated *w* is in good agreement with the FEM calculations and the conductors usually consist of small strands.

The values of loss exponents depend on the transformer design. For the winding harmonic loss exponent, a value of 2 has been used by Crepaz [36]. A value of 2 at lower harmonics and a little less than 2 for higher harmonics was used in [37]. For foil windings J. Drisen et al. [35] used a rational exponent of 0.7 due to the fact that different layers showed different frequency dependence ranging from linear to square-root characteristics. For other stray losses, Karasev [38] suggested 1, 0.9 is used by Bendapudi [34] and 1.5 is used by Emmanual and Wang [39].

5.5 Evaluation of transformer loading capability

International standards recommend a method to determine the loading capability of transformers subject to non-sinusoidal load currents. The recommended method in [28] for dry type transformers is based on the condition that the pu value of the non-sinusoidal current will cause the same hot spot losses as the rated sinusoidal current. This can be expressed as

$$I_{\max}(pu) = \sqrt{\frac{P_{W-R}(pu)}{1 + F_{HL} \times P_{EC}(pu)}} \tag{5.24}$$

This assumes that the normal life of the unit will be maintained.

The calculation for liquid filled transformers is similar to the dry type except the other stray losses must be included. The temperature rises are proportional to the losses according to the suggested standard exponents in Table 2.1 and thus can be calculated as follows:

The top oil temperature rise over ambient:

$$\Delta\Theta_{To} = \Delta\Theta_{To-R}\left(\frac{P_{NL}+P_{LL}}{P_{NL-R}+P_{LL-R}}\right)^{n} \tag{5.25}$$

where,

$\Delta\Theta_{To-R}$ is the top oil temperature rise over ambient under rated conditions.

P_{NL} are the no load losses.

P_{LL} are the load losses, increased to account for harmonic load currents $P + F_{WE}.P_{EC-R} + F_{OSL}.P_{OSL-R}$

P_{NL-R} are the no load losses at rated condition.

P_{LL-R} Load losses at rated condition.

The winding hot spot to top oil rise due to the increase in the losses at the hot spot location:

$$\Delta\Theta_{H} = \Delta\Theta_{H-R}\left(\frac{P_{W}(pu)}{P_{W-R}(pu)}\right)^{m} \tag{5.26}$$

where,

$P_{W}(pu)$ are the increased winding pu losses due to the harmonics at the hot spot location. $\frac{\sum_{h=1}^{h=max} I_h^2}{I_R^2} + \frac{\sum_{h=1}^{h=max} I_h^2}{I_R^2} h^2.P_{EC-R(pu)}$

$P_{W-R}(pu)$ are the losses at the hot spot location under rated conditions.

If the current spectrum is measured at a substation, the transformer steady state temperature rise can be checked. The following example illustrates a comparison between the harmonic order squared and the corrected loss factor.

5.6 Comparison between h^2 and the eddy current corrected loss factor in a practical situation

5.6.1 Example calculation for a dry type transformer

An example in [28] is reworked to compare the presented corrected harmonic loss factor with the harmonic order squared and the harmonic loss factor suggested in [30]; it consists of a standard transformer with 1200 A rated current and $P_{EC\text{-}R} = 0.15$. The secondary winding is assumed to consist of copper strands of 3.65×11 mm, given the non-sinusoidal load current with the harmonic distortion as shown in Fig. 5.4.

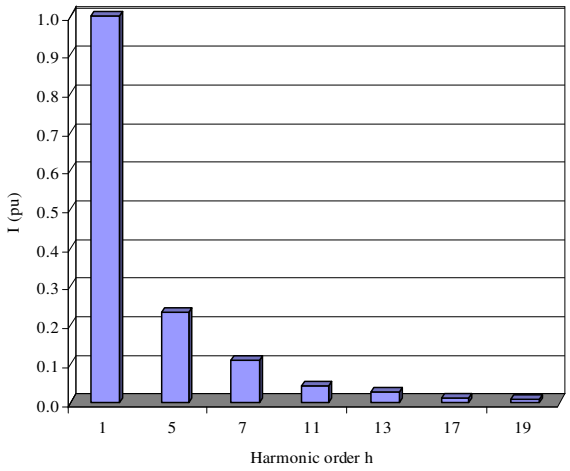

Fig.5.4 The harmonic current spectrum load

The presented corrected harmonic loss factor is compared with the harmonic order squared standard factor and the harmonic loss factor presented in [30].

$$F_{HL} = \frac{\sum_{h=1}^{h=h_{\max}} h^2 \left(\frac{I_h}{I_1}\right)^2}{\sum_{h=1}^{h=h_{\max}} \left(\frac{I_h}{I_1}\right)^2} = \quad 3.219$$

$$I_{\max}(pu) = \sqrt{\frac{1.15}{1+0.15\times 3.129}} = 0.885 \ \ pu \ \text{ or } \ I_{\max} = 0.885\times 1200 = 1062 \ \ A$$

$$F_{HL} = \frac{\sum_{h=1}^{h=h_{\max}} \frac{F(\xi_h)}{F(\xi_R)} h^2 \frac{I_h^2}{I_1^2}}{\sum_{h=1}^{h=h_{\max}} \frac{I_h^2}{I_1^2}} = \quad 2.875$$

$$I_{\max}(pu) = \sqrt{\frac{1.15}{1+0.15\times 2.875}} = 0.9 \ \ pu \ \text{ or } \ I_{\max} = 0.9\times 1200 = 1075.65 \ \ A$$

As shown in the Table below, the presented loss factor taking into account the skin effect allows only a 1.32% increase compared to the h^2-rule. This is due to the low harmonics spectrum. The harmonic loss factor presented in [30] would allow an 8.6 % increase in the current.

Table 5.1 Comparison of the max. allowed non-sinusoidal load current for different harmonic loss factors F_{HL}

Harmonic Factor	F_{HL}	$I_{\max}(A)$
$h^2\,(I_h/I)^2$	3.129	1062
$(h^2F(\xi_h)/(\xi_R))\,(I_h/I)^2$	2.875	1075
$h(\xi_h)/F(\xi_R)\,(I_h/I)^2$	1.683	1157

Fig. 5.5 shows a comparison of the transformer de-rating factor when it is subject to different THD. For this transformer it can be seen that when high frequency components increase, the standard calculation, which ignores skin effect, becomes conservative.

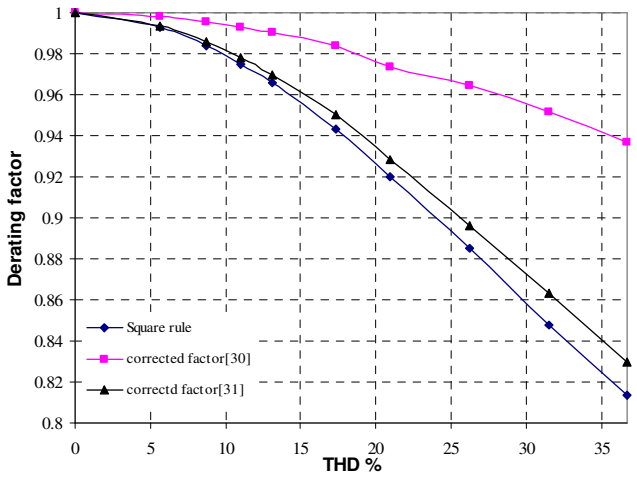

Fig.5.5 Comparison of transformer de-rating factor for different THD%

5.6.2 Example calculation for a 31.5 MVA oil-filled transformer

After installation of a 31.5 MVA, 115/6.3 kV oil-immersed transformer, the harmonic currents were measured and the current spectrum supplied to the manufacturers with a request to check the transformer temperature rise. The measured current spectrum with the expected highest degree of distortion is assumed to pass through the transformer as shown in Table. 5.2. The fundamental current is assumed to be equal to the rated current.

Table 5.2 Measured current spectrum

h	$\frac{I_h}{I_1}$
1	1.0000
5	0.1760
7	0.1100
11	0.0447
13	0.0264
17	0.0118
19	0.0106
23	0.0087
25	0.0086

At rated load and fundamental frequency, the measured losses were:

No Load	16.1 kW
P_{dc}	123.9 kW
Stray and eddy losses	22.4 kW
Load losses	146.3 kW

The division of stray losses based on FEM calculations and factory test results was estimated to be:

Winding eddy losses	11.4 kW
Other stray losses	11 kW

The measured temperature rises were:

Top oil temperature rise	50.7 °C
Hot spot temperature rise	25.6 °C

The hot spot rise over ambient $= 50.7 + 25.6 = 75.7°C$

Using the harmonic order square rule

To calculate the top oil temperature rise transformer total losses must be corrected for the given harmonic contents according to the loss factors to reflect the harmonic content. Similarly, to determine the hot spot temperature rise over top oil, the losses at the hot spot location that occur in the upper disc of the HV winding must be corrected.

The calculations using the harmonic load currents in Table 5.2 give:

$$\sum_{h=1}^{h=\max} \left(\frac{I_h}{I_R} \right)^2 = \quad 1.046$$

$$\sum_{h=1}^{h=\max} h^2 \left(\frac{I_h}{I_R} \right)^2 = \quad 2.894$$

$$\sum_{h=1}^{h=\max} h \left(\frac{I_h}{I_R} \right)^2 = \quad 1.278$$

Using (5.25), the steady-state top oil rise for the specified harmonic spectrum will be:

$$\Delta\theta_{TO} = 50.7 \left(\frac{192.749}{162.40} \right)^{0.9} = 59.15°C$$

The hot spot rise over top oil and the pu loss calculated by FEM at the hot spot location must be corrected for the given harmonic content using (5.26).

$$\Delta\theta_H = 25.61 \left(\frac{2.544}{1.52} \right)^{0.8} = 37.71°C$$

The hot spot rise over ambient $= 59.15 + 37.71 = 97.86°C$

Using the corrected winding eddy current loss factor

To calculate the top oil temperature rise in a way that reflects the harmonic content, the transformer's total losses must be corrected for the given harmonic content according to the corrected loss factor based on the conductor dimensions (5.18). Similarly, to determine the hot spot temperature rise over top oil the loss at the hot spot location that occur in the upper disc of the HV winding must be corrected.

The top oil rise for the specified harmonic spectrum

$$\Delta\theta_{TO} = 50.7\left(\frac{192.02}{162.3}\right)^{0.9} = 58.93°C$$

The hot spot rise over top oil gradient

$$\Delta\theta_{H} = 25.61\left(\frac{2.32}{1.52}\right)^{0.8} = 36.03°C$$

The hot spot rise over ambient $= 58.93 + 36.03 = 94.7°C$

In this example the spectrum used has small values of higher harmonics, which makes the temperature difference compared to the I^2 value about 3 °C. However, with a spectrum rich in higher harmonics the difference would be higher.

Chapter Six
Dynamic Thermal Modeling

The winding hot spot temperature is considered to be the most important parameter in determining the transformer loading capability. It determines the insulation loss of life and the potential risk of releasing gas bubbles during a severe overload condition. This has increased the importance of knowing the hot spot temperature at each moment of the transformer operation at different loading conditions and variable ambient temperature.

The commonly used models for top oil and hot spot temperature calculations are described in the IEC and IEEE loading guides [8]-[9] . As suggested in [42], the problem is that the IEEE top oil rise model does not properly account for variations in ambient temperature and an improved model is proposed. A more rigorous method is suggested in IEEE loading guide Annex G [9]. The equations require the use of bottom oil rise over ambient at rated conditions. Duct oil temperature is introduced, which may be higher than the top oil temperature under certain conditions, leading to more accurate hot spot temperature located at some point in the winding duct.

A thermal model for power transformers in the form of an equivalent circuit based on the fundamentals of heat transfer theory has been suggested by Swift in [44]. The proposed thermal model was established to determine the hot spot temperature. The top oil temperature is calculated from the air-to-oil model. The top oil temperature becomes the ambient temperature for the winding-to-oil model. The top oil temperature model was validated by measurements from a 250 MVA transformer in the field [45].

This chapter will re-examine and review the applicability of the existing thermal dynamic models used within transformers and arrive at a model which is not only accurate but easy to use for practical applications.

6.1 Transformer loading guides

The long-standing calculations described in clause 7 of the IEEE loading guide and IEC 354 use a dynamic loading model for top oil and hot spot temperature rises [8]-[9]. The steady state relationship is as shown in Fig. 2.1. The differential equations approach is quite similar.

The hot spot is usually assumed to be near the top of the HV or LV winding, although there are arguments that it could be lower within the cooling ducts, in particular if the transformer oil is not assumed to be directly pumped through the ducts [40]-[41].

6.1.1 Top oil temperature rise model

The basic idea of the top oil temperature rise over ambient model is that an increase in the transformer current will result in an increase in the losses within the transformer and thus an increase in the overall temperature. This temperature change depends on the heat capacity of the transformer, i.e. the mass of the core, coils and oil, and the rate of heat transfer out of the transformer. The top oil rise is calculated as a first order exponential response from the initial temperature state to the final temperature state.

$$\Delta\Theta_{TO} = \left[\Delta\Theta_{TO,U} - \Delta\Theta_{TO,i}\right]\left[1 - e^{\frac{-t}{\tau_o}}\right] + \Delta\Theta_{TO,i} \tag{6.1}$$

Equation (6.1) is the solution of the first order differential equation

$$\tau_{TO}\frac{d\Delta\Theta_{TO}}{dt} = \left[\Delta\Theta_{TO,U} - \Delta\Theta_{TO}\right] \tag{6.2}$$

$$\Delta\Theta_{TO,U} = \Delta\Theta_{TO-R}\left(\frac{1+R\cdot K^2}{1+R}\right)^n \tag{6.3}$$

where,

$\Delta\Theta_{TO}$ is the top oil temperature rise over ambient temperature.

$\Delta\Theta_{TO,U}$ is the ultimate top oil temperature rise over ambient temperature.

K is the load current per unit

τ_{TO} is the top oil rise time constant.

$\Delta\Theta_{TO-R}$ is the rated top oil temperature rise over ambient temperature.

R is the ratio of load losses at rated load to no load losses.

n is an empirically derived exponent that depends on the cooling method

6.1.2 Winding hot spot temperature rise model

The basic idea behind the hot spot temperature rise model is that an increase in the transformer current will result in an increase in the losses and thus an increase in the temperature. The hot spot rise is calculated as a first order exponential response from the initial temperature state to the final temperature state.

$$\Delta\Theta_{H} = \left[\Delta\Theta_{H,U} - \Delta\Theta_{H,i}\right]\left[1 - e^{\frac{-t}{\tau_H}}\right] + \Delta\Theta_{H,i} \tag{6.4}$$

Equation (6.4) is the solution of the first order differential equation

$$\tau_H \frac{d\Delta\Theta_H}{dt} = \left[\Delta\Theta_{H,U} - \Delta\Theta_H \right] \tag{6.5}$$

$$\Delta\Theta_{H,U} = \Delta\Theta_{H,R} \cdot K^{2m} \tag{6.6}$$

where,

$\Delta\Theta_H$ is the hot spot temperature rise over top oil temperature.

$\Delta\Theta_{H,U}$ is the ultimate hot spot temperature rise top oil temperature.

K is the load current per unit

τ_H is the hot spot rise time constant.

$\Delta\Theta_{H,R}$ is the rated hot spot temperature rise over top oil temperature.

m is an empirically derived exponent that depends on the cooling method

The suggested exponents n and m define the non-linearity and they depend on the ambient fluid and the transformer cooling method. The exponents generally used were presented in chapter 2.

Finally, the hot spot temperature is calculated by adding the ambient temperature to the top oil temperature rise and to the hot spot temperature rise, using

$$\Theta_H = \Theta_A + \Delta\Theta_{TO} + \Delta\Theta_H \tag{6.7}$$

where,

Θ_H is the hot spot temperature.

Θ_A is the ambient temperature

The temperature calculations assume a constant ambient temperature. This is a conservative estimate since it does not account for the effects of ambient temperature

dynamics on top oil temperature. The guide also includes a method to modify the top oil time constant τ_{TO} as a function of n if desired for greater accuracy. The loading guide equations have proven to be reasonably accurate for moderate longer term overloads [41].

6.1.3 The simulation model

Fig 6.1 shows a simplified diagram for the thermal dynamic loading equations. The continuous form of equations (6.2) and (6.5) are solved using Simulink. At each discrete time the hot spot temperature is assumed to consist of three components Θ_A, $\Delta\Theta_{TO}$ and $\Delta\Theta_H$. Different numerical techniques can be applied and different time steps can be assigned for accuracy [52].

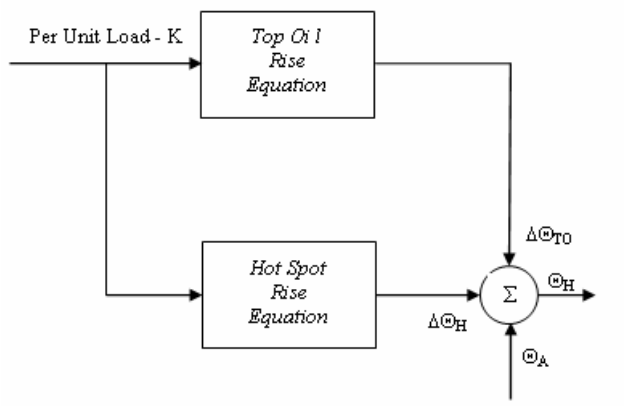

Fig 6.1 Simplified diagram of the thermal dynamic model

A block diagram to calculate the top oil temperature rise is shown in Fig. 6.2.

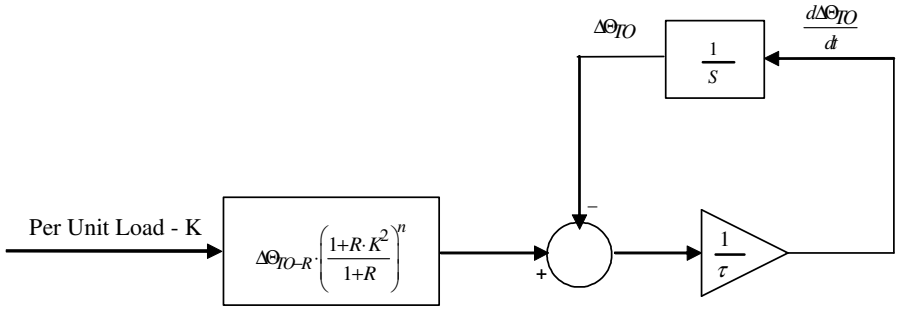

Fig. 6.2 Block diagram of top oil rise model

6.1.4 Example calculation for a 250 MVA transformer

For this example the transformer input parameters used for the hot spot calculation are

Table 6.1 Thermal model parameters

Rated top oil rise over ambient	38.3 ° C
Rated hot spot rise over top oil	20.3 ° C
Ratio of load loss to no load loss	6.20
Top oil time constant	170 min
Hot spot time constant	7 min
Exponent *n*	0.9
Exponent *m*	0.8

The data used in the model is based on the transformer manufacturer's testing. The top oil temperature time constant is less than the calculated based on the total heat capacity of the transformer according to the IEEE loading guide [9].

The transformer was tested under the load cycle shown in Fig. 6.3. The top oil and the hot spot temperatures were recorded in the factory.

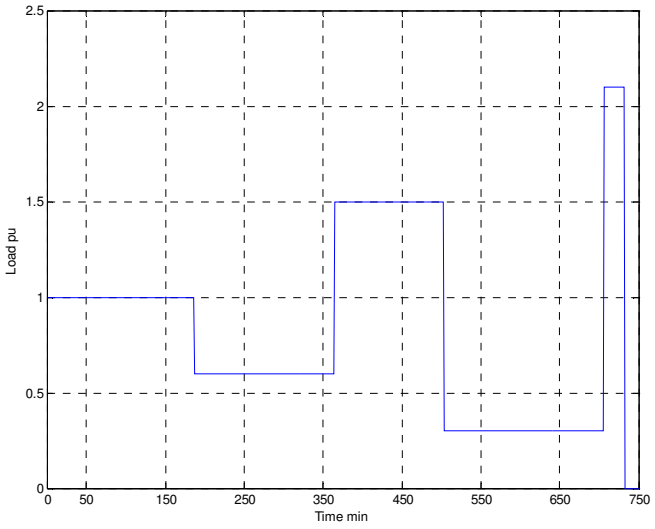

Fig. 6.3 250 MVA transformer load used in the test

The transformer hot spot temperature, calculated according to the loading guide model using the transformer input data shown in the above table and compared with the measured temperature hot spot, is shown in Fig. 6.4.

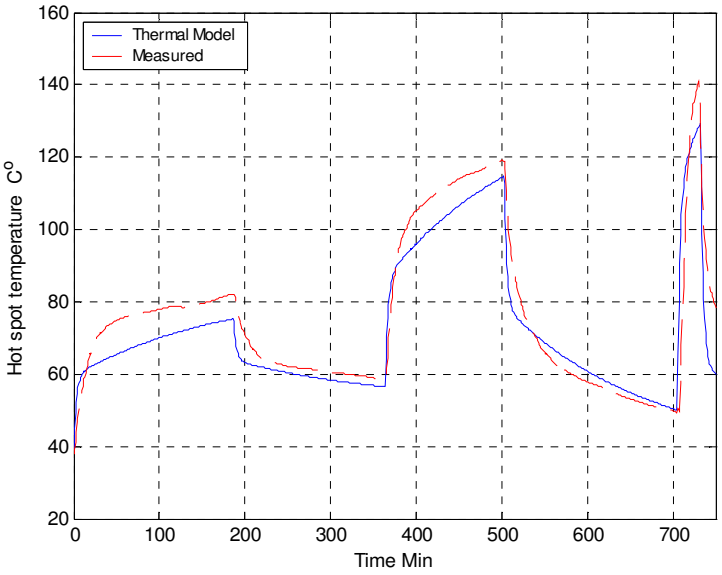

Fig. 6.4 The calculated hot spot temperature of the 118 KV winding compared with measured

It can be clearly seen that the hot spot temperature is under estimated for the applied loads.

6.2 Loss of insulation life

Insulation in power transformers is subject to ageing due to the effects of heat, moisture and oxygen content. From these parameters the hottest temperature in the winding determines the thermal ageing of the transformer and also the risk of bubbling under severe load conditions.

The IEEE Guide [9] recommends that users select their own assumed lifetime estimate. In this guide, 180 000 hours (20.6 years) is used as a normal life.

It is assumed that insulation deterioration can be modelled as a per unit quantity as follows

$$Per\ unit\ life = A\ e^{\left[\frac{B}{\Theta_H + 273}\right]} \tag{6.10}$$

where

A is a modified constant based on the temperature established for one per unit life.

B is the ageing rate.

For a reference temperature of 110 °C, the equation for accelerated ageing is

$$F_{AA} = e^{\left(\frac{15000}{383} - \frac{15000}{\Theta_H + 273}\right)} \quad pu \tag{6.11}$$

The loss of life during a small interval dt can be defined as

$$dL = F_{AA}\ dt \tag{6.12}$$

The loss of life over the given load cycle can be calculated by

$$L = \int F_{AA}\, dt \tag{6.13}$$

And the per unit loss of life factor is then

$$L_F = \frac{\int F_{AA}\, dt}{\int dt} \tag{6.14}$$

The insulation loss of life is usually taken to be a good indicator of transformer loss of life. To illustrate, if a transformer hot spot temperature is approximately 117 °C, then L_F would be about 2. i.e. the transformer would lose all of its life in half of its chosen normal life. A simulation function is shown in appendix III

6.3 An improved top oil rise temperature model

The top oil rise equation in clause 7 of the IEEE guide is modified to allow for continuously varying ambient temperature. The ambient temperature Θ_A is included in the top oil rise model where it allows the top oil temperature to respond dynamically to changes in ambient temperature [42]-[43].

$$\tau_{TO} \frac{d\Theta_{TO}}{dt} = \left[\Theta_{TO,U} + \Theta_A\right] - \Theta_{TO} \tag{6.15}$$

where,

Θ_A is the ambient temperature, ° C

Θ_{TO} is the top oil rise over ambient temperature,° C

$\Theta_{TO,U}$ is the ultimate top oil temperature rise over ambient temperature,° C

τ_{TO} is the top oil rise time constant, min.

Then, the top oil temperature rise over ambient is added to the hot spot rise to get the hot spot temperature

$$\Theta_H = \Theta_{TO} + \Delta\Theta_H \tag{6.16}$$

6.4 IEEE Annex G

IEEE loading guide Annex G presents an alternative temperature calculation method in which the bottom oil temperature is used as the calculation starting point. It also introduces the duct oil temperature, which may be higher than the top oil temperature under certain conditions, leading to a more accurate prediction of the hot spot temperature located at some point in the winding duct [9] and [41].

6.4.1 Loading equations

The hot spot temperature calculation presented in the guide is made up of the following components.

$$\Theta_H = \Theta_A + \Delta\Theta_{BO} + \Delta\Theta_{WO} + \Delta\Theta_{HSWO} \tag{6.16}$$

where,

$\Delta\Theta_{BO}$ is the bottom oil temperature rise over ambient temperature, °C.

$\Delta\Theta_{WO}$ is the oil temperature rise at winding hot spot location over bottom oil, °C.

$\Delta\Theta_{HSWO}$ is the winding hot spot temperature rise over oil at hot spot location, °C.

The temperature rises in equation (6.16) are obtained in [9] and [41] based on the conservation of energy over each time interval Δt. For such an interval, there must be a balance between the amounts of all energy changes in Joules. The equations were solved by the finite difference Forward Euler Method. At each step new calculated temperature values are added to the old value. The calculated losses and viscosity changes with temperature are corrected for each time step. The equations were programmed in Basic as documented in [9] and [41].

Alternatively, the equations presented in [9] and [41] can be written on the basis that at any instant *t* there must be a balance between all energy rates in watts. The equations are then in a continuous form and can be solved using different numerical techniques and time steps depending on the required accuracy [50]. Such an approach is adopted in this thesis and the equations are as follows:

Average winding equation

The average winding temperature can be calculated from the energy balance equation:

$$Q_{GW} = Q_{AW} + Q_{LW} \tag{6.17}$$

where,

Q_{GW} is the heat generated by the winding losses, W.

Q_{AW} is the heat absorbed by the windings, W.

Q_{LW} is the heat lost by the windings, W.

The heat generated by the windings at any instant *t* is

$$Q_{GW} = L^2 \left[P_{dc} \cdot K_W + \frac{P_{EC}}{K_W} \right] \tag{6.18}$$

where,

$$K_W = \frac{\Theta_W + \Theta_K}{\Theta_{WR} + \Theta_K} \tag{6.19}$$

L is the per unit load

P_{dc} are the winding losses due to the dc resistance, W.

P_{EC} are the winding losses due to the eddy currents, W.

K_W is a temperature correction for winding losses

Θ_W is the average winding temperature, °C.

Θ_K is the temperature factor for resistance change with temperature: 234.5 for copper, 225 for Aluminium

Θ_{WR} is the rated average winding temperature, °C.

The heat absorbed by the windings at any instant *t* is

$$Q_{AW} = M_W Cp_W \frac{d\Theta_W}{dt} \tag{6.20}$$

where

M_W is the mass of the windings, kg

Cp_W is the specific heat of the windings, W. min/kg. °C.

The thermal capacitance can be estimated from the winding time constant as follows:

$$M_W Cp_W = \frac{(P_{dc} + P_{EC})\tau_W}{\Theta_{WR} - \Theta_{DAOR}} \tag{6.21}$$

where,

τ_W is the winding time constant, min

Θ_{DAOR} is the rated average temperature of oil in the winding ducts, °C.

The heat lost by the windings at any instant *t* is

$$Q_{LW} = \left[\frac{\Theta_W - \Theta_{DAO}}{\Theta_{WR} - \Theta_{DAOR}}\right]^{5/4} \left[\frac{\mu_{WR}}{\mu_W}\right]^{1/4} (P_{dc} + P_{EC}) \tag{6.22}$$

where,

Θ_{DAO} is the average temperature of the oil in the winding ducts, °C.

μ_W is the viscosity of the oil film in the ducts at time instant *t,* Centipoise.

μ_{WR} is the rated viscosity of the oil film in the ducts at rated load, Centipoise.

Substituting (6.18), (6.20) and (6.22) into (6.17) gives

$$L^2\left[P_{dc}\cdot K_W + \frac{P_{EC}}{K_W}\right] = M_W Cp_W \frac{d\Theta_W}{dt} + \left[\frac{\Theta_W - \Theta_{DAO}}{\Theta_{WR} - \Theta_{DAOR}}\right]^{5/4} \left[\frac{\mu_{WR}}{\mu_W}\right]^{1/4} (P_{dc} + P_{EC}) \tag{6.23}$$

Winding duct equation

The winding duct oil rise can be determined from the following equation:

$$\Theta_{DO} - \Theta_{BO} = \Delta\Theta_{DO} = \left[\frac{Q_{LW}}{P_{dc} + P_{EC}}\right]^{x} \left(\Theta_{DOR} - \Theta_{BOR}\right) \tag{6.24}$$

where,

Θ_{DO} is the temperature of the oil exiting the winding ducts, °C.

Θ_{DOR} the rated temperature of the oil exiting the winding ducts, °C.

$\Delta\Theta_{DO}$ is the temperature rise of the oil at the top of the duct over the bottom oil temperature, °C.

Θ_{BO} is the temperature of the bottom oil entering the winding, °C.

Θ_{BOR} is the rated temperature of the bottom oil entering the winding, °C.

x is 0.5 for OA, FA and NDFOA; 1.0 for DFOA.

The heat lost by the winding to the duct oil is given by (6.22).

The hot spot may not be located at the top of the winding. The oil temperature at the hot spot elevation is given by:

$$\Delta\Theta_{WO} = H_H \left(\Theta_{DO} - \Theta_{BO}\right) \tag{6.25}$$

$$\Theta_{WO} = \left(\Theta_{BO} + \Delta\Theta_{WO}\right) \tag{6.26}$$

where

H_H is the per unit value representing the winding height to hot spot location.

Θ_{WO} is the temperature of the oil in the ducts at the hot spot location, °C.

If the winding duct oil temperature is less than in the top oil in the tank then the oil temperature adjacent to the hot spot is assumed equal to the top oil or, in equation form,

$$IF \quad \Theta_{DO} < \Theta_{TO} \quad \text{THEN} \quad \Theta_{WO} = \Theta_{TO} \tag{6.27}$$

where

Θ_{TO} is the top oil temperature in the tank °C.

Winding hot spot equation

The hot spot temperature can be written similar to the average temperature equation

$$Q_{GH} = Q_{AH} + Q_{LH} \tag{6.28}$$

where,

Q_{GH} is the heat generated by losses at the hot spot location, W.

Q_{AH} is the heat absorbed at the hot spot location, W.

Q_{LH} is the heat lost at the hot spot location, W.

$$Q_{GH} = L^2\left[P_{dcH}\cdot K_H + \frac{P_{ECH}}{K_H}\right] \tag{6.29}$$

$$K_H = \frac{\Theta_H + \Theta_K}{\Theta_{HR} + \Theta_K} \tag{6.30}$$

where,

L is the per unit load

Θ_H is the winding hot spot temperature, °C.

P_{dcH} are the winding losses due to the dc resistance at the hot spot location.

P_{ECH} are the winding losses due to the eddy currents at the hot spot location.

K_H is the temperature factor for the change in resistance with temperature at the hot spot location: 234.5 for copper, 225 for Aluminium

Θ_H is the temperature at the hot spot location, °C.

Θ_{HR} is the rated temperature at the hot spot location, °C.

The heat absorbed at the hot spot at any instant *t* is

$$Q_{AH} = M_H C p_H \frac{d\Theta_H}{dt} \tag{6.31}$$

The hot spot equation presented in [9] and [40] used the total winding losses and hence the total winding thermal capacitance. This equation is modified using the calculated highest losses at the hot spot location and the calculated thermal capacitance at the hot spot location as follows [50]:

$$M_H Cp_H = \frac{(P_{dcH} + P_{ECH})\tau_H}{\Theta_{HR} - \Theta_{WOR}} \tag{6.32}$$

where,

M_H is the mass of windings at the hot spot location, kg

Cp_H is the specific heat of the windings, W.min/kg .°C.

τ_H is the windings time constant at the hot spot location, min.

Θ_{WOR} is the rated temperature of the oil in the ducts at the hot spot location, °C.

$$Q_{LH} = \left[\frac{\Theta_H - \Theta_{WO}}{\Theta_{HR} - \Theta_{WOR}}\right]^{5/4} \left[\frac{\mu_{HR}}{\mu_H}\right]^{1/4} (P_{dcH} + P_{ECH}) \tag{6.33}$$

where,

Θ_{WO} is the temperature of the oil in the ducts at the hot spot location, °C.

μ_{WH} is the viscosity of the oil film at the hot spot location at time instant *t,* Centipoise.

μ_{HR} is the rated viscosity of the oil film at the hot spot location, Centipoise.

Substituting (6.29), (6.31) and (3.33) into (6.28) gives

$$L^2\left[P_{dcH}\cdot K_H + \frac{P_{ECH}}{K_H}\right] = M_H Cp_H \frac{d\Theta_H}{dt} + \left[\frac{\Theta_H - \Theta_{WO}}{\Theta_{HR} - \Theta_{WOR}}\right]^{5/4} \left[\frac{\mu_{HR}}{\mu_H}\right]^{1/4} \left(P_{dcH} + P_{ECH}\right) \tag{6.34}$$

Average oil equation

The equation to determine the oil temperature is

$$Q_{LW} + Q_{GC} + Q_{GSL} = Q_{AO} + Q_{LO} \tag{6.35}$$

where,

Q_{LW} is the heat lost by the windings, W.

Q_{GC} is the heat generated by the core losses, W.

Q_{GSL} is the heat generated by stray losses, W.

Q_{AO} is the heat absorbed by the tank core oil, W.

Q_{LO} is the heat lost by the oil, W.

The heat generated by the core losses for normal excitation is assumed constant as they are determined by system voltages.

$$Q_{GC} = P_{CR} \tag{6.36}$$

where

P_{CR} are the rated core losses, W.

As noted in this model, transformers subject to an over-excitation, which increases the core losses, can be included in the model.

The heat generated by stray losses

$$Q_{G-OSL} = L^2 \left[\frac{P_{OSL}}{K_W} \right] \tag{6.37}$$

where,

P_{OSL} are the rated other stray losses, W.

The heat absorbed by the tank, core and oil is given by

$$Q_{AO} = \sum MCp \frac{d\Theta_O}{dt} \tag{6.38}$$

$$\sum MCp = M_T Cp_T + M_C Cp_C + M_O Cp_O$$

where,

Θ_O is the average oil temperature, °C.

M_T is the mass of the tank, kg.

Cp_T is the specific heat of the tank, W.min/kg °C.

M_C is the mass of the core, kg.

Cp_C is the specific heat of the core, W.min/kg °C.

M_O is the mass of oil, kg.

Cp_O is the specific heat of the oil, W.min/kg °C.

The heat lost to the ambient air

$$Q_{LO} = \left[\frac{\Theta_O - \Theta_A}{\Theta_{OR} - \Theta_{AR}} \right]^{1/y} (P_T) \tag{6.39}$$

where,

Θ_A is the ambient air temperature, °C.

Θ_{AR} is the rated ambient air temperature, °C.

P_T are the rated total losses, W.

y is 0.8 for OA, 0.9 for FA and NDFOA, and 1.0 for DFOA.

Substituting (6.36), (6.37), (6.38) and (6.39) into (6.35) gives

$$Q_{LW} + P_C + L^2 \left[\frac{P_{SL}}{K_W} \right] = \sum MCp \frac{d\Theta_O}{dt} + \left[\frac{\Theta_O - \Theta_A}{\Theta_{OR} - \Theta_{AR}} \right]^{1/y} (P_T) \tag{6.40}$$

Top and bottom oil equation

The top and bottom oil temperatures are determined similar to the duct oil rise equation:

$$\Theta_{TO} - \Theta_{BO} = \Delta\Theta_{TB} = \left[\frac{Q_{LO}}{P_T}\right]^Z \left(\Theta_{TOR} - \Theta_{BOR}\right) \tag{6.41}$$

where

Θ_{TOR} is the rated top oil temperature, °C.

Θ_{BOR} is the rated bottom oil temperature, °C.

$\Delta\Theta_{TB}$ is the top to bottom oil temperature difference, °C.

Z is 0.5 for OA and FA, and 1.0 for NDFOA and DFOA.

The heat lost by the oil to the duct oil is given by (6.39).
The top and bottom oil temperatures are

$$\Theta_{TO} = \Theta_O + \frac{\Delta\Theta_{TB}}{2} \tag{6.42}$$

$$\Theta_{BO} = \Theta_O - \frac{\Delta\Theta_{TB}}{2} \tag{6.43}$$

Fluid Viscosity

The fluid viscosity is highly temperature dependent. The fluid viscosity at any temperature can be obtained using

$$\mu = B \cdot e^{C/(\Theta+273)} \tag{6.44}$$

where,

μ is the fluid viscosity, Centipoise.

B is a constant

C is a constant

Θ is the temperature used to calculate the viscosity, °C.

The constants *B* and *C* have different values for the different fluids used in transformers. For example, *B* and *C* for oil are 0.0013573 and 2797.3, respectively [41]. The temperature used for calculating viscosity is given in the following table

Table 6.2 Viscosity terms and model equations

Equation	Viscosity term	Temperature used for calculation
6.22	μ_{WR}	$(\Theta_{WR} + \Theta_{DAOR}) / 2$
6.22	μ_{W}	$(\Theta_{W} + \Theta_{DAO}) / 2$
6.33	μ_{HR}	$(\Theta_{HR} + \Theta_{WOR}) / 2$
6.33	μ_{H}	$(\Theta_{H} + \Theta_{WO}) / 2$

6.4.2 The simulation model

Fig. 6.5 shows the simplified diagram for the thermal dynamic model. The continuous form of equations (6.23) (6.24) (6.34) (6.40) and (6.41) are solved using Simulink. Different numerical techniques and different time steps can be assigned to obtain the required level of accuracy (see Appendix III for model details).

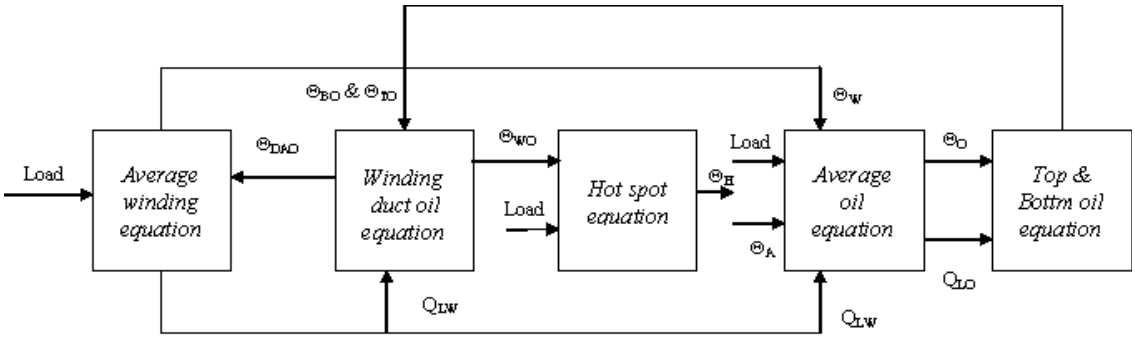

Fig. 6.5 Simplified model of IEEE Annex G

The block diagram to solve the hot spot temperature equation is shown in Fig. 6.6.

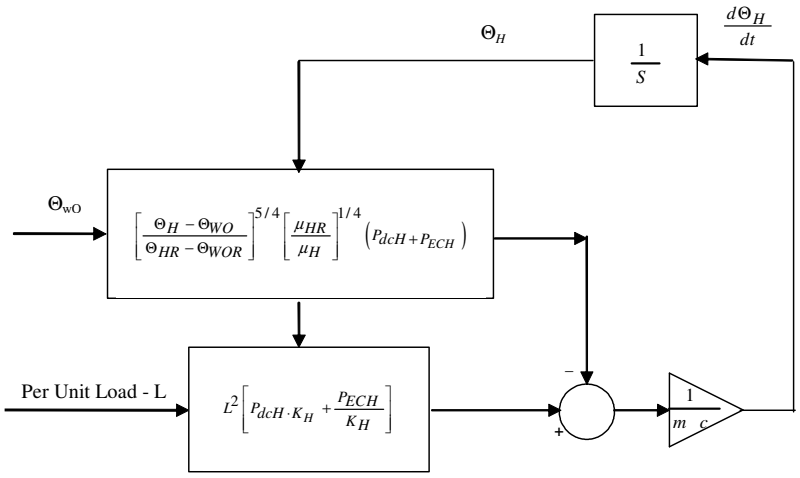

Fig. 6.6 Block diagram for the hot spot equation

6.4.3 Example calculation for a 250 MVA transformer

For this example the transformer data needed for the thermal model are as follows:

Table 6.3 Transformer characteristics of the 250 MVA unit

Transformer Losses, W.		
No Load	78100	
P_{dc} losses ($I^2 R_{dc}$)	411780	
Eddy losses	41200	
Stray losses	31660	
	118 KV	230KV
P_{dc} at hot spot location	467	527
Eddy current losses at hot spot location	309 (0.65 pu)	157 (0.3 pu)
Per unit height to winding hot spot	1	1

Temperature Rise °C.

Rated top oil rise	38.3	
Rated top duct oil rise	38.8	
Rated hot spot rise	58.6	50.8
Rated average winding rise	41.7	39.7
Rated bottom oil rise	16	
Initial top oil	38.3	
Initial top duct oil	38.3	
Initial average winding	33.2	
Initial bottom oil	28	
Initial hot spot	38.3	
Transformer component weights, kg		
Mass of core and coil assembly	172200	
Mass of tank	39700	
Mass of oil	37887	
Transformer exponents		
Based on the type of cooling		
x	0.5	
y	0.9	
z	0.5	
Other Exponents		
n	0.25	
B	0.0013573	
C	2797.3	
Cp oil	13.92×2.2	
Cp steel	3.51×2.2	
Cp copper	2.91×2.2	

The data were taken from the transformer manufacturer's test report and the FEM model developed in this thesis.

The calculated top oil temperature compared with measured is shown in Fig. 6.7, and which indicates that it is lower than the measured temperature.

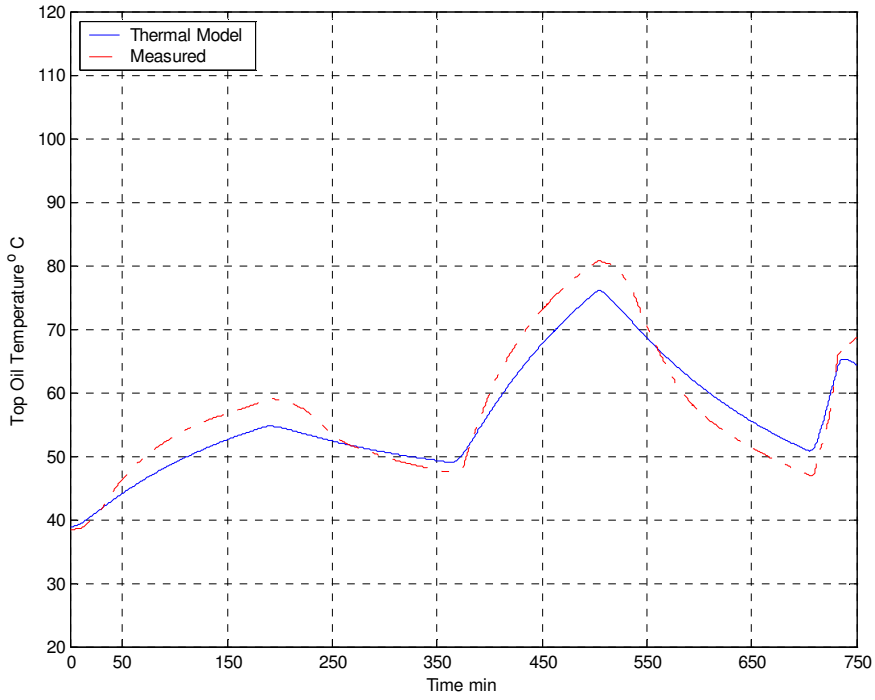

Fig. 6.7 The calculated top oil temperature compared with measured

The hot spot temperature for each individual winding can be calculated according to the losses concentrated in the top of the winding. Figs. 6.8 and 6.9 show the calculated hot spot temperature of the 118 kV and 230 kV windings compared with the measured temperature. It can be seen that the calculated hot spot temperature for both windings is in good agreement with the measured.

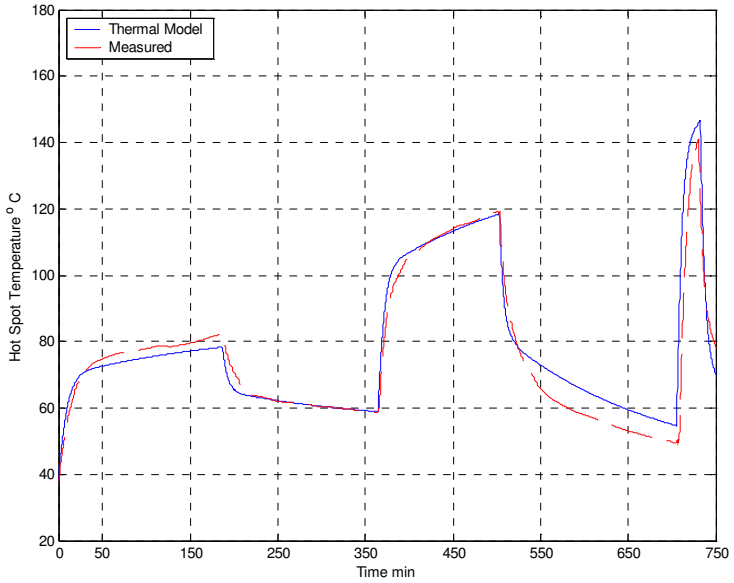

Fig. 6.8 The calculated hot spot temperature of the 118 kV winding compared with the measured

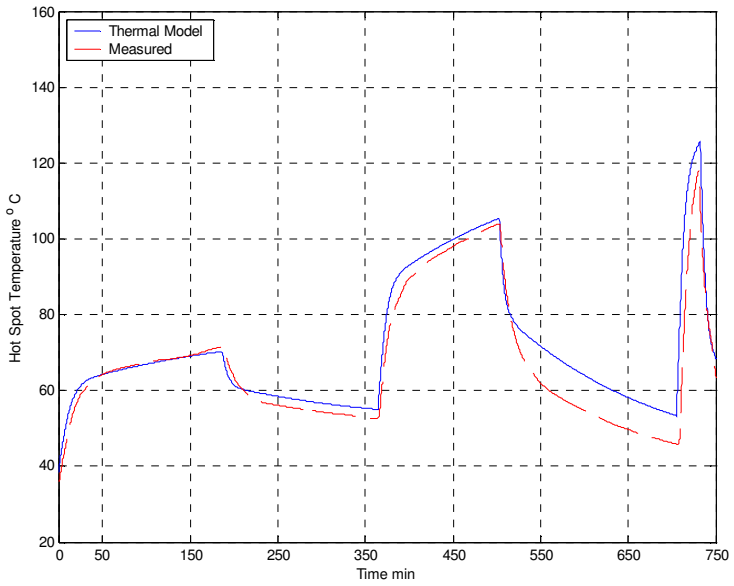

Fig. 6.9 The calculated hot spot temperature of the 230 kV winding compared with the measured

6.5 Thermal model based on an electrical -thermal equivalent circuit

A thermal model of a power transformer in the form of an equivalent circuit based on the fundamentals of heat transfer theory has been suggested by Swift in [44]. The proposed

thermal model was established to determine the hot spot temperature. The top oil temperature was calculated from the air-to-oil model. The top oil temperature becomes the ambient temperature for the winding to oil model.

Based on this approach a model which considers the non-linear thermal oil resistance has been introduced by Susa [46]. The oil viscosity changes and loss variation with temperature were included in the method. The model was shown to be valid for different transformer units.

In this thesis a hot spot model equation based on [44] is presented. The model is analogous to the top oil model equation. The losses used in the model are the estimated highest losses that generate the heat at a specific location in the LV or HV winding. The model is easy to implement and is validated by comparison with measured results.

6.5.1 Background

There is an analogy between an electrical circuit and a thermal circuit as shown in the table below. Due to the similarity between heat transfer and electric charge transport, an equivalent electrical circuit can be used to solve the heat transfer problem.

Table 6.4 Analogy between thermal and electric quantities

Thermal	Electrical
Heat transfer rate *q,* watt	Current, *i* amps
Temperature Θ, °C	Voltage, v volts
Thermal resistance R_{th}, °C/watt	Resistance, R Ω
Thermal capacitance, joules/ °C	Capacitance, farads

In transformers, oil is typically used as the coolant. The heat generated by losses in transformers is taken up by the oil and carried into a heat exchanger, which in most cases is an oil-air cooler. The cooler dissipates heat to the surroundings by natural or forced flow.

The non linear thermal resistance is related to the many physical parameters of an actual transformer. The exponent defining the non linearity is traditionally *n* if the moving fluid is air and *m* if it is oil.

6.5.2 Top oil thermal model

The top oil thermal model is based on the equivalent thermal circuit shown in Fig. 6.11. A simple RC circuit is employed to predict the top oil temperature Θ_{ol}.

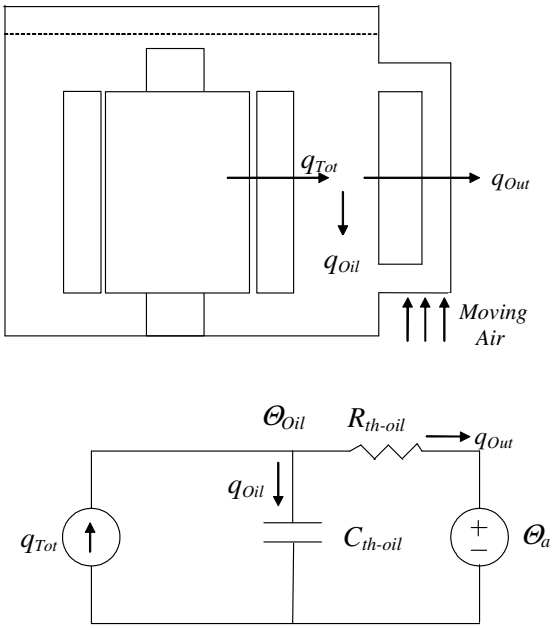

Fig.6.11 Thermal model for top oil temperature

In the thermal model all transformer losses are represented by a current source injecting heat into the system. The capacitances are combined as one lumped capacitance. The thermal resistance is represented by a non-linear term.

The differential equation for the equivalent circuit is

$$q_{Tot} = C_{th-oil}\frac{d\Theta_{oil}}{dt} + \frac{1}{R_{th-oil}}\left[\Theta_{oil} - \Theta_A\right]^{1/n} \tag{6.46}$$

where,

q_{Tot} is the heat generated by total losses, W

C_{th-Oil} is the oil thermal capacitance W.min/° C,

R_{th-Oil} is the oil thermal resistance° C/W,

Θ_{oil} is the top oil temperature, ° C.

Θ_A is the ambient temperature, ° C.

n is the exponent that defines the non-linearity

Equation (6.46) is then reduced as in [44]

$$\frac{I_{pu}^2\beta + 1}{\beta + 1}\cdot\left[\Delta\Theta_{oil-R}\right]^{1/n} = \tau_{oil}\frac{d\Theta_{Oil}}{dt} + \left[\Theta_{oil} - \Theta_A\right]^{1/n} \tag{6.47}$$

where,

I_{pu} is the load current per unit.

β is the ratio of load to no-load losses, conventionally R

τ_{oil} is the top oil time constant, min.

$\Delta\Theta_{oilR}$ is the rated top oil rise over ambient, K.

The non-linear thermal resistance is related to the many physical parameters of an actual transformer. The most convenient and commonly used form is

$$q = \frac{1}{R_{th-R}}\cdot\Delta\Theta^{1/n}$$

The exponent defining the non linearity is traditionally n.

If the cooling is by natural convection, the cooling effect is more than proportional to the temperature difference because the air flow will be faster, i.e. the convection will be greater. A typical value for *n* is 0.8, which implies that the heat flow is proportional to the 1.25^{th} power of the temperature difference. If the air is forced to flow faster by fans then *n* may increase. There is another effect: R_{th-R} becomes much lower, i.e., the cooling is more effective.

The oil to air model is validated by 250 MVA transformer measurements in the field [45].

6.5.3 Winding hot spot thermal model

In the thermal model the calculated winding losses generate the heat at the hot spot location. The thermal resistance of the insulation and the oil moving layer is represented by a non-linear term. The exponent defining the non linearity is traditionally *m*. The typical value used for *m* is 0.8.

The hot spot thermal equation is based on the thermal lumped circuit shown in Fig. 6.12. [51].

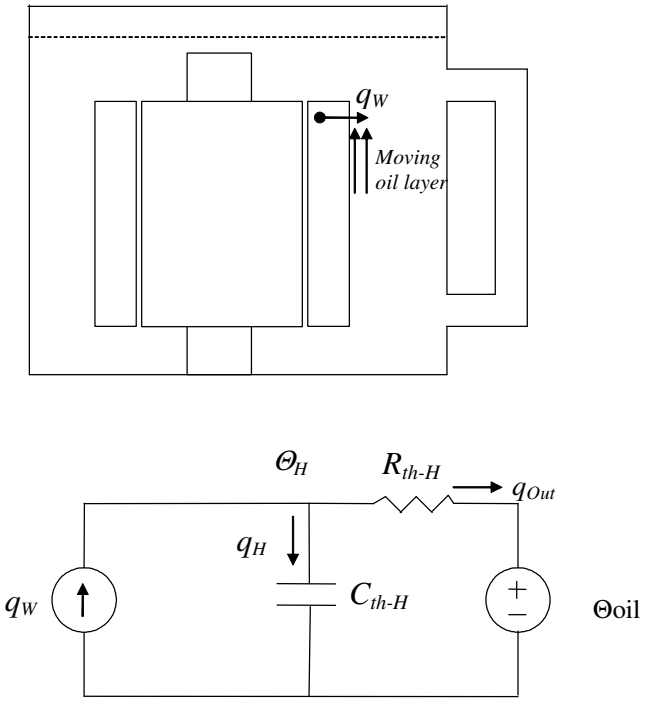

Fig.6.12 Thermal model for hot spot temperature

The differential equation for the equivalent circuit is

$$q_W = C_{th-H}\frac{d\Theta_H}{dt} + \frac{1}{R_{th-H}}\left[\Theta_H - \Theta_{oil}\right]^{1/m} \tag{6.48}$$

where,

q_W is the heat generated by losses at the hot spot location, W.

C_{th-H} is the winding thermal capacitance at the hot spot location, W.min/° C.

R_{th-H} is the thermal resistance at the hot spot location, ° C/W.

Θ_H is the hot spot temperature, ° C.

m is the exponent defining non-linearity.

Equation (6.48) is then reduced to:

$$\frac{I_{pu}^2\left[1+P_{EC-R(pu)}\right]}{1+P_{EC-R(pu)}}\cdot\left[\Delta\Theta_{H-R}\right]^{1/m} = \tau_H\frac{d\Theta_H}{dt} + \left[\Theta_H - \Theta_{oil}\right]^{1/m} \tag{6.49}$$

where

$P_{EC-R(pu)}$ are the rated eddy current losses at the hot spot location

$\Delta\Theta_{H-R}$ is the rated hot spot rise over ambient, K.

τ_H is the winding time constant at the hot spot location, min.

The variation of losses with temperature is included in the equation above using the resistance correction factor.

6.5.4 The simulation model

Fig 6.12 shows a simplified diagram of the thermal dynamic model. Equations (6.47) and (6.49) are solved using Simulink. At each discrete time the top oil temperature Θ_{oil} is calculated and it becomes the ambient temperature in the calculation of the hot spot Θ_H.

Different numerical techniques and different time steps can be assigned for accuracy (see Appendix III for model details).

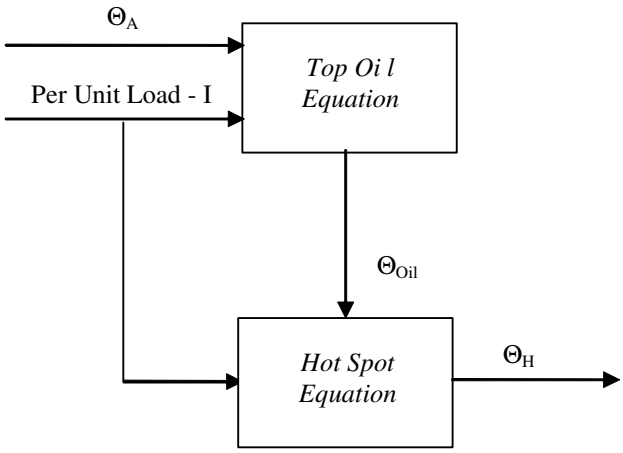

Fig.6.13 Simplified transformer thermal model

A block diagram of the hot spot model is shown in Fig. 6.14.

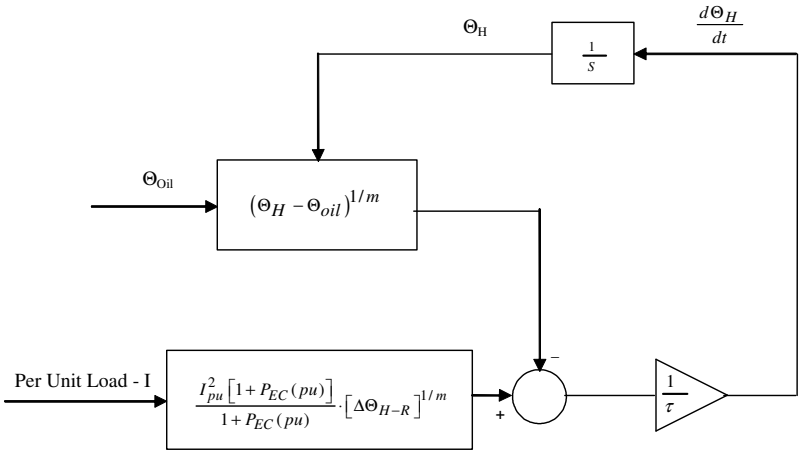

Fig. 6.14 Block diagram of the winding hot spot model

6.5.5 Example calculation for a 250 MVA transformer

For this example the transformer input parameters needed for the thermal model are as follows:

Table 6.5 Thermal model parameters

Rated top oil rise over ambient	38.3 ° C
Rated hot spot rise over top oil	20.3 ° C
Ratio of load losses to no load losses	6.20
pu eddy current losses at hot spot location, LV	0.65
pu eddy current losses at hot spot location, HV	0.3
Top oil time constant	170 min
Hot spot time constant	6 min
Exponent *n*	0.9
Exponent *m*	0.8

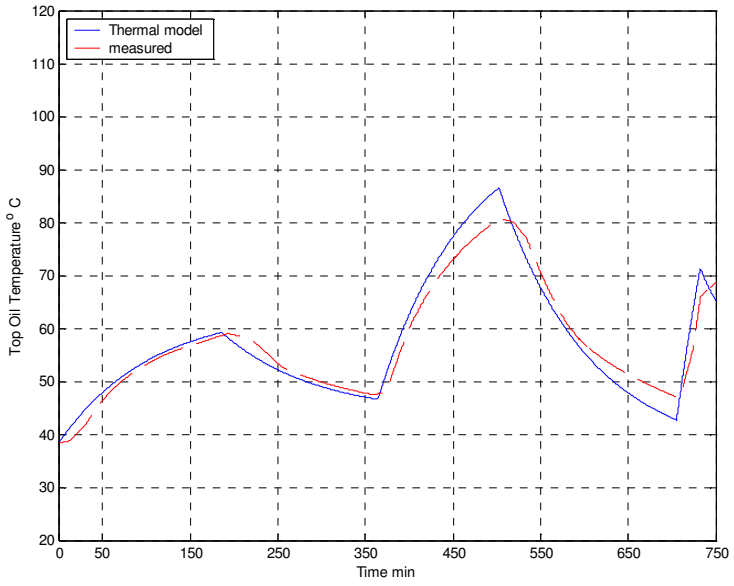

Fig. 6.15 The calculated top oil temperature compared with measured

Fig. 6.15 shows the calculated top oil temperature to be in good agreement with the measured temperature. The same applies to the hot spot temperature of the 118 kV and 230 kV windings, as shown in Figs. 6.16 and 6.17, respectively. The model gives a more accurate temperature predictions compared to the IEEE loading guide [52].

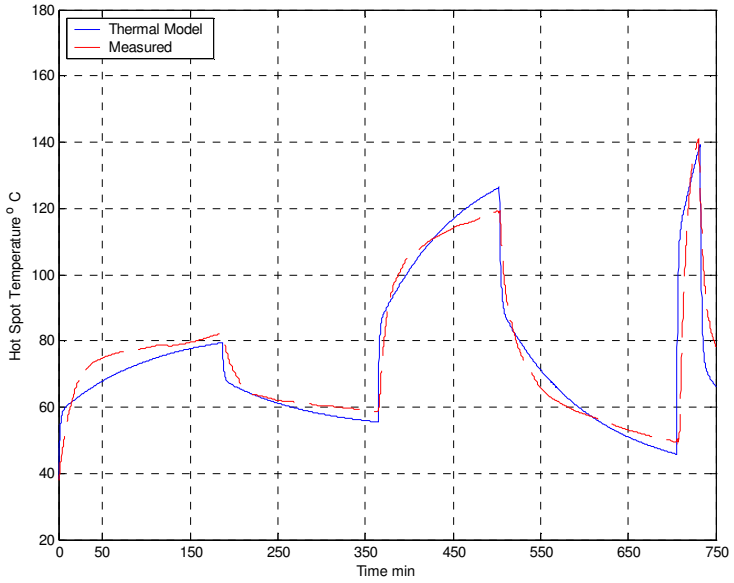

Fig. 6.16 The calculated hot spot temperature of the 118 kV winding compared with measured

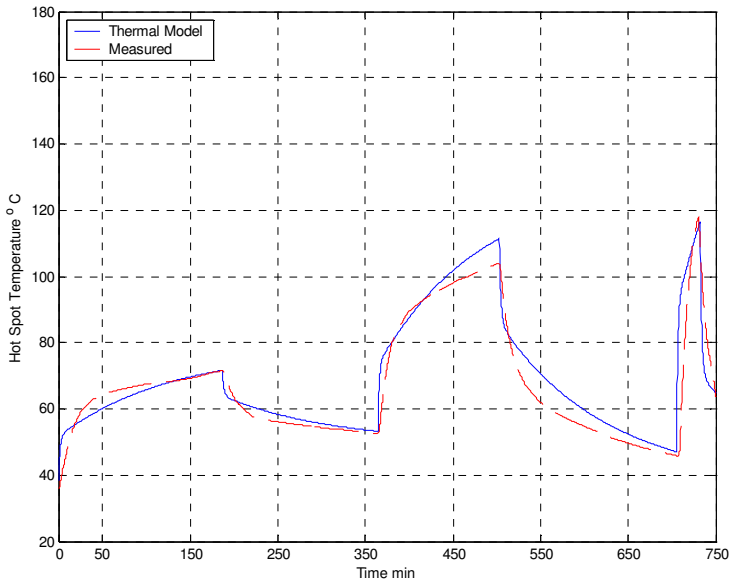

Fig. 6.17 The calculated hot spot temperature of the 230 kV winding compared with measured

6.5.6 Example calculation of a 2500 kVA transformer

The parameters used for this example of the hot spot calculation are based on factory measurements published in [47] and FEM calculations.

Table 6.4 Thermal model parameters

Rated top oil rise over ambient	48 ° C
Rated hot spot rise over top oil	17.9 ° C
Ratio of load losses to no load losses	5.44 ° C
pu eddy current losses at the hot spot location	0.13
Top oil time constant	190 min
Hot spot time constant	7 min
Exponent *n*	0.9
Exponent *m*	0.8

The transformer was tested under the load shown in Fig. 6.18 and the top oil and the hot spot temperatures were recorded in the factory.

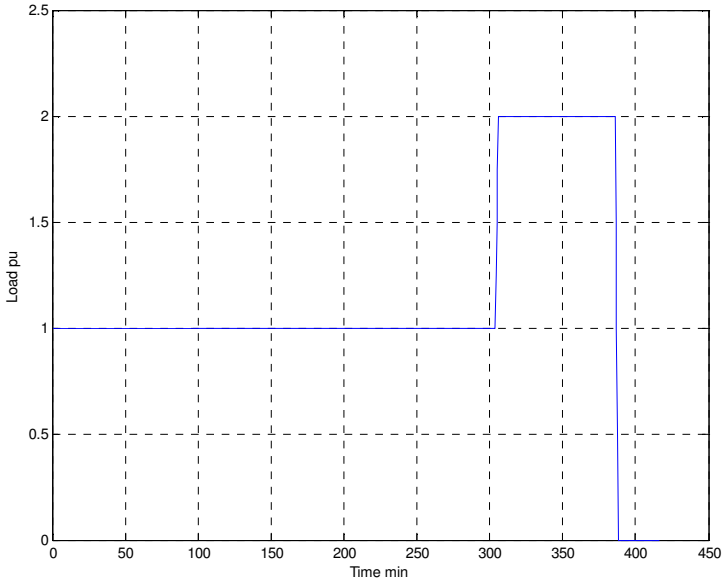

Fig. 6.18 2500 kVA transformer load used in the test

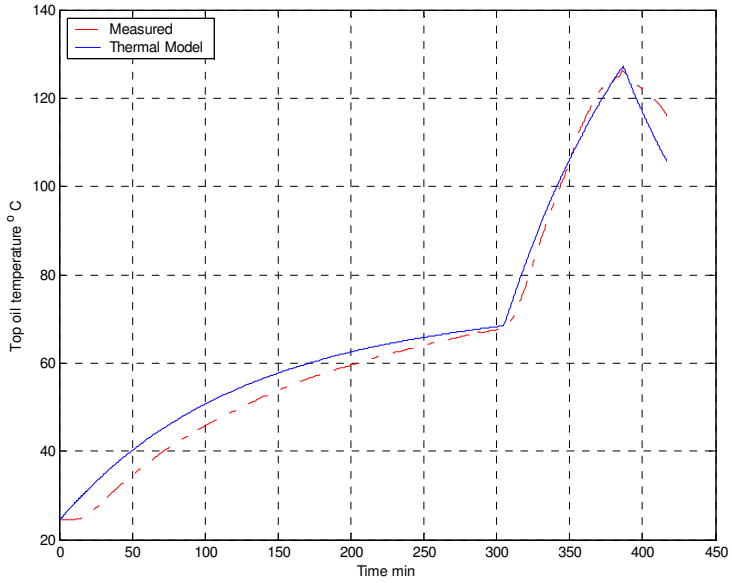

Fig.6.19 The calculated top oil temperature compared with measured

The transformer hot spot temperature was calculated using the thermal model with the transformer data shown in the above table and compared with the measured temperatures shown in Fig. 6.19 for the top oil and in Fig. 6.20 for the HV winding hot spot.

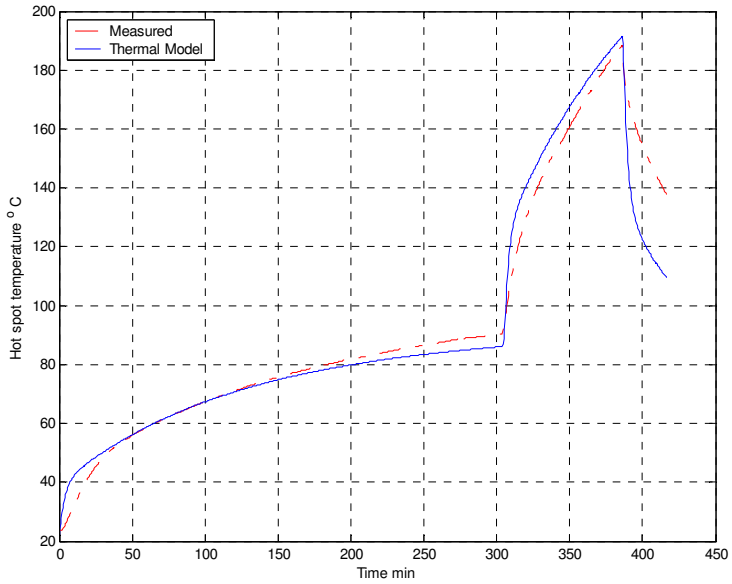

Fig. 6.20 The calculated hot spot temperature of the HV winding compared with measured

Chapter Seven

Dynamic Thermal Modelling in the Presence of Non-sinusoidal Load Currents

The international IEEE and IEC guides [27] [28] give a conservative approach to check the transformer steady state temperature rises to which industrial or distribution transformers would be subjected while in service. An accurate and applicable method is needed to estimate the effect of harmonics on the transformer hot spot temperature and hence on the transformer loss of life. Such a method should consider distorted load cycle variation on the transformer hot spot temperature.

The aim of this chapter is to modify the thermal dynamic models in order to consider a distorted load cycle variation, i.e. the real operating conditions that a transformer is subject to. The model needs to be able to evaluate the loading capability of both existing transformers and new installations. The model has to be accurate and easy to use for practical application.

7.1 Predicting transformer temperature rise and loss of life in the presence of harmonic load currents

Power system harmonic distortion can cause additional losses and heating leading to a reduction of the expected normal life. The load ability of a transformer is usually limited by the allowable winding hot spot temperature and the acceptable loss of insulation life (ageing) owing to the hot spot heating effect.

Existing loading guides have been based on the conservative assumptions of constant daily peak loads and the average daily or monthly temperatures to which a transformer would be subjected while in service.

To correctly predict transformer loss of life it is necessary to consider the real distorted load cycle in the thermal model. This would predict the temperatures more accurately and hence the corresponding transformer insulation loss of life (ageing). Other forms of deterioration caused by ageing are not considered in the analysis and the approach here is limited to the transformer thermal insulation life.

Based on the existing loading guides the impact of non-sinusoidal loads on the hot spot temperature have been studied in [39], [48] and [49]. In order to estimate the transformer loss of life correctly, it is necessary to take into account the real load (harmonic spectrum), ambient variations and the characteristics of transformer losses.

7.1.1 Transformer loading guides

The equations to calculate the hot spot temperature should be modified to account for the increase in winding losses and the corresponding temperature rise. The load ratio must account for the non-linear currents introduced. The modified equations become

The top oil equation (6.3):

$$\frac{1+R.K^2}{1+R} = \left[\frac{P_{NL} + \left(\sum_{h=1}^{h=\max} \frac{I_h^2}{I_R^2}.P_{dc} + P_{EC} \sum_{h=1}^{h=\max} \frac{I_h^2}{I_R^2} h^2 + P_{OSL} \sum_{h=1}^{h=\max} \frac{I_h^2}{I_R^2} h^{0.8} \right)}{P_{NL-R} + P_{LL-R}} \right] \tag{7.1}$$

The hot spot equation (6.6):

$$K^2 = \frac{\sum_{h=1}^{h=\max} \frac{I_h^2}{I_R^2} + P_{EC-R(pu)} \sum_{h=1}^{h=\max} \left(\frac{I_h}{I_R} \right)^2 h^2}{1+P_{EC-R(pu)}} \tag{7.2}$$

When applying the above equation, the left hand side term is replaced by the right hand side in (6.3) and (6.6).

7.1.2 IEEE Annex G

The loading equations presented in [41] separate eddy and stray losses from the losses due to the winding resistance. This allows for the consideration of oil and winding heating effects due to increased stray and eddy losses when harmonic currents are present. The model is modified to consider non-linear currents as follows:

The average winding equation (6.23):

$$L^2.\left[P_{dc} \cdot K_W + \frac{P_{EC}}{K_W} \right] = \left[\sum_{h=1}^{h=\max} \frac{I_h^2}{I_R^2}.P_{dc} \cdot K_W + \frac{P_{EC} \cdot \sum_{h=1}^{h=\max} \frac{I_h^2}{I_R^2} h^2}{K_W} \right] \tag{7.3}$$

The hot spot equation (6.34):

$$L^2.\left[P_{dcH}\cdot K_H+\frac{P_{ECH}}{K_H}\right]=\sum_{h=1}^{h=\max}\frac{I_h^2}{I_R^2}\left[\sum_{h=1}^{h=\max}\frac{I_h^2}{I_R^2}P_{dcH}\cdot K_H+\frac{P_{ECH}\sum_{h=1}^{h=\max}\frac{I_h^2}{I_R^2}h^2}{K_H}\right] \tag{7.4}$$

The average oil equation (6.40):

$$L^2.\left[\frac{P_{OSL}}{K_W}\right]=\left[\frac{P_{OSL}\sum_{h=1}^{h=\max}\frac{I_h^2}{I_R^2}h^{0.8}}{K_W}\right] \tag{7.5}$$

7.1.3 Thermal model based on the electrical-thermal circuit

The thermal model has to be modified to account for the increased losses due to the harmonic currents as follows [53]:

The top oil equation (6.47):

$$\frac{\beta.I_{pu}^2+1}{\beta+1}=\left[\frac{P_{NL}+(\sum_{h=1}^{h=\max}\frac{I_h^2}{I_R^2}P_{dc}+P_{EC}\sum_{h=1}^{h=\max}\frac{I_h^2}{I_R^2}h^2+P_{OSL}\sum_{h=1}^{h=\max}\frac{I_h^2}{I_R^2}h^{0.8})}{P_{NL-R}+P_{LL-R}}\right] \tag{7.6}$$

The hot spot equation (6.49):

$$\frac{I_{pu}^2\left[1+P_{EC-R}(pu)\right]}{1+P_{EC-R(pu)}}=\frac{\frac{\sum_{h=1}^{h=\max}I_h^2}{I_R^2}+P_{EC-R(pu)}\sum_{h=1}^{h=\max}h^2\frac{I_h^2}{I_R^2}}{1+P_{EC-R(pu)}} \tag{7.7}$$

For high order harmonics and large winding conductors, the corrected harmonic loss factor (5.18) is used to account for the fact that the flux may not totally penetrate the conductors. The hot spot equation would then be modified as follows:

$$\frac{I_{pu}^2\left[1+P_{EC-R}(pu)\right]}{1+P_{EC-R(pu)}}=\frac{\dfrac{\sum_{h=1}^{h=\max} I_h^2}{I_R^2}+P_{EC-R(pu)}\sum_{h=1}^{h=\max} F_{WE}\dfrac{I_h^2}{I_R^2}}{1+P_{EC-R(pu)}} \tag{7.8}$$

where, the corrected loss factor F_{WE} is calculated as presented in section 5.3, in equations (5.13) and (5.18).

Example Calculation for the 2500 KVA transformer

The transformer was tested under a 0.62 pu load at 250 Hz. The top oil and hot spot temperatures were recorded in the factory. The thermal model equations (7.6) and (7.7) and transformer data were used to calculate the transformer temperatures and are compared with measurements.

The measured and calculated temperatures for 0.62 pu and 250 Hz frequency are shown in Figs. 7.1 and 7.2

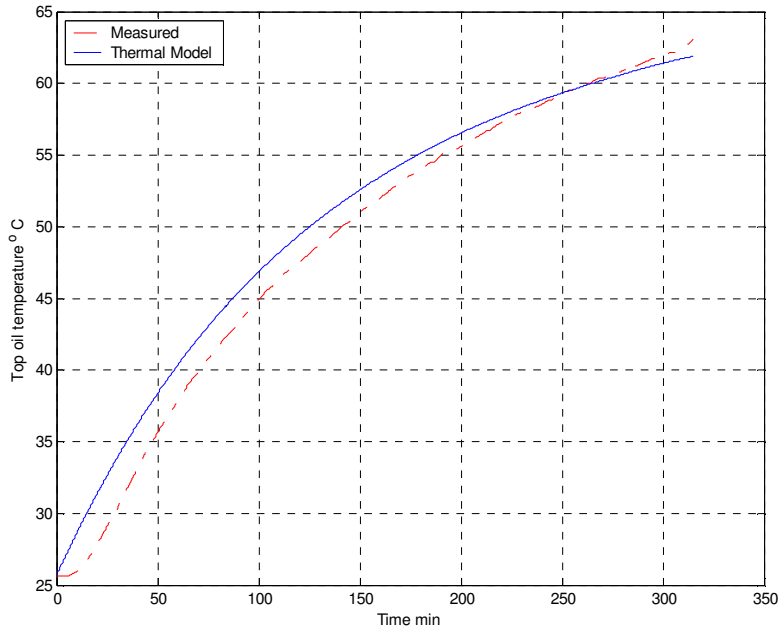

Fig. 7.1 The calculated top oil temperature compared with measurements

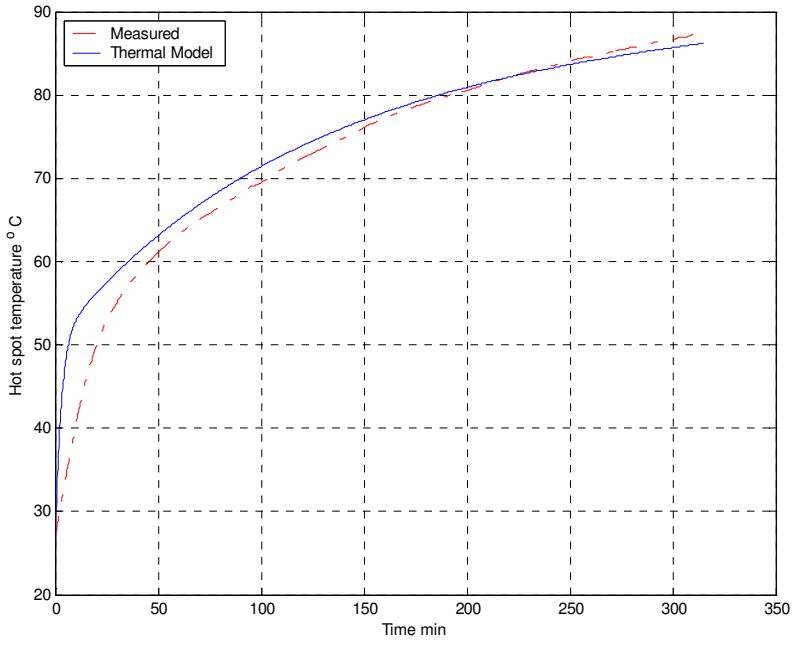

Fig. 7.2 The calculated hot spot temperature of the HV winding compared with measurements

It can be seen that the calculated top oil and hot spot temperatures are fairly in good agreement with measurements.

Example Calculation for the 31.5 MVA transformer [53]

Consider that the 31.5 MVA transformer is subject to a real daily load cycle profile and ambient temperature for a peak summer day as shown in Figs. 7.3 and 7.4 respectively. The load cycle is presented without harmonics. Then the transformer is assumed to be subject to distorted loads with THDs of about 21.6% and 10 %. The spectrum used is shown in Fig. 7.5. The assumed harmonics include major harmonics 5th, 7th, 11th, 13th, 17th, 19th, 23th and 25th.

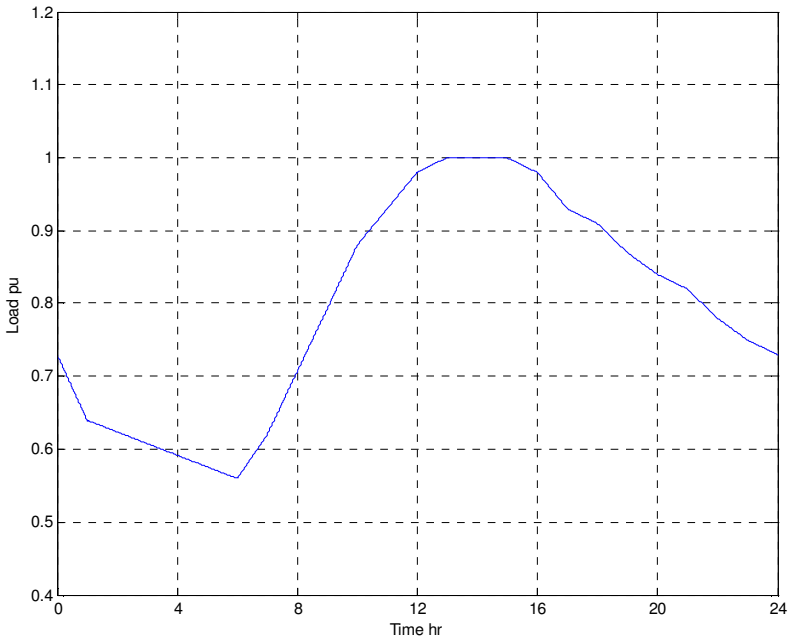

Fig. 7.3 Load cycle considered for the transformer

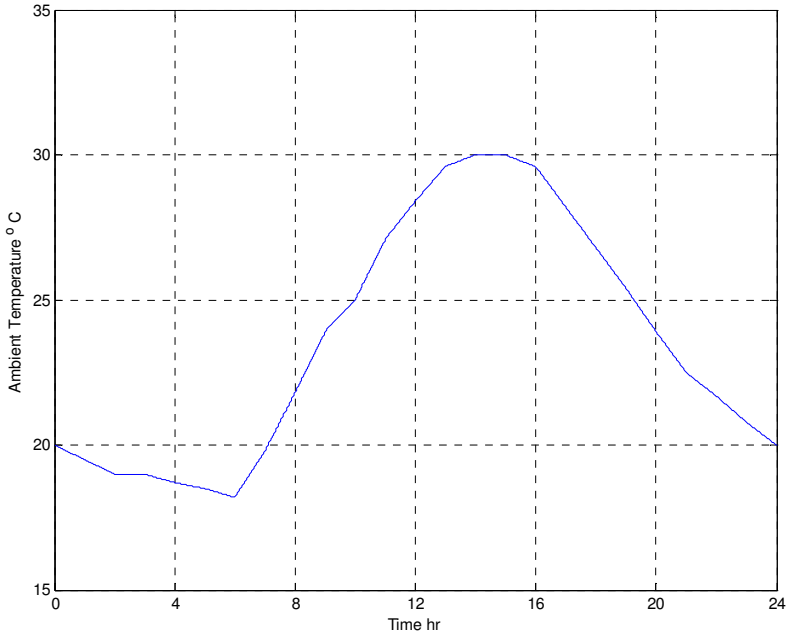

Fig. 7.4 Ambient temperature

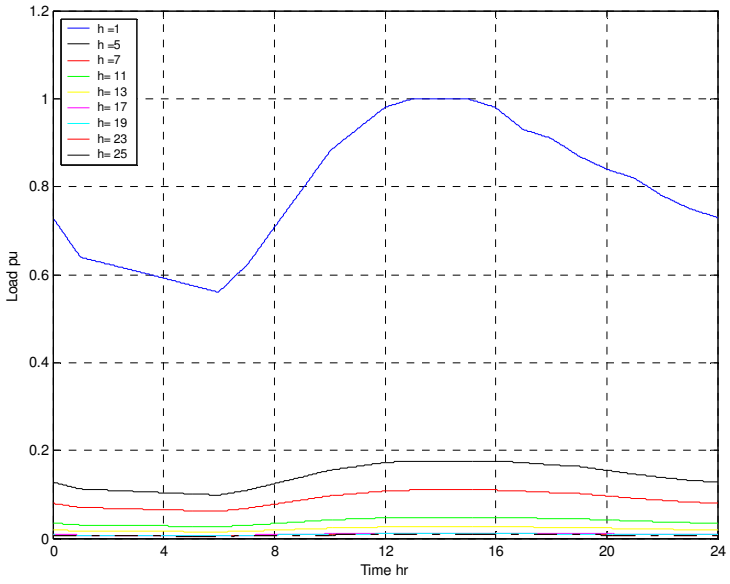

Fig. 7.5 Distorted load cycle with THD= 21.5%

Fig. 7.6 shows the top oil temperature for the assumed harmonics produced by the load supplied by the transformer. The THD of 21.5% gives a temperature rise about 8.5 °C

above the temperature where there are no harmonics, whereas the increase is just 2 °C for a THD of 10 % when compared with the rise that occurs if there are no harmonics.

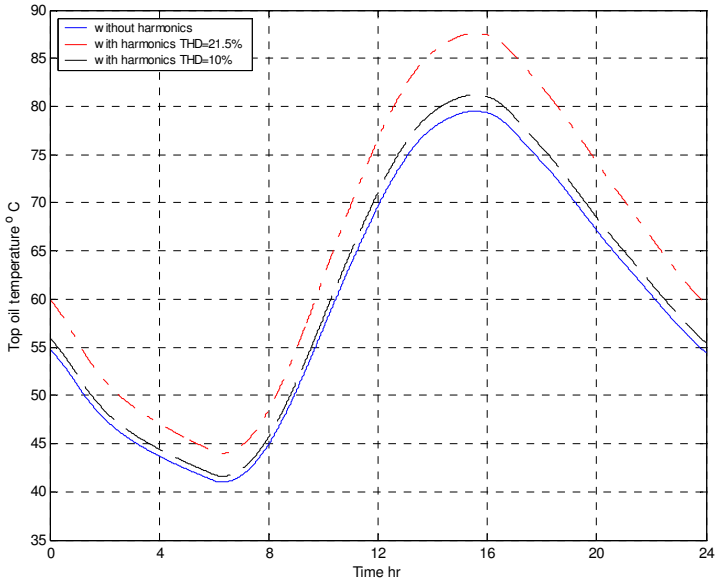

Fig.7.6 The calculated top oil temperature of the secondary winding for different load cycles

The temperature varies according to the distorted load and ambient temperature that the transformer will be subjected to

Fig. 7.7 shows the hot spot temperature for the assumed harmonics produced by the load supplied to the transformer. The THD of 21.5% gives a temperature rise of more than 20 °C above the temperature rise for no harmonics.

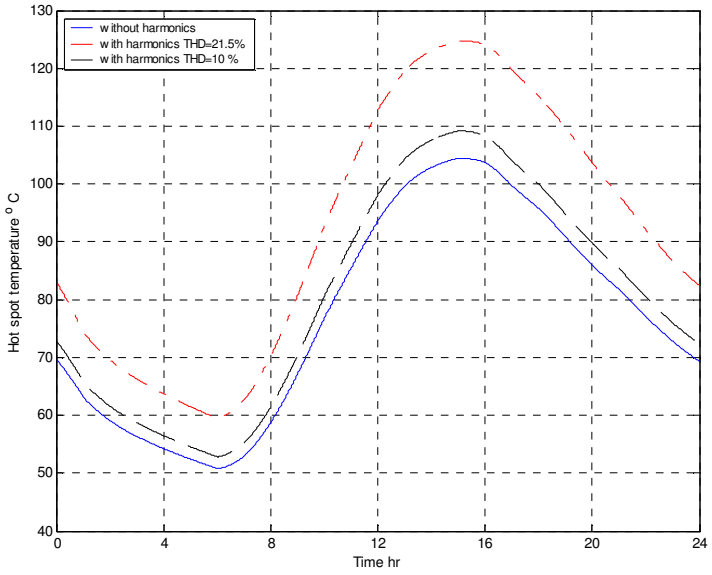

Fig. 7.7 The calculated hot spot temperature of the secondary winding for different load cycles

Fig. 7.8 shows the instant pu loss factor (equivalent ageing factor) for different load cycles. The calculated loss of life factor for the load cycles is shown in Table. 7.1. The pu loss factor for a load cycle with a THD of 21.5% is just below 1.

Table 7.1 Transformer loss of life calculation

	No harmonics	THD=21.6%	THD=10%
Loss of life over a cycle	2.85	23.31	4.95
Load cycle duration	24	24	24
pu loss of life factor	0.12	0.971	0.21

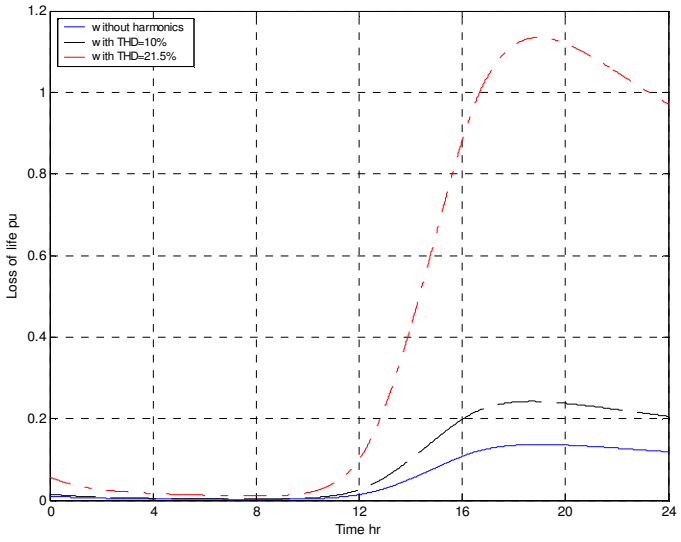

Fig . 7.8 The transformer insulation loss of life for different load cycles, pu

The calculated hot spot temperature and the instant loss factor using the harmonic order square rule is compared with the corrected harmonic pu loss of life factor for a load cycle with a THD of 21.5%, as demonstrated in Figs. 7.9 and 7.10, respectively.

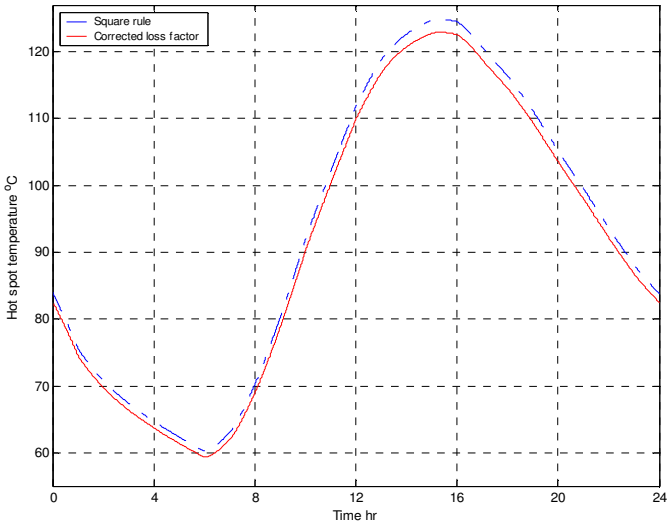

Fig. 7.9 The calculated hot spot temperature of the secondary winding using the square rule and the corrected loss factor for a load cycle with THD=21.5%

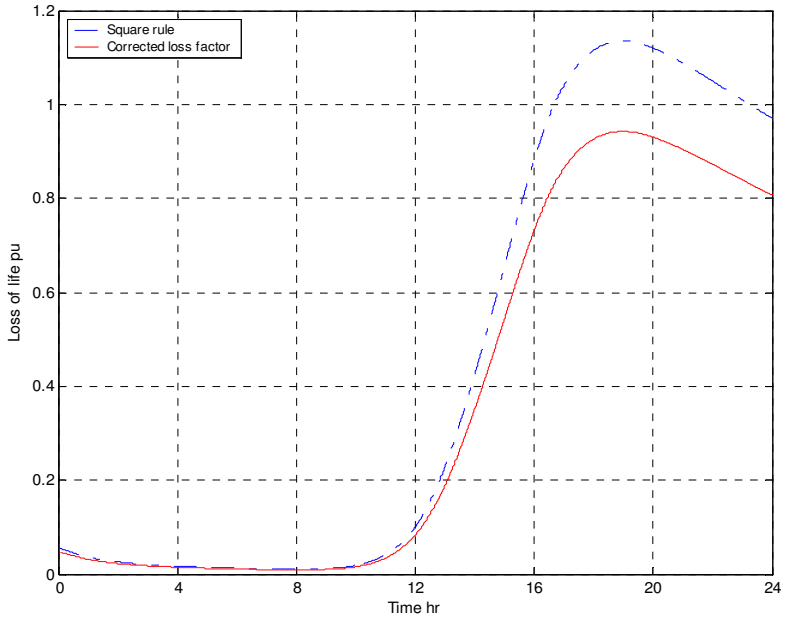

Fig .7.9 Comparison of the transformer insulation loss of life, pu

The calculated pu loss of life factor for the load cycle becomes 0.81, as shown in Table.7.2.

Table 7.2 Transformer loss of life calculation

	Corrected loss factor	Square rule
Loss of life over a cycle	19.38	23.31
Load cycle duration	24	24
pu loss of life factor	0.81	0.971

Chapter Eight
Conclusions

The significance of harmonics in power systems has increased substantially due to the use of solid state controlled loads and other high frequency producing devices. An important consideration in evaluating the impact of harmonics is their effect on power system components and loads. Transformers are major components in power systems. The increased losses due to harmonic distortion can cause excessive winding loss and hence abnormal temperature rise.

An electromagnetic analysis using a finite element model has been adapted to predict transformer winding losses. This can be used to calculate the eddy losses in individual turns/discs to enable location of the winding losses that cause the hot spot and to predict the hot spot factor H.

Conventionally, eddy losses are assumed to vary with the square of the current and the square of the frequency (harmonic order *h*). This assumption is reasonable when conductors are small. For a combination of large conductors and high frequencies, the electromagnetic flux may not totally penetrate the strands in the winding and such an assumption leads to conservative results. A corrected loss factor which considers the skin effect is presented and verified experimentally. This leads to a more accurate prediction of transformer capability when subject to non-sinusoidal load currents.

The differential equations of the loading guides were modelled using Simulink and revealed that the predicted hot spot is not accurate for applied overloads when compared with measurements.

Annex G of the IEEE loading guide equations were modelled in Simulink/Matlab on the basis that at any instant *t* there must be a balance between all energy rates in watts. The hot spot equation is modified using the calculated winding losses that cause the hot spot.

A new thermal model has been established to determine the hot spot temperature. The top oil temperature is calculated from the top oil equation. The top oil temperature becomes the ambient temperature for a hot spot equation model. The equations are modelled in Simulink and validated using transformer data from measurements in the factory.

The increased transformer temperatures due to harmonics are estimated based on a constant harmonic load currents pattern and average daily or monthly temperatures. Transformer loading generally changes with time. It may, for example, operate in an overload condition for a short period followed by a period at less than rated load with different harmonic currents. The thermal model is modified to consider the actual load cycle that a transformer is subjected to while in service. The insulation loss of life is usually taken as a good indicator of transformer loss of life. The pu loss of life function has been developed to assess the effect of distorted load cycle on transformer lifetime.

The main contributions of this thesis can be summarised as

- A FEM model was adapted and used to predict the transformer losses. The knowledge of flux density was used with conductor dimensions to predict the eddy losses for a specific design. The model can be used to calculate the eddy loss in individual turns/discs, to locate the winding hot spot location, and to predict the hot spot factor *H*. Such information is very important for winding hot spot determination.

- A corrected eddy current loss factor was developed that considers the actual flux impinging on the conductor due to the skin effect. The factor can be applied to predict more accurately the transformer increased losses due to harmonics and hence the temperature rise. The factor was verified experimentally.

- The hot spot equation of IEEE Annex G was modified using the calculated winding losses that cause the hot spot. The thermal dynamic model was also modified to consider distorted load cycle variation.

- The winding-to-oil model proposed by Swift was developed to predict the hot spot temperature based on loading, oil temperature and the estimated losses that cause a winding hot spot. The thermal dynamic model was also modified to consider distorted load cycle variation. The model was verified using measured data from a transformer factory.

References

[1] L. W. Pierce, "Transformer design and application consideration for non-sinusoidal load currents," IEEE Trans. on Industry Applications, vol.32, no.3 1996, pp.633-645.

[2] S. A. Stigant and A. C. Franklin, The J & P Transformer Book. 10th ed. New York: Wiley, 1973

[3] J. Lammeraner and M. Stafl, Eddy Currents. London: Iliffe, 1966

[4] R. L. Stool, The Analysis of Eddy Currents. Clarendon, 1974.

[5] O. W. Anderson, "Transformer leakage flux program based on finite element method," IEEE Trans Power Apparatus and systems, vol. PAS-92, 1973, pp.682-689.

[6] R. Komulainen and H. Nordman, "Loss evaluation and use of magnetic and electromagnetic shields in transformers," Paper no. 12-03, CIGRE 1988.

[7] D. Pavlik, D. C. Johnson, and R. S. Girgis, "Calculation and reduction of stray and eddy losses in core form transformers using a highly accurate finite element modelling technique," IEEE Trans Power Delivery, vol. 8, no. 1 Jan. 1993, pp.239-245.

[8] IEC 354 Standard Publications: 1991, Loading Guide for Oil-Immersed Power Transformers.

[9] IEEE standard C57.91-1995, Loading Guide for Mineral-Oil-Immersed Immersed Transformers.

[10] Working Group 12-09, "Heat Run Test For Power Transformers" Electra, no.129, pp.37-39.

[11] Working Group 12-09, "Experimental Determination of Power Transformer Hot-Spot Factor" Electra, no.161, Aug 1995, pp.35-39.

[12] IEC Publication 76-2:1993, Power Transformers, Part 2. Temperature rises.

[13] Working Group 12-09, "Analytical Determination of Transformer Windings Hot-Spot Factor" Electra, no.161, Aug 1995, pp.29-33.

[14] Working Group 12-09, "A survey of facts and opinions on the maximum safe operating temperature of power transformers under emergency conditions" Electra, no.129, pp.53-63.

[15] J. Saitz, T. Holopainen and A. Arkkio, Modelling and Simulation in Electromechanics Field Problems, HUT , Electromechanics Lab. 2002.

[16] K. Haymer and R. Belmans, Numerical Modelling and Design of Electric Machines and Devices, WIT-Press, 1999.

[17] M. David and Others, Finite Element Method Magnetic FEMM.

[18] A. Konard, "Inegrodifferential Finite Element Formulation of Two-Dimensional Steady-State Skin Effect Problems," IEEE Trans. on Magnetics, vol. MAG-18, no.1, Jan 1982, pp.284-292.

[19] J. Weiss and Z. J. Csendes "A One Step Finite Element Method for Multi-conductor Skin Effect Problems," IEEE Trans. on Power Apparatus and Systems, vol. PAS-101, no.10, Oct. 1982, pp.3796-3800.

[20] A. Konard, M. V. K. Chari, and Z. J. Csendes "New Finite Element Techniques for Skin Effect Problems," IEEE Trans. on Magnetics, vol. MAG-18, no.2, Mar. 1982, pp.450-455.

[21] Lates L. V., Electromagnetic calculation of Transformers and Reactors: Moscow ENERGY, 1981 (In Russian), p.313.

[22] FEMLAB V2.3, Electromagnetics Module. Comsol, 2002.

[23] A. Elmoudi, M. Lehtonen, "Eddy losses calculation in transformer windings using FEM," The 44th International Scientific Conference of Riga Technical University, Riga, Latvia, October 9-11, 2003, Series 4, Vol. 10, pp. 46-51.

[24] J. Driesen, R. Belmans, K. Hameyer, "Study of Eddy Currents in Transformer Windings caused by Non-Linear Rectifier Load," Proceedings EPNC 98 circuits, Sept. 98, Liege, Belgium, pp.114-117.

[25] M. T. Bishop, J. F. Baranowski, D. Heath, S. J. Benna, " Evaluating Harmonic-Induced Transformer Heating," IEEE Trans. on Power Delivery, vol. 11, no.1, Jan 1996, pp.305-311.

[26] A Girgis, E. Makram, J. Nims," Evaluation of temperature rise of distribution transformer in the presence of harmonic distortion," Electric Power Systems Research, vol. 20, no.1, Jan 1990, pp.15-22.

[27] IEC 61378-1 Standard Publication: 1997, Transformers for Industrial applications.

[28] IEEE Std C57-110-1998, Recommended Practice for Establishing Transformer Capability when Supplying Non sinusoidal Load currents.

[29] S. P. Kennedy, C. L. Ivey , "Application, Design and Rating of Transformers Containing Harmonic Currents," IEEE Pulp and paper industry conference, 18-22 Jun. 90, pp.19-31.

[30] S. N. Makarov, A. E. Emanual, "Corrected Harmonic Loss Factor For Transformers supplying Non-sinusoidal Load current," Proc. of the 9th International conference on Harmonics and Power Quality, vol. 1, Oct. 2000, pp.87-90.

[31] Elmoudi, Asaad, Lehtonen, Matti and Nordman, Hasse, "Corrected Winding Eddy Current Harmonic Loss Factor for Transformers Subject to Non-sinusoidal Load Currents," 2005 IEEE PowerTech'2005, St. Petersburg, Russia, June, 27-30, 2005, Paper 226, 6 p.

[32] E. J. Davis and P. Simson, Induction Heating Hand Book London: McGraw-Hill, 1979 Ch. 12.

[33] Working Group 12/14.10, “Load Loss In HVDC Converter Transformers” Electra, no.174 pp.53-57

[34] S. R. Bendapudi J. C. Forrest, G. W. Swift “Effect of Harmonics on Converter Transformer Load Losses,” IEEE Trans. on Power Delivery, vol. 6, no.1, Jan 1991, pp.153-157.

[35] J. Driesen, T. V. Craenenbroeck, B. Brouwers, K. Hameyer, R. Belmans, “Practical Method to Determine Additional Load Losses due to Harmonic Currents in Transformers with Wire and Foil Windings,” IEEE Power Engineering Society Winter Meeting, 2000,Vol. 3, 23-27 Jan. 02 pp.2306 – 2311

[36] S. Crepaz, “Eddy Current Losses in Rectifier Transformers,” IEEE Trans. on Power Apparatus and Systems, vol. 89, 1970, pp.1651-1656.

[37] M.S. Hwang, W. M. Grady W. H. Sanders, "Assessment of Harmonic Current Effects in Power System Transformers," Ph.D. dissertation, Dept. Elec. Eng., Univ. of Texas at Austin, 1985.

[38] V.V Karasev, "The Dependence of losses in transformer tanks upon current, Frequency and Temperature," All-Union Electro Institute, vol. 79, pp. 628-636, 1969.

[39] A. E. Emanuel, X. Wang, “Estimation of Loss of Life of Power Transformers supplying Non-Linear Loads,” IEEE Trans. on Power Apparatus and Systems, vol. PAS-104 No.3, March 1985, pp.628-636.

[40] L. W. Pierce, “An Investigation of the Thermal Performance of an Oil Transformer Winding,” IEEE Trans. on Power Delivery, vol.7, no.3 July 1992, pp.1347-1358.

[41] L. W. Pierce, “Predicting Liquid Filled Transformer Loading Capability,” IEEE Trans. on Industry Applications, vol.30, no.1 1992, pp.170-178.

[42] B.C. Lesieutre W.H. Hagman J.L. Kirtley Jr. , “An Improved Transformer Top Oil Temperature Model for Use in An On-Line Monitoring and Diagnostic System,” IEEE Trans. on Power Delivery, vol.12, no.1 Jan 1997, pp.249-256.

[43] G.W. Swift, S.E. Zocholl, M. Bajpai, J. F. Burger, C.H. Castro, S.R. Chano, F. Cobelo, P. de Sa, E.C. Fennel, J.G. Gilbert, S.E. Grier, R. W. Hass, W. G. Hartmann, R. A. Hedding, P. Kerrigan, S. Mazumdar, D. H. Miller, P.G. Mysore, M. Nagpal, R.V Rebbapragada, M. V. Thaden, J. T. Uchiyam, S M. Usman, J. D. Wardlow, and M. Yalla "Adaptive Transformer Thermal Overload Protection," EEE Trans. on Power Delivery, vol.16, no.4 Oct. 2001, pp.516-521.

[44] G.W. Swift, T.S. Molinski, W. Lehn , "A Fundamental Approach to Transformer Thermal Modelling–Part I: Theory and Equivalent Circuit," IEEE Trans. on Power Delivery, vol.16, no.2 April 2001, pp.171-175.I

[45] G.W. Swift, T.S. Molinski, R. Bray and R. Menzies, "A Fundamental Approach to Transformer Thermal Modelling–Part II: Field Verification," IEEE Trans. on Power Delivery, vol.16, no.2 April 2001, pp.176-180.

[46] D. Susa, M. Lehtonen, H. Nordman, "Dynamic Thermal Modelling of Power Transformers," IEEE Trans. on Power Delivery, vol.20, Iss.1 Jan 2005, pp.197-204.

[47] D. Susa, M. Lehtonen, H. Nordman, "Dynamic Thermal Modelling of distribution Transformers," The paper has been approved for publication in the IEEE Trans. on Power Delivery

[48] P.T. Staats, W.M. Grady, A. Arapostathis, R. S. Thallam, "A Procedure for Derating a Substation Transformer in the Presence of Widespread Electric Vehicle battery Charging," IEEE Trans. on Power Delivery, vol.12, No.4 Oct 1997, pp.1562-1568.

[49] L. Pierrat, M.J. Resende, J. Santan, "Power Transformers Life Expectancy under Distorting Power Electronic Loads," Proceedings of ISIE 96, Vol.2 Jun. 96, pp.578-583.

[50] A. Elmoudi, M. Lehtonen, H. Nordman, "Predicting Liquid Filled Transformer Loading Capability" Accepted at CMD conference 2006 – South Korea

[51] A. Elmoudi, M. Lehtonen, H. Nordman, "Transformer Thermal Model Based on Thermal-Electrical Equivalent Circuit" Accepted at CMD conference 2006 – South Korea

[52] A. Elmoudi, M. Lehtonen, H. Nordman, "A Thermal Model for Power Transformers Dynamic Loading" Accepted at IEEE conference 2006 – Canada

[53] A. Elmoudi, M. Lehtonen, H. Nordman, "Effect of Harmonics on Transformers Loss of Life" Accepted at IEEE conference 2006 – Canada

Appendix I

Test setup and results for Eddy Loss Factor validation

A test set-up (calorimetric method) was built to check the validity of the corrected eddy loss factor [31] (see the photographs in Fig.1). The idea was to show the effect of harmonics on eddy losses induced in a conductor by an external varying magnetic field. Prof. M. Lehtonen suggested making an air core coil to create a homogenous magnetic field parallel to the axis of the coil. J. Millar and A. Elmoudi constructed the test setup and performed the analysis.

Coil design and the magnetic field

The magnetic field in the coil, which should be homogeneous and parallel to the axis of the coil is:

$$B_{coil} = \frac{N\mu_0 I}{Coil\_length} K = 0.54 \quad I \quad \text{mT}$$

where,

I is the current in the coil (in A).

This relationship was verified with measurements. The main point to note is that the magnetic field is proportional to the coil current. When corrected for current there was a slight variation in the measured field over the 50-500 Hz range. The error was within 5%.

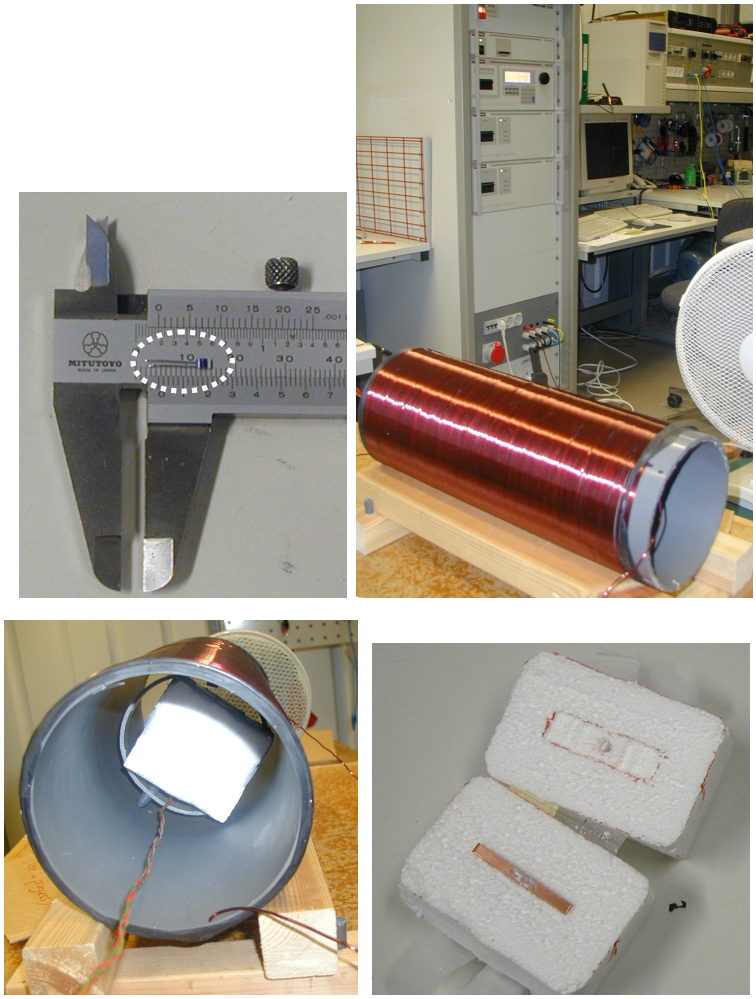

Figure 1 Photographs of the test equipment, which includes a tiny Pt100 temperature sensor (top left) attached with thermal paste to the thermally insulated sample (bottom right), a coil wound on a PVC tube, a high quality AC power supply (top right), capable of supplying a good sinusoidal current at a range of frequencies, and suitable cooling.

Heat equation

If we assume the conductor sample to be a perfect thermal conductor with perfectly insulating boundary conditions, then the losses can be calculated from the temperature rise:

$$q = \rho \; c \; \frac{\Delta\Theta}{\Delta t}$$

where, $\Delta\Theta$ is the temperature rise, ρ is the density of the sample, c is the specific heat capacity.

Experimental procedure

The process adopted was to measure the temperature rise of the samples with a single sensor when subjected to a magnetic field in order to determine the relationship of losses to frequency. Ideal conditions are impossible to achieve, but were approximated by attaching a tiny Pt100 sensor to the conductor sample and packing the sample in polystyrene. The thermally insulated sample was then suspended in the heating tube in a swivel bracket, which minimised the thermal contact between the sample and the solenoid. Fans were directed at and through the coil but even so, there was a period of little more than 40 s before the heat flux from the coil started to noticeably affect the sample.

Losses at fundamental frequency are problematic to measure, as the field must be very strong to produce a measurable temperature rise in samples with small conductor sections. Nevertheless, by controlling the ambient conditions and using as high a supply current as possible, results were obtained that are at least indicative of trends, and show the relationship of losses with frequency. The Shaffner generator was used to supply voltage and frequency steps automatically.

The temperature gradients obtained at each frequency were scaled by the inverse square of the currents to enable comparison with the fundamental response, the current of which was used as a base. The entire test period was logged, which meant that the temperature behaviour at the sensor on the sample could be modelled prior to each power step. The temperature rise above ambient was then estimated.

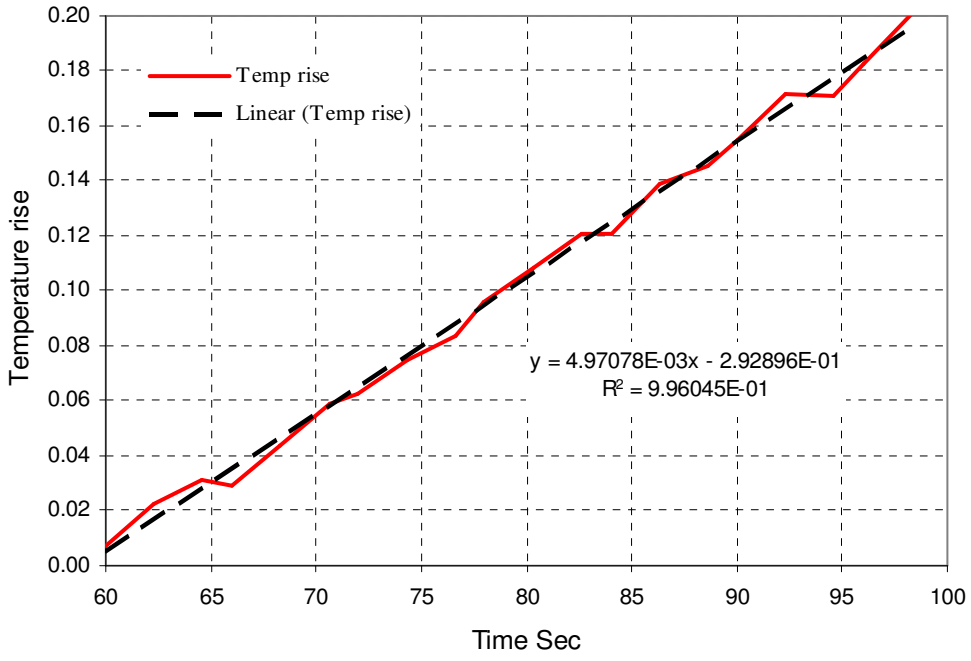

Fig. 2 *The line of best fit (using the least squares method) gives a gradient of* $4.97 \cdot 10^{-3}$ *K/s at 50 Hz*

For frequencies higher than 500 Hz, the lower power HP6834B power supply was used manually, noting that at higher frequencies the eddy current losses are much higher, and so lower coil currents are permissible.

Results

The test samples were 50 mm long, to ensure good clearance from the hot coil, and are shown in Fig.3

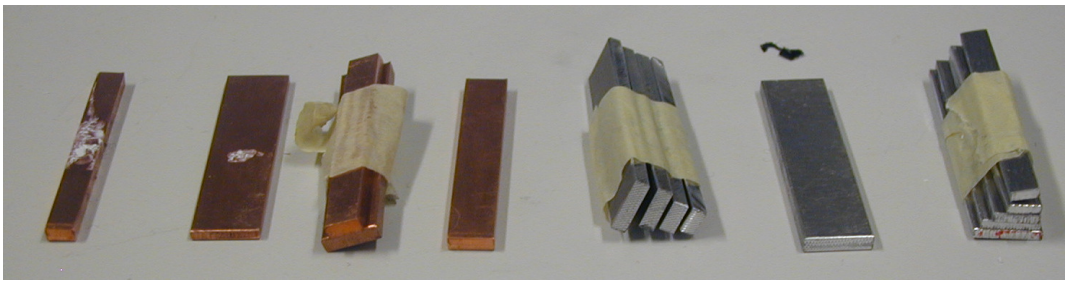

Fig. 3 *Solid conductor samples*

The results gave a near perfect fit with the response predicted for 12 mm and 8 mm conductors positioned perpendicular to the magnetic field as shown in Figs. 4 and 5.

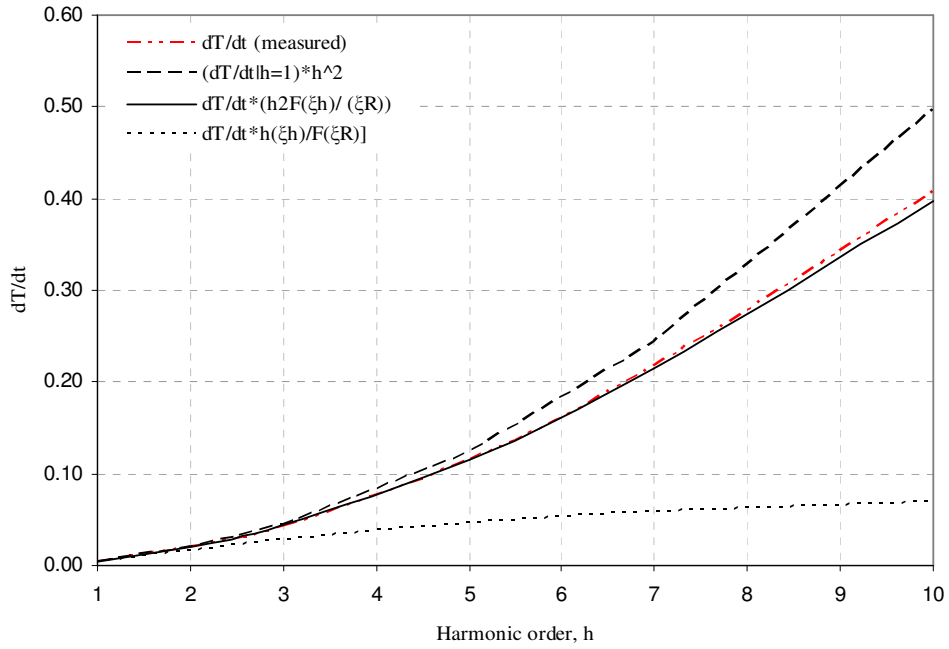

Fig. 4 The response of the conductor with the 12 mm edge facing the field

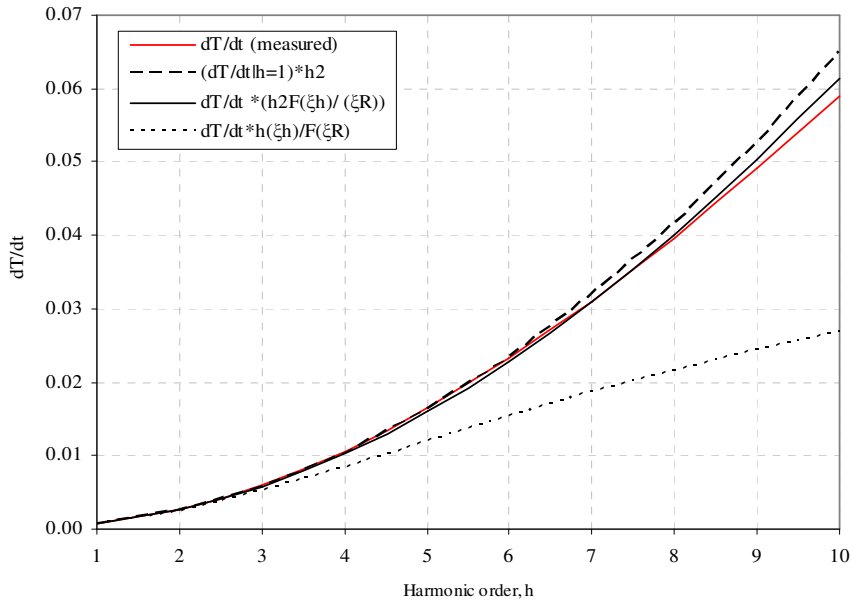

Fig. 5 The response of the conductor with the 8 mm edge facing the field

Since the results were very promising we were encouraged to measure up to the 25th harmonic. As shown in Fig. 6 the corrected loss factor gives a good prediction of the increased losses due to harmonics.

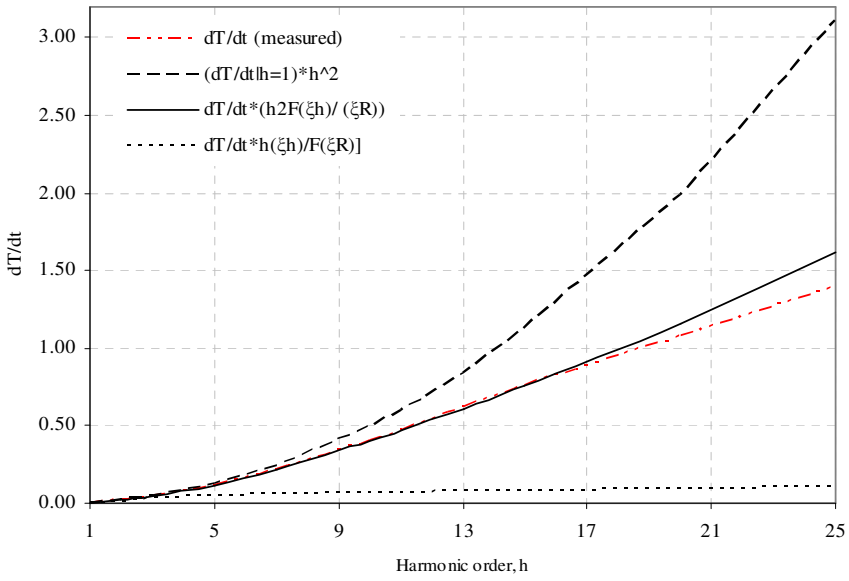

Fig. 6 The response of the conductor with the 12 mm edge facing the field

For smaller 2mm conductors the results were as shown in Fig.7 although it must be admitted that the temperature response became so small for small sections, that the gradient at 50 Hz could only be estimated. Losses at higher harmonics are greater, and thus gave rise to temperature gradients that were high enough to be accurately measured.

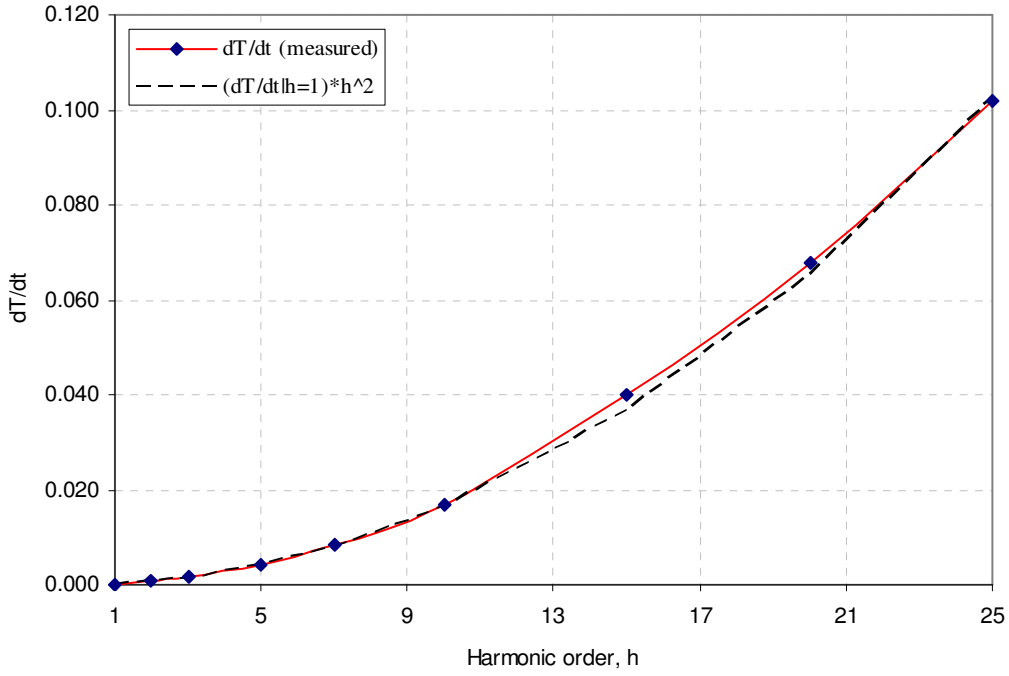

Fig. 8 The response of the conductor with the 2 mm edge facing the field

Fig. 9 shows the normalised response for different conductor sizes and, up to the 10th harmonic order, the comparison with the calculated results shows good agreement.

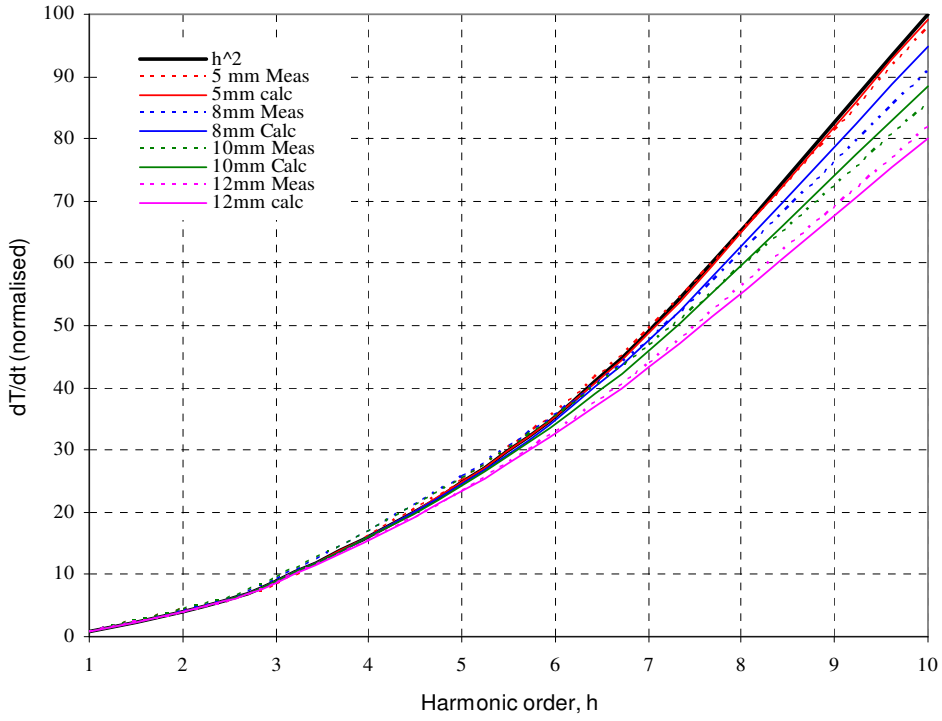

Fig. 8 Normalised responses for different conductor sizes compared with measurements

Appendix II

FEM Simulation Models

$$-\nabla\cdot(\frac{1}{\mu}\nabla\mathbf{A})+j\omega\sigma\mathbf{A}=\sigma\frac{\mathbf{V}}{\ell}=\mathbf{J}_s \qquad (3.19)$$

Input data for 250 MVA

Subdomain	Sig σ	μr	Current density
LV Winding	0	1	-1.95 A/mm2
HV Winding	0	1	1.72 A/mm2
Inn. Reg. Winding	0	1	1.32 A/mm2
Outer. Reg. Winding	0	1	0
Core	0	2000	0

Input data for 31.5 MVA

Subdomain	Sig σ	μr	Current density
LV Winding	0	1	-2.67A/mm2
HV Winding	0	1	1.98 A/mm2
Reg. Winding	0	1	0
Core	0	2000	0

Input data for 2500 KVA

Subdomain	Sig σ	μr	Current density
LV Winding	0	1	-1.58A/mm2
HV Winding	0	1	1.43 A/mm2
Reg. Winding	0	1	0
Core	0	2000	0

Boundary Conditions

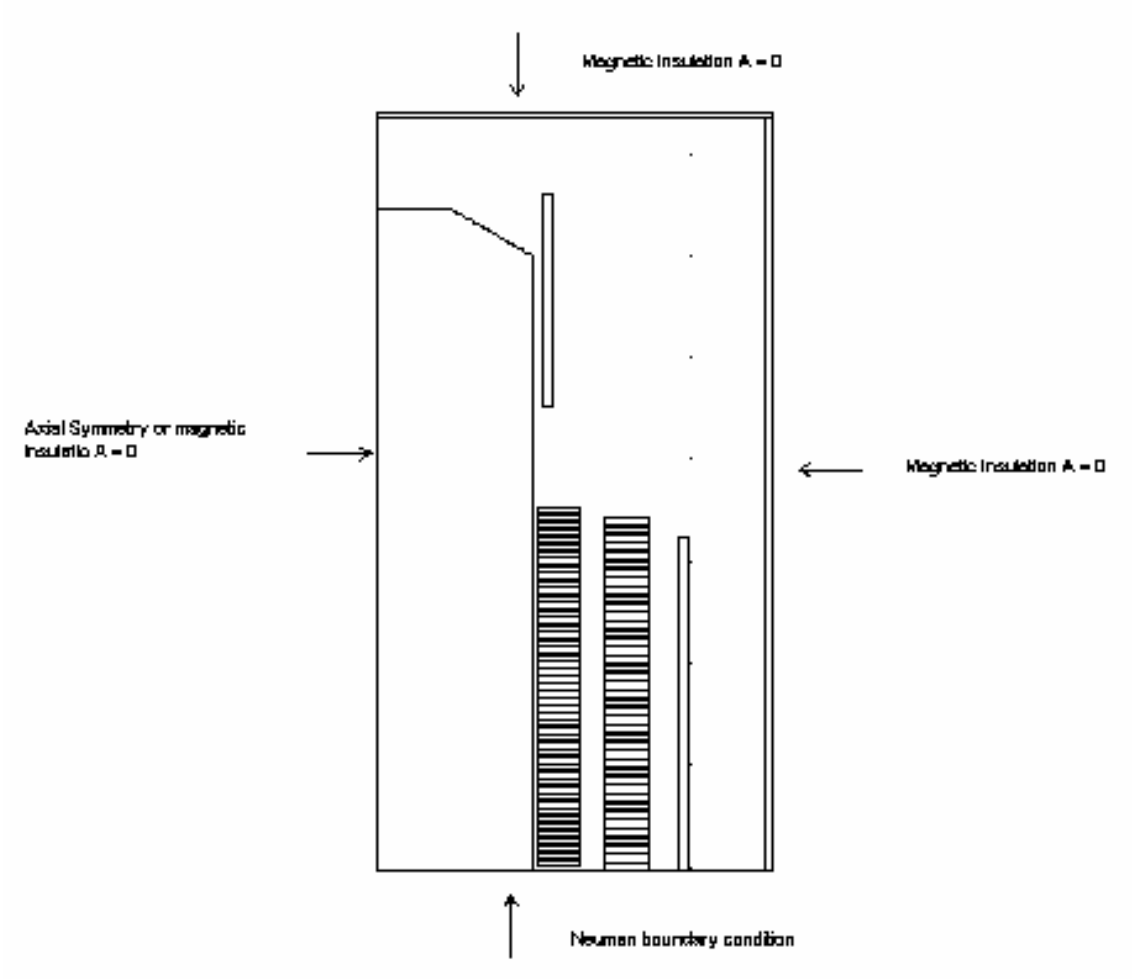

Appendix III
Simulation Models

1. IEEE Annex G Model

Fig. 1. shows IEEE Annex G model developed in Simulink. The model equations (6.23) (6.24) (6.34) (6.40) and (6.41) are solved straight forward using different numerical techniques, different time step can be assigned for required accuracy.

The Modified Hot Spot Model

$$L^2\left[P_{dcH}\cdot K_H+\frac{P_{ECH}}{K_H}\right]=M_H Cp_H\frac{d\Theta_H}{dt}+\left[\frac{\Theta_H-\Theta_{WO}}{\Theta_{HR}-\Theta_{WOR}}\right]^{5/4}\left[\frac{\mu_{HR}}{\mu_H}\right]^{1/4}\left(P_{dcH}+P_{ECH}\right) \quad (6.34)$$

and

$$M_H Cp_H = \frac{(P_{dcH} + P_{ECH})\tau_H}{\Theta_{HR} - \Theta_{WOR}} \tag{6.32}$$

Input variables (Function of time, *t*)

Θ_{WO} is the temperature of the oil in the ducts at the hot spot location, °C.

L is load current per unit.

μ_{WH} is the viscosity of the oil film at the hot spot location at time instant *t,* Centipoise.

Output variable (Function of time, t)

Θ_H is the winding hot spot temperature, °C.

Parameters (constants)

P_{dc} are the winding losses due to the dc resistance at the hot spot location.

P_{EC} are the winding losses due to the eddy currents at the hot spot location.

Θ_{HR} is the rated temperature at the hot spot location, °C

Θ_{WOR} is the rated temperature of the oil in the ducts at the hot spot location, °C

K_H Is the temperature factor for resistance change with temperature at hot spot location

τ_H is the winding time constant at hot spot location, min.

μ_{HR} is the rated viscosity of oil film at hot spot location, Centipoise.

Fig. 2 shows the equation above modeled in Simulink.

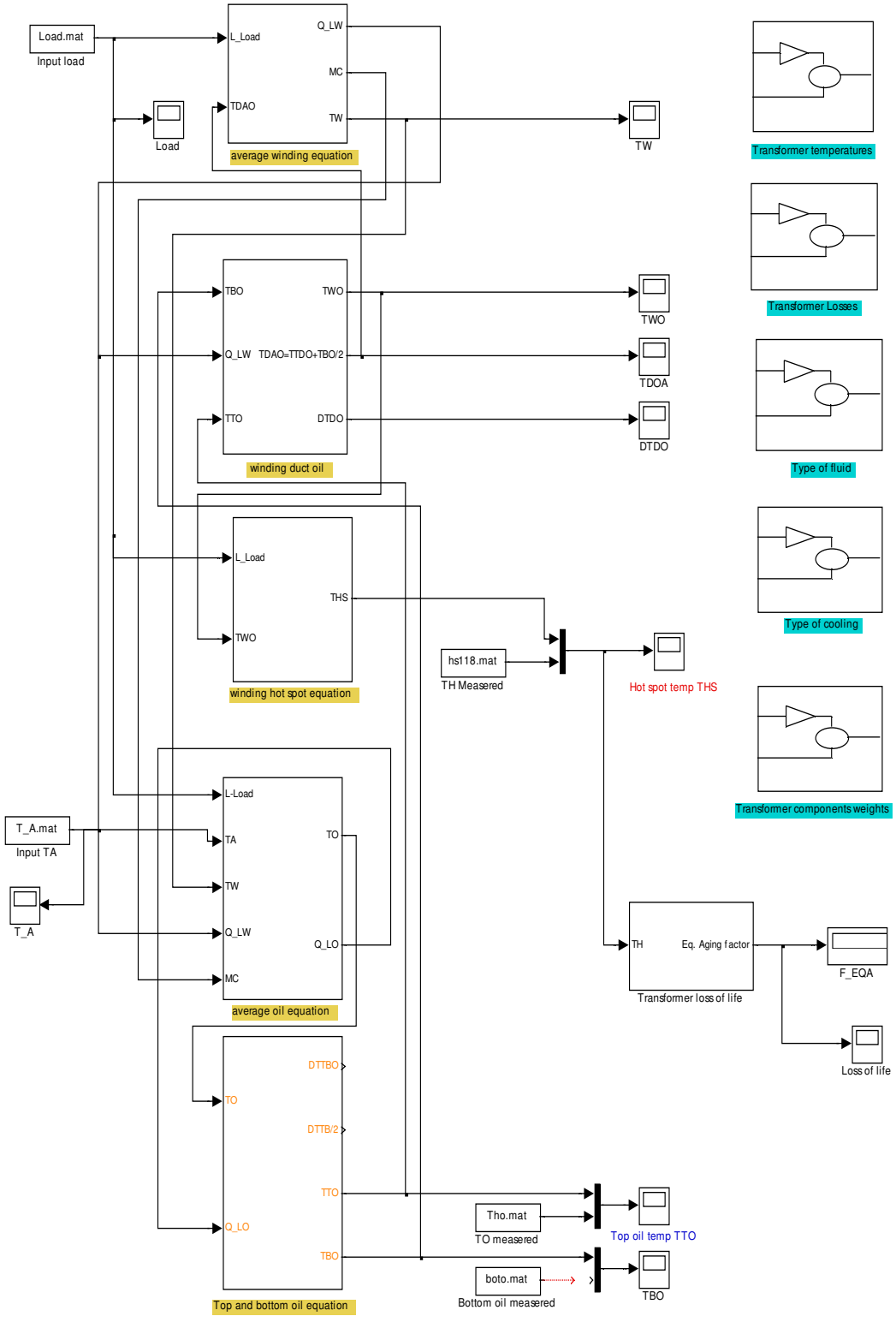

Fig. 1 Annex G IEEE Model

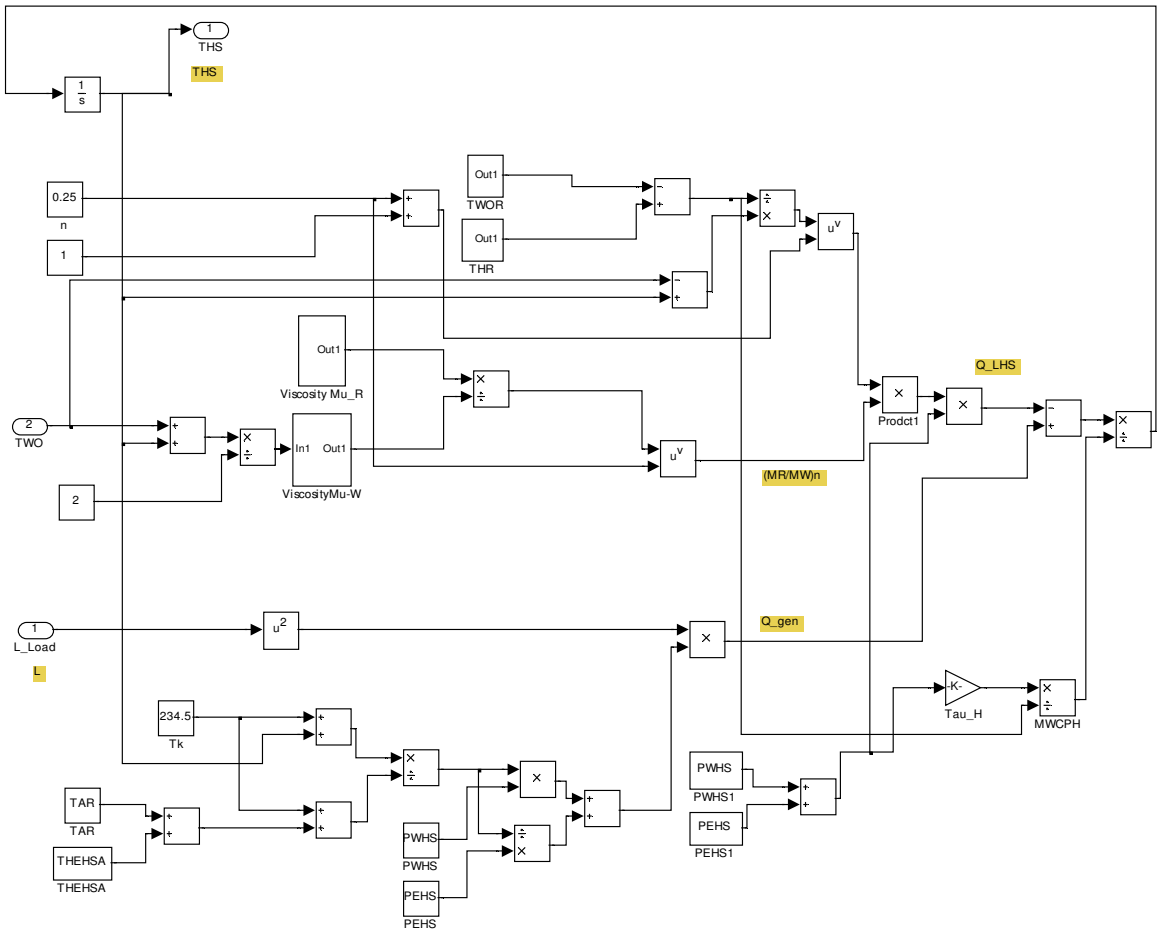

Fig. 2 the hot spot equation model

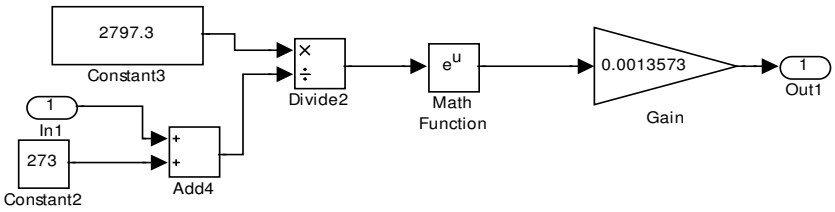

Fig. 3 The viscosity equation μ_R

The input parameters needed for the equations is shown in Fig. 4.

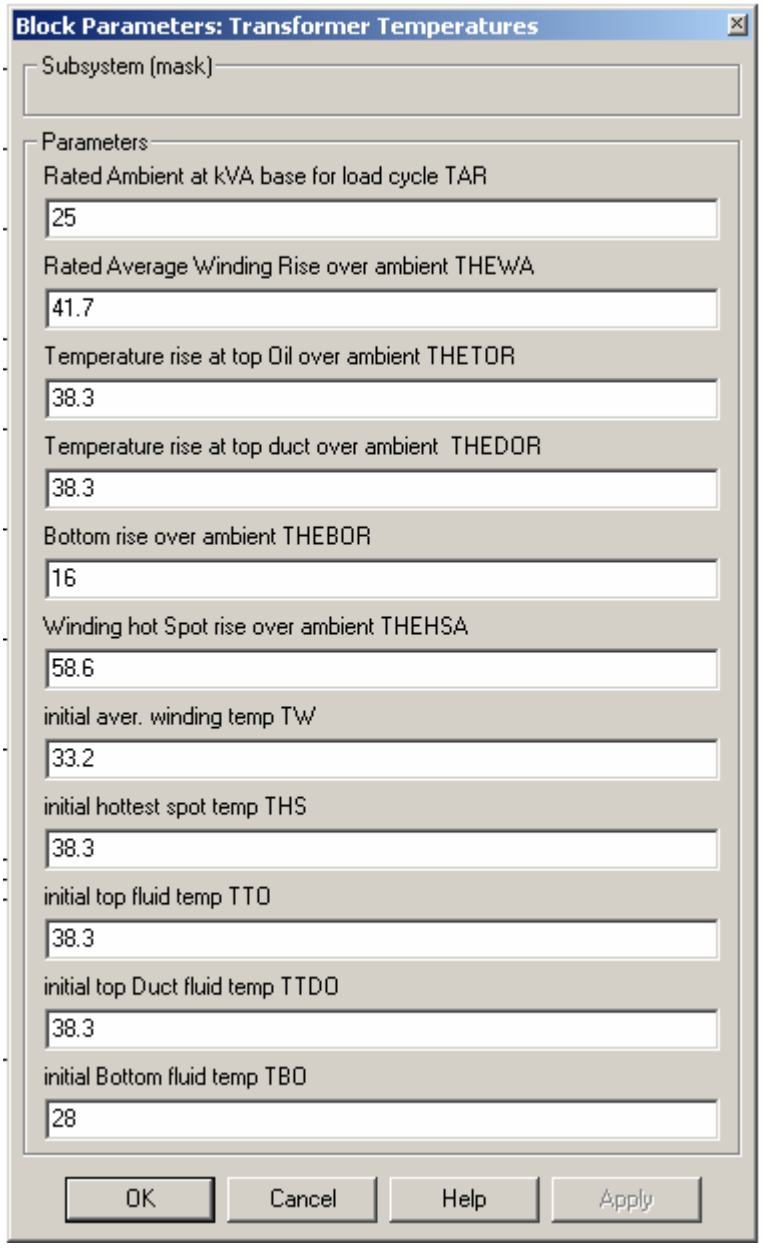

Fig. 4 Input temperature data for the model

Thermal Model based on Thermal-Electric equivalent circuit

Fig. 5 shows the thermal dynamic loading model developed in Simulink. The continuous form of equations (6.47) and (6.49) are solved straightforward.

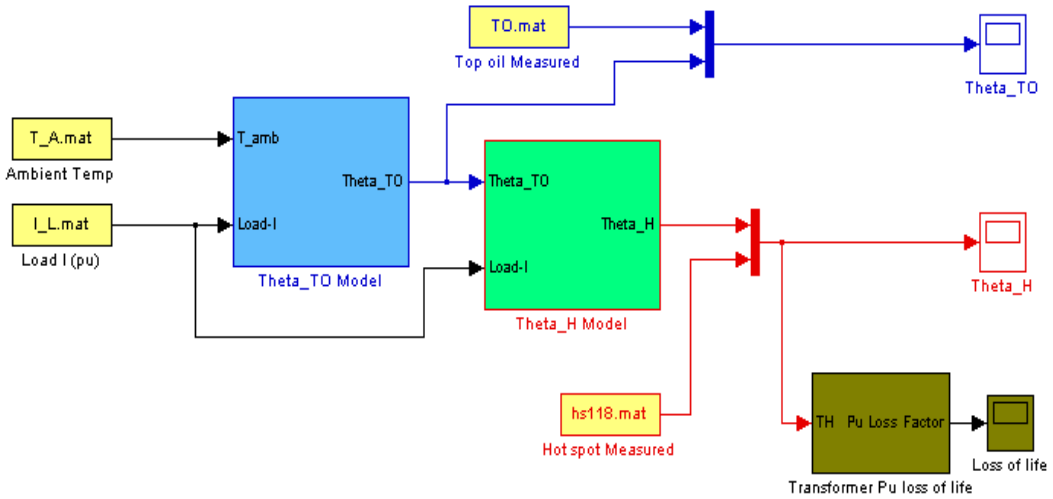

Fig. 5 Simulation model for the thermal model equations

The top oil model

$$\frac{I_{pu}^2\beta+1}{\beta+1}\cdot\left[\Delta\Theta_{oil-R}\right]^{1/n}=\tau_{oil}\frac{d\Theta_{Oil}}{dt}+\left[\Theta_{oil}-\Theta_A\right]^{1/n} \qquad (6.47)$$

Input variables (Function of time, *t*)

I_{pu} is the load current per unit.

Θ_A is the ambient temperature, ° C.

Output variable (Function of time, t)

Θ_{oil} is the top oil temperature, ° C.

Parameters (constants)

β is the ratio of load to no-load losses, conventionally *R*

τ_{oil} is the top oil time constant, min.

$\Delta\Theta_{oilR}$ is the rated top oil rise over ambient, K.

n is constant defines non-linearity.

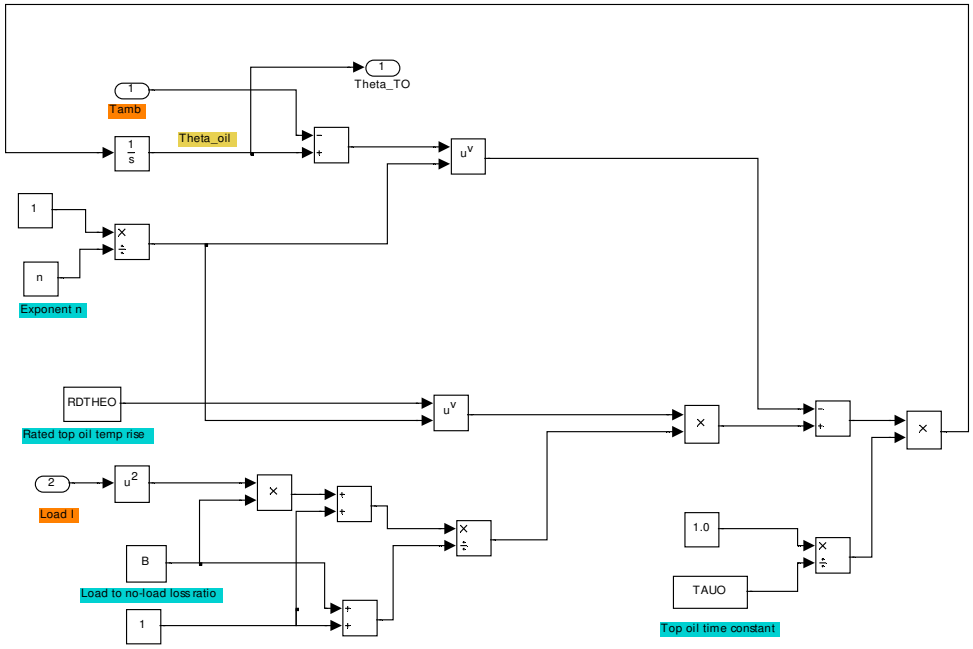

Fig. 6 Top oil model equation

The input parameters block for the top oil rise equation in the model is shown in Fig.7.

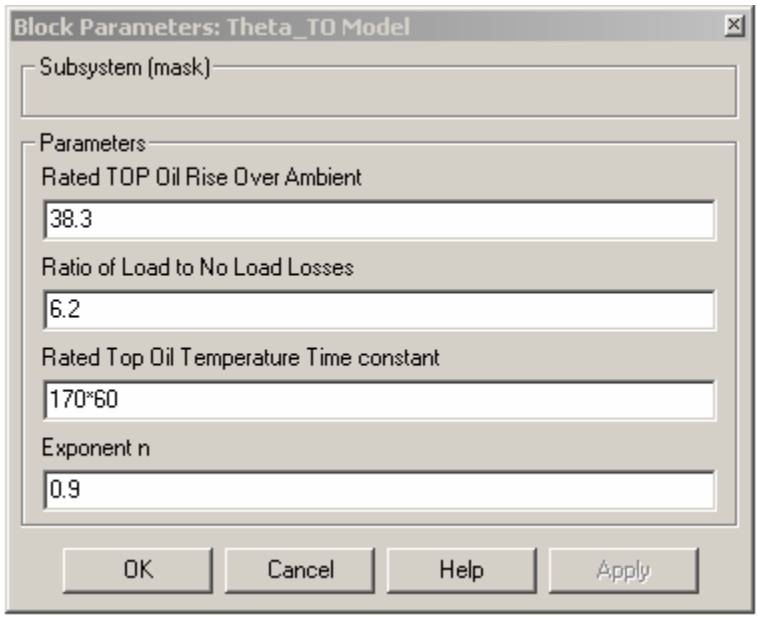

Fig. 7 Input parameters for top oil model

Loss of life equation

Fig. 8 shows the insulation loss of life simulation model as implemented in Simulink.

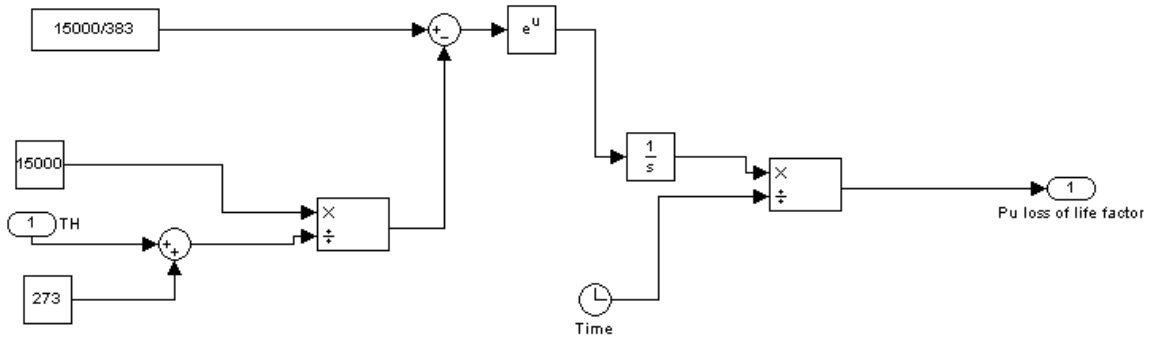

Fig. 8 Insulation loss of life simulation model

ISBN 951-22-8077-9
ISBN 951-22-8078-7 (PDF)
ISSN 1795-2239
ISSN 1795-4584 (PDF)